ABSTRACT

DISTRIBUTION OF VELOCITIES AND VELOCITY GRADIENTS IN MIXING AND FLOCCULATION VESSELS: COMPARISON BETWEEN LDV DATA AND CFD PREDICTIONS

by
Changgen Luo

Flocculation is an operation of significant industrial relevance commonly encountered in many processes, including water and wastewater treatment. The physico-chemical phenomena of this process is strongly affected by the magnitude of the velocity gradients generated, typically through agitation, in rapid mix devices and flocculation vessels.

In this work the fluid dynamic characteristics of mechanically agitated systems, namely three different types of stirred tanks, which can be used as flocculation vessels, were studied. Both the mean and fluctuating velocities in all three directions were measured by using a Laser-Doppler Velocimeter (LDV). The velocity distribution, fluctuating velocities, power consumption and local velocity gradient were numerically predicted with *FLUENT*, a computational fluid dynamic (CFD) software, using k-ε model, algebraic stress model (ASM), or Reynolds Stress Model (RSM) to simulate turbulence effect. The experimentally obtained mean velocities and turbulent kinetic energies on the top and bottom horizontal surfaces of the region swept by the impeller were used as boundary conditions in the simulations.

Significant agreement between the experimental data and the numerical predictions of the three dimensional velocities and turbulent kinetic energies was obtained in all cases.

A novel approach to numerically calculate the local velocity gradient (G) in turbulent flocculation tanks was developed. The distribution of local G values in three mixing systems was mapped through two new methods: the complete definition of local velocity gradient method and the local energy dissipation method. Results show that both methods can provide similar information about the local G value distribution. The trajectory of a solid particle with physical properties similar to those to a floc particle moving in three different mixing systems was numerically determined. The G value experienced by the particle as a function of time was also determined. A new parameter, the velocity gradient-time integral along a particle trajectory, was proposed and calculated. It is expected that the approach developed in this study will provide the foundations for a more accurate characterization of the fluid dynamics of flocculation systems.

DISTRIBUTION OF VELOCITIES AND VELOCITY GRADIENTS IN MIXING AND FLOCCULATION VESSELS: COMPARISON BETWEEN LDV DATA AND CFD PREDICTIONS

by
Changgen Luo

A Dissertation
Submitted to the Faculty of
New Jersey Institute of Technology
in Partial Fulfillment of the Requirements for the Degree of
Doctor of Philosophy

Department of Chemical Engineering,
Chemistry, and Environmental Science

May 1997

APPROVAL PAGE

DISTRIBUTION OF VELOCITIES AND VELOCITY GRADIENTS IN MIXING AND FLOCCULATION VESSELS: COMPARISON BETWEEN LDV DATA AND CFD PREDICTIONS

Changgen Luo

Dr. Piero M. Armenante, Dissertation Advisor — Date
Professor of Chemical Engineering, Chemistry, and Environmental Science, NJIT

Dr. Gordon A. Lewandowski, Committee Member — Date
Professor of Chemical Engineering, Chemistry, and Environmental Science, NJIT

Dr. Ching-Rong Huang, Committee Member — Date
Professor of Chemical Engineering, Chemistry, and Environmental Science, NJIT

Dr. Ernest S. Geskin, Committee Member — Date
Professor of Mechanical Engineering, NJIT

Dr. Robert G. Luo, Committee Member — Date
Assistant Professor of Chemical Engineering, Chemistry, and Environmental Science, NJIT

BIOGRAPHICAL SKETCH

Author: Changgen Luo

Degree: Doctor of Philosophy in Chemical Engineering

Date: May 1997

Undergraduate and Graduate Education:

- Doctor of Philosophy in Chemical Engineering
  New Jersey Institute of Technology, New Jersey, 1997
- Master of Science in Chemical Engineering
  East China University of Chemical Technology, Shanghai, P. R. China, 1988
- Bachelor of Science in Chemical Engineering
  East China University of Chemical Technology, Shanghai, P. R. China, 1985

Major: Chemical Engineering

Publications:

Armenante P. M., Luo C., Chou C. C., Fort I. and Medek J., "Velocity Profiles in a Closed, Unbaffled Vessel: Comparison between Experimental LDV Data and Numerical CFD Predictions", *Chemical Engineering Science*, in press, 1997.

This dissertation is dedicated to
my wife and my daughter

ACKNOWLEDGMENT

I would like to take this opportunity to thank Dr. Piero M. Armenante for his help and guidance. Without his support, this work would not have been done.

I would also like to express my sincere thanks to Dr. Gordon A. Lewandowski, Dr. Ching-Rong Huang, Dr. Ernest S. Geskin and Dr. Robert G. Luo for serving as Committee Members.

Special thanks go to Dr. Chun-Chiao Chou, Dr. Ding-Wei Zhou and Dr. Gong-Wei Wang, Dr. Socrates Ioannidis. Their knowledge, wisdom, time, and effort have made invaluable contributions to the conduct of the research and the completion of this work. More importantly their friendship has made my time at NJIT an enjoyable experience.

This work was partially supported by the National Science Foundation (Grant Number EEC 9520573), whose contribution is gratefully acknowledged.

I would like to give special credit to many specialists from both TSI Inc. and Fluent Inc. for their technical support in LDV experiment and CFD program usage.

Appreciation goes to our co-investigators from the Czech Republic and Queen's University, Northern Ireland, for the information they provided and exchanged with me.

Finally, I would like to express my deep appreciation to my wife for her patience and considerate support.

TABLE OF CONTENTS

TABLE OF CONTENTS
(Continued)

Chapter **Page**

TABLE OF CONTENTS
(Continued)

Chapter **Page**

LIST OF TABLES

Table **Page**

LIST OF FIGURES

LIST OF FIGURES
(Continued)

Figure **Page**

LIST OF FIGURES
(Continued)

Figure **Page**

LIST OF FIGURES
(Continued)

Figure **Page**

LIST OF FIGURES
(Continued)

Figure **Page**

NOMENCLATURE

C_1, C_2, C_3, C_4, C_5, C_D, C_μ Constants used in the CFD simulation; dimensionless

d Particle diameter in flocculation process; m

D Impeller diameter; m

Fl Impeller flow number ($Q/N D^3$); dimensionless

G Velocity gradient; s^{-1}

G_{ave} Average velocity gradient within the entire vessel; s^{-1}

G_k Generation of turbulence kinetic energy, k; $kg/m \cdot s^3$

H Height of liquid in mixing vessel; m

k Turbulent kinetic energy; m^2/s^2

m Mass of liquid in vessel; kg

n Particle concentration in flocculation process; dimensionless

n_o Initial particle concentration in flocculation process; dimensionless

N Agitation speed; rotations/s

N_p Power number; dimensionless

P Power dissipation; W

P_{ave} Average power dissipation for the entire vessel; W

Q, Q_{ij}, Q_{ij} Variables used in CFD simulation (ASM model); m^2/s^3

Q_c Impeller discharge flow rate; m^3/s

r Radial distance from vessel centerline; m

R Radius of impeller; m

t Time; s

NOMENCLATURE
(Continued)

T Vessel diameter; m

u Velocity; m/s

$\mathbf{u}$ Velocity vector; m/s

$\overline{\mathbf{u}}$ Time averaged velocity vector; m/s

$\mathbf{u}'$ Fluctuating velocity vector; m/s

u_a Axial (vertical) velocity; m/s

u_r Radial velocity; m/s

u_t Tangential velocity; m/s

u_x', u_y', u_z' Fluctuating velocity in three directions, respectively; m/s

U_{tip} Impeller tip velocity; m/s

w Vertically projected width of impeller blade; m

x_i, x_j, x_l Coordinate variables; m

Z Axial (vertical) distance from vessel bottom; m

Z_b Axial (vertical) distance from vessel bottom to bottom of impeller region; m

Z^+ Axial (vertical) distance from vessel bottom up to the point on the impeller tip where the radial flow on the impeller side is directed outwards; m

Greek Letters

α Constant used during the numerical simulation of turbulence (equation 2); dimensionless

NOMENCLATURE
(Continued)

δ_{ij} Kronecker delta

ε Turbulence energy dissipation rate; m^2/s^3

ε_{ave} Average turbulence energy dissipation rate within the entire vessel; m^2/s^3

η Collision efficiency in flocculation process; dimensionless

μ_t Turbulent viscosity; kg/(m·s)

μ Liquid viscosity; kg/(m·s)

ν Kinematic viscosity; $m^2 \cdot s^{-1}$

ρ Liquid density; kg/m^3

σ_k Constant used in the CFD simulation; dimensionless

σ_ε Constant used in the CFD simulation; dimensionless

τ Torque at shaft; N·m

Ω Volume fraction of colloidal particles in flocculation process; dimensionless

Dimensionless Groups:

$N_p = \frac{P}{\rho N^3 D^5}$ Power number

$Re = \frac{ND^2\rho}{\mu}$ Impeller Reynolds number

CHAPTER 1

INTRODUCTION

Mechanically agitated mixing vessels are widely used in a variety of industrial applications, such as precipitation, flocculation, polymerization, fermentation, as well as crystallization and heterogeneous catalysis. As a result, a significant literature exists on the subject, and design principles have been determined for many situations of industrial significance. In recent years the flow distribution in agitated vessels has been studied primarily using two complementary techniques, Laser-Doppler Velocimetry (LDV) and Computational Fluid Dynamics (CFD) simulations. Computational fluid dynamics (CFD) is a tool that is becoming increasing popular to study complex fluid flows such as those typically found in mixing vessels. The main advantage of this approach is in its potential for reducing the extent and number of experiments required to describe such types of flow. These two tools have enabled investigators to experimentally and non-intrusively determine the velocity distribution in mixing vessels, and make quantitative predictions about the same velocities (Armenante and Chou, 1996; Bakker, 1992; Costes et al., 1991; De Groot, 1991; Dong, 1994; Hirata et al., 1991; Jaworski et al., 1991; Kresta and Wood, 1991; Mahouast et al., 1989; Weetman, 1991; Ranade et al., 1989, 1992)

Some industrial processes, such as flocculation, are strongly affected by the magnitude of the velocity gradients generated, typically through agitation. However, only rough estimates of such velocity gradients (based on the average power dissipation in the flocculation vessel) are currently available. Very little information is available from the literature on the distribution of velocity gradients throughout the flocculation vessel (especially the fluctuating velocity gradients produced by turbulence effects).

Furthermore, although the product of the average velocity gradient by the retention time of the flocculating water has often been used as a the main parameter in the design of flocculators even less information is available on the time the individual floc particles spend in different zones of the vessel while being exposed to velocity gradients of different intensities. This indicates that the need exists for a better quantification of both the velocity gradient distribution and the velocity gradient-time integral for the floc particles being formed during flocculation.

Therefore, this work has been focused on the determination of the spatial distribution of local velocity gradients (through the determination of local power dissipation rates) along with the determination of tri-dimensional velocity distribution in mixing vessel with identical configurations to an existing flocculation pilot plant run at the Questor Centre at Queen's University, Belfast, Northern Ireland, U.K., using both an non-intrusive experimental approach (via Laser-Doppler Velocimetry) and a rigorous computational approach (via Computational Fluid Dynamics). This work is one part of the collaborative research project entitled "Fundamental Studies and Chemical and Engineering Innovations in Flocculative Water Cleaning" between HSMRC at New Jersey Institute of Technology, Newark, NJ and Questor Centre at Queen's University, Belfast, Northern Ireland, U.K.

Turbulent fluid dynamic effects play a significant role in the flocculation process. The reason for this can be traced back to the effect that the transport of the chemical species and floc aggregates throughout the vessel have on the final results of the process. Since such transfer phenomena are very significantly affected by parameters such as shear rate and bulk flow it is evident that the fluid dynamic characteristics of flocculators

are of paramount importance for both an understanding of the process and its actual practical results. This is a very well recognized aspect of flocculation known to any practitioner in the field. In fact, the most common flocculation test, the jar test, is an attempt to capture the essence of both the fluid dynamic characteristics and the particle destabilization and floc aggregation aspects of the process. Unfortunately, this approach is very crude and results it produces are difficult to extrapolate.

The main difficulty at the basis of a precise definition of the fluid dynamic characteristics of flocculators is that flocculation is dominated by turbulence, a phenomenon still poorly understood. In recent years the study of turbulent phenomena has been greatly been enhanced by experimental tools such as Laser-Doppler Velocimetry. In addition, fluid dynamic problems have been successfully tackled by numerically solving the equations commonly used to described turbulent phenomena. This work is aimed at utilizing these tools to quantitatively describe the fluid dynamics of flocculators.

In this study the velocities in four mixing and flocculation systems (System A: an unbaffled, flat-bottom, cylindrical vessel provided with a lid, completely filled with water, and agitated by a six-blade, 45° pitched-blade turbine; System B: a baffled rectangular tank agitated by a 2-blade paddle-type impeller; System C1 and C2: baffled, flat-bottomed cylindrical vessels agitated by six-blade, 45° pitched-blade turbines of different sizes) were experimentally determined with a laser-Doppler velocimetry (LDV) apparatus. The velocities at a number of locations in the impeller region (defined as the outer surface of the volume swept by the impeller) were then used as boundary conditions in CFD simulations. The velocity distribution, fluctuating velocities, power

consumption and local velocity gradient were numerically predicted with *FLUENT*, a computational fluid dynamic (CFD) software, using k-ε model, algebraic stress model (ASM), or Reynolds Stress Model (RSM) to simulate turbulence effect. Comparisons were made between the experimental LDV data obtained for all three systems and the results of the numerical predictions, in order to determine the best approach to CFD simulation of complex flows in mixing and flocculation vessels.

In addition, a novel approach to numerically calculate the local velocity gradient (G) in turbulent flocculation tanks was developed. The distribution of local G values in two mixing systems was mapped through two new methods: the complete definition of local velocity gradient method and the local energy dissipation method. Results show that both methods can provide similar information about the local G value distribution. The trajectory of a solid particle with physical properties similar to those to a floc particle moving in three different mixing systems was numerically determined. The G value experienced by the particle as a function of time was also determined.

In order to better characterize the effect of fluid dynamics on the flocculation process, a new parameter, the velocity gradient-time integral, was proposed in this work. A rigorous program to quantify this new parameter from the information obtained by CFD simulation has been developed in this work by using Visual Basic language incorporated with Microsoft Excel 5.0. Finally, a comparison was made between the G average value obtained through the conventional method and the new method in this work.

CHAPTER 2

OBJECTIVES

The primary objective of this work was the determination of the spatial distribution of local velocity gradients (through the rigorous methods proposed in this work, i.e., the complete definition of local velocity gradient method and the local energy dissipation rate method) and the determination of tri-dimensional velocity distribution in four mixing/flocculation systems. The trajectory of a virtual particle with physical properties similar to those of a floc particle moving in three different systems was also numerically determined. Both an non-intrusive experimental approach (via Laser-Doppler Velocimetry) and a rigorous computational approach (via Computational Fluid Dynamics) were used to achieve these objectives.

A new variable, the velocity gradient-time integral along a particle trajectory, taking into account the local velocity gradient and the time a moving floc particle is exposed to it, was then defined and calculated for three different systems to better model the flocculation process. It is expected that the results of this approach will eventually be incorporated in some of the many models available in the literature for floc aggregation and breakage. So far these models have typically relied on averages of the velocity gradient derived from simplified turbulence theories rather than their actual values.

CHAPTER 3

THEORETICAL BACKGROUND

3.1 Flocculation Process

Flocculation process is an operation of significant industrial relevance commonly encountered in water and wastewater treatment plants. Coagulation and flocculation refer, respectively, to the process of destabilization of colloidal particles upon the addition of some chemicals to the water containing them, and to the process through which these destabilized particles collide and aggregate to form larger floc particles that can be separated via sedimentation or other physical methods. The two terms are often used interchangeably - a practice that will also be followed in this work, unless leading to possible misunderstanding. Flocculation is a process extremely difficult to quantify because of the complexities of the phenomena at its origin, and also because these phenomena affect each other in ways that are difficult to resolve into separate effects.

When a coagulant is added to a solution containing colloidal particles a number of aspects must be considered to fully explain the overall results. Chemical hydrolysis, particle agglomeration and breakup, and turbulent fluid dynamic effects all play a significant role in the overall process (Amirtharajah and Mills, 1982). These characteristics of flocculation processes will now be briefly reviewed.

3.1.1 Chemical Hydrolysis

Most of the chemicals commonly used as coagulants react with water forming hydrolysis products. In many cases the number and nature of these products are such that complex equilibria among such species is possible. Furthermore, the composition of the resulting

solution is a strong function of pH and temperature. For example, the addition of ferric chloride to water results in its hydrolysis to $Fe(OH)_3$ which then results in the formation of species such as $Fe(OH)_4^-$, $Fe(OH)_2^+$, $Fe(OH)^{2+}$, Fe^{3+} and others. Equilibrium diagram for all the species involved have been produced and are quite complex. An additional complication results from the fact that the kinetics of the formation of the various products during coagulation must be taken into account, and that only some of these species are effective as coagulants.

3.1.2 Destabilization and Aggregation of Colloidal Particles

After its initial formation the coagulation products are typically adsorbed on the surface of the colloid particles, destabilizing them. This is usually a fast reaction. However, in order for the destabilized particles to aggregate they must come in contact with each other and be maintained in such close proximity for a sufficient period of time for the floc to be formed. Successive floc growth occurs when floc particles come in contact with other particles, producing flocculation. This is typically a slower process. The two aspects of the process have resulted in the common practice of carrying out flocculation first under rapid mix conditions (where interactions among destabilized particles are promoted) and then under slow mix conditions (where floc breakup is minimized and sedimentation is promoted).

3.1.3 Fluid Dynamics Effects

The two previous aspects of the coagulation/flocculation process can be significantly affected by the fluid dynamic conditions inside the flocculation vessel. The reason for this can be traced back to the effect that the transport of the chemical species and floc aggregates throughout the vessel have on the final results of the process. Since such transfer phenomena are very significantly affected by parameters such as shear rate and bulk flow it is evident that the fluid dynamic characteristics of flocculators are of paramount importance for both an understanding of the process and its actual practical results. This is a very well recognized aspect of flocculation known to any practitioner in the field. The common alternation of "rapid mix" and "slow mix" regimes during flocculation is a recognition that agitation is indeed a key parameter. In fact, the most common flocculation test, the jar test, is an attempt to capture the essence of both the fluid dynamic characteristics and the particle destabilization and floc aggregation aspects of the process. Unfortunately, this approach is very crude and results it produces are difficult to extrapolate.

The main difficulty at the basis of a precise definition of the fluid dynamic characteristics of flocculators is that flocculation is dominated by turbulence, a phenomenon still poorly understood. In recent years the study of turbulent phenomena has been greatly enhanced by experimental tools such as laser-Doppler Velocimetry (LDV). In addition, fluid dynamic problems have been successfully tackled by numerically solving the equations commonly used to describe turbulent phenomena. This work is aimed at utilizing these tools to quantitatively describe the fluid dynamics of

flocculators so that it can be eventually incorporated in more comprehensive chemical-physical flocculation models.

3.2 Effect of Velocity Gradients on Flocculation

Flocculation process is strongly affected by the magnitude of the velocity gradients generated, typically, through agitation. In flocculation the velocity gradient is important not only because it can produce contact between particles, but also because it can produce floc breakup if it has too high a value.

3.2.1 Conventional Method to Estimate the Velocity Gradient

Because of the complexity of the flocculation process a number of simplified models as well as rules of thumb are available from the literature (Bhargava and Ojha, 1993; Delichatsios and Probstein, 1975; Dharmappa et al., 1993; Glasgow and Kim, 1986; Glasgow and Liu, 1991; Mhaisalkar et al., 1991; Wiesner, 1992). In the vast majority of these models the effect of agitation and turbulence on flocculation is typically expressed using a single key parameter, namely the root mean square velocity gradient in the vessel, G, first introduced by Camp and Stein (1943):

$$G = \sqrt{\left(\frac{\partial u}{\partial y} + \frac{\partial v}{\partial x}\right)^2 + \left(\frac{\partial u}{\partial z} + \frac{\partial w}{\partial x}\right)^2 + \left(\frac{\partial v}{\partial z} + \frac{\partial w}{\partial y}\right)^2} \qquad (3.1)$$

where u, v, w are the velocities components in x, y, z coordinates. Camp and Stein (1943) called this G as the *absolute velocity gradient* at a point. They considered that the angular distortion of an elemental volume of water due to tangential surface forces or

shears. Therefore, they related this *absolute velocity gradient* with the work done per unit volume per unit time in the following way.

$$\frac{P}{V} = \mu G^2 \tag{3.2}$$

where P = power dissipation, V = vessel volume, μ = liquid viscosity.

Rearranging Eq. 3.2, they had

$$G = \sqrt{\frac{P}{V\mu}} = \sqrt{\frac{\varepsilon}{\nu}} \tag{3.3}$$

where ε = dissipation rate, ν = kinematic viscosity.

Theoretically, if the power dissipated or the work done at any point within agitated vessel is known, then the *absolute velocity gradient* can be calculated by using the above equation. However, realistically, the dissipated power varies from position to position within the agitated vessel. Therefore, the velocity gradient in this expression is a function of both time and position within the vessel. Since the velocity gradients are quite difficult to calculate, an approximation typically made to estimate G is to replace it with its average value throughout the vessel G_{ave} :

$$G_{ave} = \sqrt{\frac{P_{ave}}{V\mu}} \tag{3.4}$$

where the average power consumption, P_{ave}, can easily be obtained from the power requirement to agitate the vessel:

$$P_{ave} = N_p \rho N^3 D^5 \tag{3.5}$$

with N_p = power number for a given impeller, ρ = density of liquid, N = rotational speed of impeller, D = impeller diameter.

G_{ave} obtained through equation 3.4 is referred to in this work as the G average value obtained through the *conventional method.*

G_{ave} or another mean value for G is typically included in most flocculation models. For example, O'Melia (1972) assumed that the rate of change in the total concentration of particles during flocculation is:

$$\frac{dn}{dt} = -\frac{2\eta d^3 n^2}{3} G_{ave} \tag{3.6}$$

where n = particle concentration, η = collision efficiency, d = particle diameter. Upon integration this equation becomes:

$$ln\frac{n}{n_o} = -\frac{4\eta\Omega}{\pi} G_{ave} t \tag{3.7}$$

where n_o = initial particle concentration, Ω = volume fraction of colloidal particles, and t = time. A similar approach was also followed by Miyanami et al. (1982) who obtained an expression in which $\ln(n/n_o)$ was proportional to $G_{ave}^{1.11}$. Other recommendations for optimum flocculation include a number of different relationships in which the term G_{ave}^{α} t^{β} can be found (Camp, 1955; McConnachie, 1989).

It is evident that the use of G_{ave} instead of G greatly simplifies the calculation of the frequency collision and hence the determination of the optimal flocculation conditions. Unfortunately, in stirred tanks used in flocculation the distribution of velocity gradients is by no means uniform. In fact, it has been shown already that the

local power consumption at location of high turbulence intensity (e.g., in the vicinity of the impeller) can be many times higher than that in the rest of the tank (Wu and Patterson, 1989; Kresta and Wood, 1991; Tatterson, 1991; Geisler *et al*, 1996)). Furthermore, different mixing devices can produce identical average power dissipation values (and hence identical G_{ave} values) but very different distributions of ε and G throughout the vessel. As stated by Zhou and Kresta (1996): "Different types of impellers create different circulation patterns and different distributions of turbulence energy dissipation for the same tank geometry. The same average power input per unit mass (sometimes called the average energy dissipation) can result in widely different distributions of turbulence energy dissipation when different impellers are used with the same tank geometry". Ducoste *et al* (1997) also pointed that: "There is growing evidence that a more complex relationship exists between particle agglomeration/breakup and the fluid mechanics generated in a flocculation basin that can not be fully described by just using the G value for the whole tank. In order to fully understand the relationship between agglomeration/breakup and fluid mechanics, it is necessary to first characterize the complex fluid mechanics."

Furthermore, the time a floc particle exposed to a given velocity gradient during the flocculation processing is also very important. A particle may spend more time in zones with one G value than other zones with different G value. This will make big difference for certain flocculation process. A closer examination reveals that what can be of ever greater significance for these two phenomena is a parameter that takes into account not only the local velocity gradient but also the time a particle or floc is exposed

to it. The simplest conceivable function that includes both parameters is the product $G_{ave}\ t_{ret}$ in which t_{ret} is the retention time. In fact, this group appears in the flocculation equation by O'Melia given above. However, it is evident that even in the simple O'Melia model the cumulative change in flocculation at a generic time will depend on the integral of G as a function of time. Since during the same time interval the particle or floc has followed a certain trajectory within the vessel the integral of G vs. t must be calculated knowing what the trajectory is and the velocity that the particle has at each point. Therefore, the term $G_{ave}\ t_{ret}$ obtained through the conventional method is only a crude estimation of the actual velocity gradient-time integral.

3.2.2 Rigorous Methods to Calculate the Velocity Gradient

Although the conventional method to estimate the velocity gradient, proposed by Camp and Stein (1943), has been widely used by environmental engineers for decades, it is a very rough method. Apparently, it has two major weaknesses, at least. First, the so-called *absolute velocity gradient* is defined in such a way that only the tangential shear stresses were considered, while the normal stress terms were not included. This leads to an incomplete estimation of this parameter. Second, an average velocity gradient is calculated for the entire agitated vessel. This leads to a very inaccurate estimation of this parameter, since the velocity gradient varies greatly from position to position within the vessel. A simple value cannot represent the characteristics of this process. Besides, different agitated systems could have the same G_{ave} but produce quite different mixing or flocculating results.

Because of these weaknesses, many researchers have found that G_{ave} is not suitable to describe the turbulent flocculation process. Argaman and Kaufman (1970) experimentally observed that the maximum floc size in flocculation process was inversely proportional to G. Cleasby (1984) even proposed that power input per unit mass to the two thirds power, $\varepsilon^{2/3}$, is a more appropriate flocculation parameter than G obtained by the conventional method for common water and wastewater flocculation practice. All attempts available in the literature are based on the use of an average parameter for the entire vessel, which can be inadequate to characterize the turbulent flocculation process. No information was found in the literature about the estimation of local velocity gradient in mixing or flocculation processes.

This work aimed to solve this problem. With the assistance of new technologies in both experimental and simulation fields (LDV and CFD, respectively), we were able to calculate the real value of this parameter (local velocity gradient) at each position within the mixing or flocculation vessel, through more fundamental and rigorous methods shown below.

A differential mechanical energy balance for a fluid element can be written as (Bird et al. 1960):

$$\frac{\partial}{\partial t}\left(\tfrac{1}{2}\rho v^2\right) = -\left(\nabla \cdot \tfrac{1}{2}\rho v^2\,\mathbf{v}\right) - \left(\nabla \cdot p\,\mathbf{v}\right) - \left(\nabla \cdot [\tau \cdot \mathbf{v}]\right) + \rho(\mathbf{v}\cdot\mathbf{g}) - p(-\nabla \cdot \mathbf{v}) - (-\tau : \nabla\,\mathbf{v}) \tag{3.8}$$

where the term on the left hand side is the rate of increase in kinetic energy per unit volume, and the terms on the right hand side are the net rate of input of kinetic energy by virtue of bulk flow, the rate of work done by pressure of surroundings on volume

element, the rate of work done by viscous force on volume element, the rate of work done by gravity force on volume element, the rate of reversible conversion to internal energy, and the rate of *irreversible* conversion to internal energy, respectively.

The term $(-\tau:\nabla \mathbf{v})$ in the above equation accounts for the degradation of mechanical energy to thermal energy. It represents the energy dissipation rate, ε. Hence:

$$\varepsilon = \frac{P}{V} = (-\tau:\nabla \mathbf{v}) \tag{3.9}$$

For Newtonian fluids the term $(-\tau:\nabla \mathbf{v})$ can be rewritten as:

$$(-\tau:\nabla \mathbf{v}) = \mu \Phi_v \tag{3.10}$$

where

$$\begin{aligned}\Phi_v = 2&\left[\left(\frac{\partial u_x}{\partial x}\right)^2 + \left(\frac{\partial u_y}{\partial y}\right)^2 + \left(\frac{\partial u_z}{\partial z}\right)^2\right] \\ &+ \left(\frac{\partial u_x}{\partial y} + \frac{\partial u_y}{\partial x}\right)^2 + \left(\frac{\partial u_y}{\partial z} + \frac{\partial u_z}{\partial y}\right)^2 + \left(\frac{\partial u_x}{\partial z} + \frac{\partial u_z}{\partial x}\right)^2 \\ &- \frac{2}{3}\left[\frac{\partial u_x}{\partial x} + \frac{\partial u_y}{\partial y} + \frac{\partial u_z}{\partial z}\right]^2\end{aligned} \tag{3.11}$$

and u_x, u_y, u_z are the velocity components in the x, y, z direction, respectively.

By defining G (velocity gradient at a point) as follows:

$$\begin{aligned}G = \Bigg\{2&\left[\left(\frac{\partial u_x}{\partial x}\right)^2 + \left(\frac{\partial u_y}{\partial y}\right)^2 + \left(\frac{\partial u_z}{\partial z}\right)^2\right] \\ &+ \left(\frac{\partial u_x}{\partial y} + \frac{\partial u_y}{\partial x}\right)^2 + \left(\frac{\partial u_y}{\partial z} + \frac{\partial u_z}{\partial y}\right)^2 + \left(\frac{\partial u_x}{\partial z} + \frac{\partial u_z}{\partial x}\right)^2 \\ &- \frac{2}{3}\left[\frac{\partial u_x}{\partial x} + \frac{\partial u_y}{\partial y} + \frac{\partial u_z}{\partial z}\right]^2\Bigg\}^{1/2}\end{aligned} \tag{3.12}$$

Then we have the relationship between the G and ε as:

$$\varepsilon = \frac{P}{V} = \left(-\tau : \nabla \mathbf{v}\right) = \mu G^2 \tag{3.13}$$

For an incompressible fluid the last term in the expression for G is zero (because of continuity) and G becomes:

$$G = \left\{ 2\left[\left(\frac{\partial u_x}{\partial x}\right)^2 + \left(\frac{\partial u_y}{\partial y}\right)^2 + \left(\frac{\partial u_z}{\partial z}\right)^2 \right] + \left(\frac{\partial u_x}{\partial y} + \frac{\partial u_y}{\partial x}\right)^2 + \left(\frac{\partial u_y}{\partial z} + \frac{\partial u_z}{\partial y}\right)^2 + \left(\frac{\partial u_x}{\partial z} + \frac{\partial u_z}{\partial x}\right)^2 \right\}^{1/2} \tag{3.14}$$

If the spatial distribution of u_x, u_y, u_z is known, then the distribution of G in the fluid can be calculated by computing the derivatives on the right hand side of this equation. This method is referred to as the ***complete definition of local velocity gradient method*** in this work.

A comparison between the rigorous equation for G (Eq. 3.14) and that (Eq. 3.1) of Camp and Stein (1943) shows that these investigators forgot to include the normal shear terms in their equation for G.

Similarly, in cylindrical coordinates, the rigorous expression for G becomes:

$$G = \left\{ 2\left[\left(\frac{\partial u_r}{\partial r}\right)^2 + \left(\frac{1}{r}\frac{\partial u_\theta}{\partial \theta} + \frac{u_r}{r}\right)^2 + \left(\frac{\partial u_z}{\partial z}\right)^2 \right] + \left(r\frac{\partial}{\partial r}\left(\frac{u_\theta}{r}\right) + \frac{1}{r}\frac{\partial u_r}{\partial \theta}\right)^2 + \left(\frac{\partial u_\theta}{\partial z} + \frac{1}{r}\frac{\partial u_z}{\partial \theta}\right)^2 + \left(\frac{\partial u_z}{\partial r} + \frac{\partial u_r}{\partial z}\right)^2 - \frac{2}{3}\left[\frac{1}{r}\frac{\partial}{\partial z}(r u_r) + \frac{1}{r}\frac{\partial u_\theta}{\partial \theta} + \frac{\partial u_z}{\partial z}\right]^2 \right\}^{1/2} \tag{3.15}$$

where u_r, u_θ, u_z are the velocity components in the radial, tangential and axial direction, respectively.

For an incompressible fluid the last term in the above expression is zero (because of continuity) and G becomes:

$$G = \left\{ 2\left[\left(\frac{\partial u_r}{\partial r}\right)^2 + \left(\frac{1}{r}\frac{\partial u_\theta}{\partial \theta} + \frac{u_r}{r}\right)^2 + \left(\frac{\partial u_z}{\partial z}\right)^2 \right] + \left(r\frac{\partial}{\partial r}\left(\frac{u_\theta}{r}\right) + \frac{1}{r}\frac{\partial u_r}{\partial \theta}\right)^2 + \left(\frac{\partial u_\theta}{\partial z} + \frac{1}{r}\frac{\partial u_z}{\partial \theta}\right)^2 + \left(\frac{\partial u_z}{\partial r} + \frac{\partial u_r}{\partial z}\right)^2 \right\}^{1/2} \tag{3.16}$$

Although the above equations (Eq. 3.14 and Eq. 3.16) are valid in any flow regime (including the turbulent regime) some modifications of practical importance need be introduced if G must be calculated for turbulent flow.

In general, the shear stress can be expressed as:

$$\tau = \mu \frac{du}{ds} \tag{3.17}$$

If Boussinesq's eddy viscosity (μ_t) concept is introduced to account for turbulent effects it is:

$$\tau = \mu\left(\frac{d\bar{u}}{ds} + \frac{du'}{ds}\right) = \mu\frac{d\bar{u}}{ds} + \mu_t\frac{d\bar{u}}{ds} = \left(\mu + \mu_t\right)\frac{d\bar{u}}{ds} \tag{3.18}$$

i.e. $$\tau = \mu_{eff}\frac{d\bar{u}}{ds} \tag{3.19}$$

where $\mu_{eff} = \mu + \mu_t$

Comparing the above equations (Eq. 3.17 and Eq. 3.19), we have

$$\frac{du}{ds}=\left(\frac{\mu_{eff}}{\mu}\right)\frac{d\bar{u}}{ds} \tag{3.20}$$

This equation relates the instant velocity gradient (including the mean and fluctuating velocity gradient components) to the mean velocity gradient, which could be obtained through simulation.

Substituting the above equation into equations of G definition (Eq. 3.14 and Eq. 3.16), we get (in cartesian coordinates)

$$G=\left(\frac{\mu_{eff}}{\mu}\right)\left\{2\left[\left(\frac{\partial\bar{u}_x}{\partial x}\right)^2+\left(\frac{\partial\bar{u}_y}{\partial y}\right)^2+\left(\frac{\partial\bar{u}_z}{\partial z}\right)^2\right]+\left(\frac{\partial\bar{u}_x}{\partial y}+\frac{\partial\bar{u}_y}{\partial x}\right)^2+\left(\frac{\partial\bar{u}_y}{\partial z}+\frac{\partial\bar{u}_z}{\partial y}\right)^2+\left(\frac{\partial\bar{u}_x}{\partial z}+\frac{\partial\bar{u}_z}{\partial x}\right)^2\right\}^{1/2} \tag{3.21}$$

and in cylindrical coordinates the expression for G becomes

$$G=\left(\frac{\mu_{eff}}{\mu}\right)\left\{2\left[\left(\frac{\partial\bar{u}_r}{\partial r}\right)^2+\left(\frac{1}{r}\frac{\partial\bar{u}_\theta}{\partial\theta}+\frac{\bar{u}_r}{r}\right)^2+\left(\frac{\partial\bar{u}_z}{\partial z}\right)^2\right]+\left(r\frac{\partial}{\partial r}\left(\frac{\bar{u}_\theta}{r}\right)+\frac{1}{r}\frac{\partial\bar{u}_r}{\partial\theta}\right)^2+\left(\frac{\partial\bar{u}_\theta}{\partial z}+\frac{1}{r}\frac{\partial\bar{u}_z}{\partial\theta}\right)^2+\left(\frac{\partial\bar{u}_z}{\partial r}+\frac{\partial\bar{u}_r}{\partial z}\right)^2\right\}^{1/2} \tag{3.22}$$

FLUENT can provide the data of μ_{eff} at any position within the vessel after the simulation is complete. It also predicts the mean velocities for all three components at any position within the vessel. Therefore the mean velocity gradient in all three directions

for any position within the vessel can be calculated. Thus we were able to calculate the local velocity gradient at any position within the agitated vessel.

Another method to determine the local G value is through the usage of local energy dissipation rate, which could also be obtained numerically. The idea is following:

Recalling Eq. 3.13, i.e.

$$\varepsilon = \frac{P}{V} = \left(-\tau : \nabla \mathbf{v}\right) = \mu G^2 \tag{3.23}$$

rearranging it, we have:

$$G = \sqrt{\frac{\varepsilon}{\mu}} \tag{3.24}$$

If the local value of ε throughout the vessel is available, the local G value could be calculated with the above equation. This alternative method is referred to as the ***local energy dissipation method*** in this work.

The above equation looks the same in the form as Eq. 3.3 proposed by Camp and Stein (1960). But it differs in that the G in Eq. 3.24 is the complete definition of local velocity gradient as shown in Eq. 3.14 or Eq. 3.16, while the G in Eq. 3.3 is the incomplete definition of velocity gradient as shown in Eq. 3.1, which did not include the effect of normal stress terms. Furthermore, no information available in the literature about the obtaining the local velocity gradient in mixing or flocculation vessels. Researchers and engineers in this area almost always referred to the Eq. 3.3 at the beginning, but then turned into the average velocity gradient throughout the entire vessel as shown in Eq. 3.4, which leads to very rough estimation of this key parameter in the

mixing and flocculation processes. In this work, for the first time, the local velocity gradients for several mixing/flocculation processes were numerically obtained through the calculation of the local power dissipation rate.

Comparing the two methods mentioned above, one can clearly see that they came from the same fundamental equation and should provide identical G values. The significance of the approach used here to calculate the local velocity gradient is as following. Firstly, it provides the correct equation to calculate the local G value (somewhat imprecisely obtained by Camp and Stein in 1943). Secondly, it provides an alternative method to obtain this local G value, i.e., for the situation provided that the local mean velocities and local turbulent viscosities were known, the first method could be used, and for the situation provided that the local energy dissipation rates were known, the second method could be applied. It broadens the ability and possibility for researchers and engineers to obtain this key parameter in mixing and flocculation process.

3.3 New Parameter for Flocculation Process

Although $G_{ave}\,t$ has often been used as a main parameter in the design of flocculators even less information is available on the time the individual floc particles spend in different zones of the vessel while being exposed to velocity gradients of different intensities. In order to better study the real effect of the actual velocity gradient profiles and the time interval of a moving particle spent in each zone with certain velocity gradient value, we proposed a new parameter called *velocity gradient-time integral*

along the particle trajectory. This new parameter is the combination of these two factors (i.e., local velocity gradient, G, and the time a moving particle spent in that cell, t) with their actual values. To obtain this new parameter for certain flocculation process, firstly, we need to find the distribution of velocity gradient throughout the entire flocculation vessel; secondly, we need to track the trajectory of a normal floc particle moving in this vessel; then finally, we can obtain this new parameter for mixing or flocculation process through numerically integrating the local velocity gradient value by the time a moving floc particle spent in that zone of the vessel.

To quantify the velocity gradient-time integral on flocculation it would be advantageous to be able to measure these quantities directly from experiments and calculate them from first-principle equations. Until relatively recently this would have been an extremely difficult task. However, in recent years two tools have become available to achieve both objectives: Laser-Doppler Velocimetry (LDV) and Computational Fluid Dynamics (CFD). In this work both tools have been applied to study the most important fluid dynamic characteristics of mixing and flocculation vessels.

CHAPTER 4

EXPERIMENTAL APPARATUS AND METHOD

The experimental system comprised a mixing vessel, an agitator assembly, an LDV system, and a data acquisition system. A schematic diagram of the experimental apparatus is shown in Figure 4-1.

4.1 Mixing and Flocculation Systems

Four mixing and flocculation systems (System A, System B and System C1 and C2, shown in Fig. 4-2, Fig. 4-3 and Fig. 4-4, respectively) were studied. The study of System A was a cooperative project between the Department of Chemical Engineering, Chemistry, and Environmental Science, New Jersey Institute of Technology, Newark, NJ, USA and the Czech Technical University, Prague, Czech Republic, while the investigation of System B was a collaborative research project between HSMRC at New Jersey Institute of Technology, Newark, NJ, USA and Questor Centre at Queen's University, Belfast, Northern Ireland, U.K.

The agitated vessel in System A was an unbaffled, cylindrical, flat-bottomed, Plexiglas vessel with a diameter of 0.293 m, provided with a flat lid cover, and completely filled with water as the process fluid (vessel height = liquid height = 0.293 m). This arrangement suppressed the formation of the central free vortex that can be typically observed in unbaffled stirred vessels. The vessel was placed in a square Plexiglas tank filled with water in order to minimize refractive effects at the curved surface of the mixing vessel. The agitation system consisted of a downward-pumping, six-blade, 45° pitched-blade turbine (Fig. 4-5a) with a diameter of 0.098 m (i.e., equal

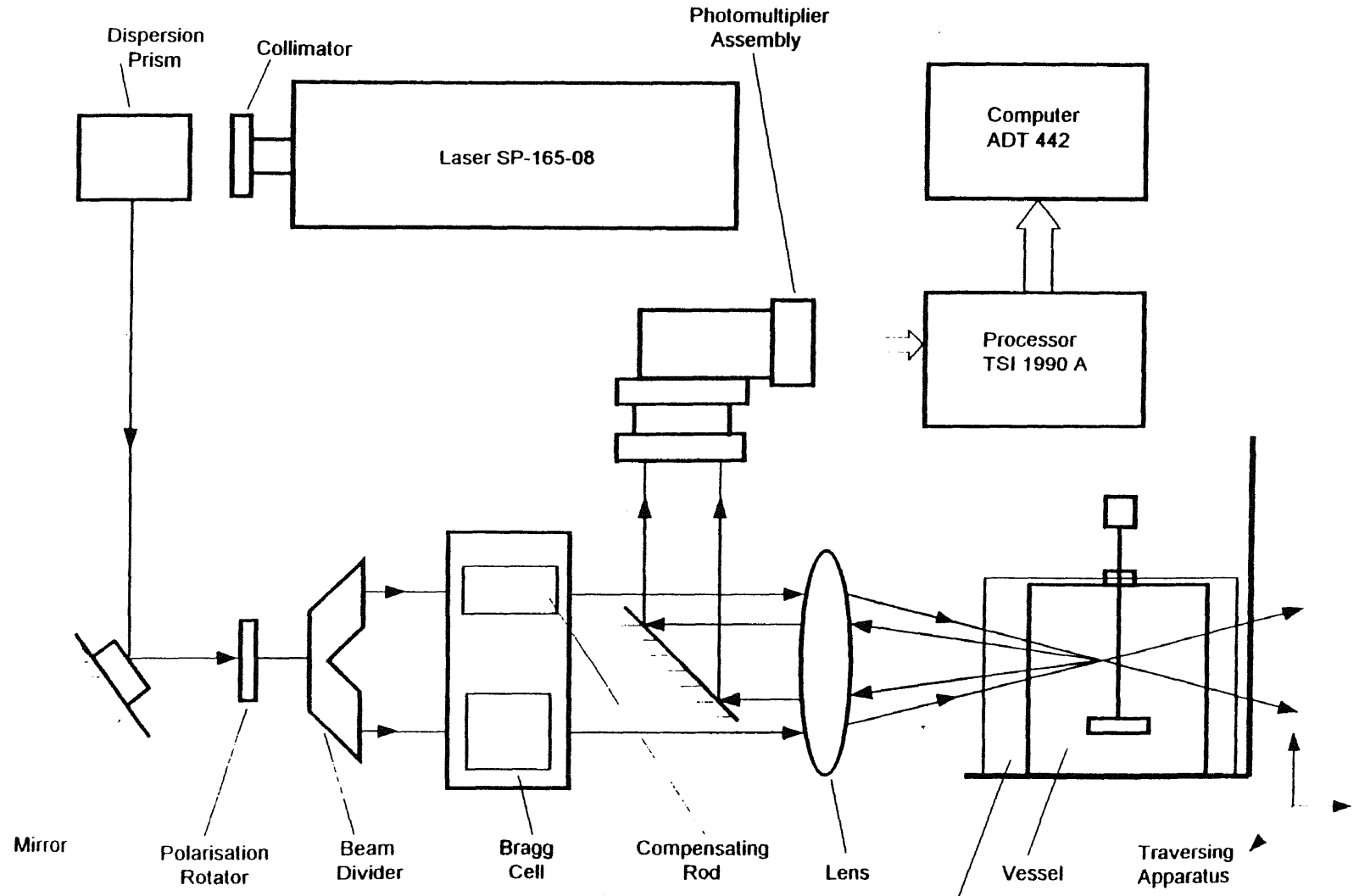

Figure 4-1 Laser-Doppler Velocimetry (LDV) apparatus

to one-third of the vessel diameter), and a projected vertical blade width of 0.013 m (corresponding to an actual blade width of 0.019 m). The impeller was mounted 0.073 m off the tank bottom, as measured from the bottom of the impeller. An electric motor connected to an external controller was used to rotate the impeller at a constant agitation speed of either 7.5 rotations/s (450 rpm) or 11.67 rotations/s (700 rpm), corresponding to impeller Reynolds Numbers of 7.1×10^4 and 11.1×10^4, respectively.

The agitated vessel in System B (presented in Figure 4-3) was a rectangular mixing tank with the identical configurations to an existing flocculation pilot plant run at the Questor Centre at Queen's University, Belfast, Northern Ireland, U.K. The flat-bottomed tank with a square base of 300 mm length and a height of 480 mm was filled with water to a height of 450 mm. Four baffles with width of 10 mm were placed in the center of each face of the tank and covered the whole length of the tank. The agitation system consisted of a radial-pumping, two-blade, paddle type impeller (Fig. 4-5b) with a diameter of 66 mm and a height of 35 mm. The impeller was mounted 130 mm off the tank bottom, as measured from the bottom of the impeller. The impeller rotational speed of 350 rpm (the same rotational speed used in the pilot plant at Queen's University, corresponding to impeller Reynolds Numbers of 2.5×10^4) was studied.

System C1 and C2 (shown in Figure 4-4) had the same configuration of System A except that the vessel had four baffles and did not have a top flat lid cover. The baffle thickness was 6.25 mm, and the baffle width-to-tank diameter ratio was 0.1. The four baffles were equally placed along the inner cylindrical surface (i.e. the angle between any two adjacent baffles was 90 degree) and extended from the top to the bottom of the

vessel. Because of the existence of baffles no top flat lid cover is necessary to prevent vortex normally occurred in unbaffled mixing vessels. The vessel was filled with water up to a height of 0.293 m and was placed in a square tank, also filled with water, to minimize the effect of diffraction on LDV measurements. The agitation system consisted of one downward-pumping, six-blade, 45° pitched-blade turbines mounted on a centrally located shaft (12.5 mm OD). Two different impeller size were used. One impeller (System C1) has a diameter 101.6 mm and a vertically projected blade width of 13.7 mm. Another impeller (System C2) has a diameter 76.2 mm and a vertically projected blade width of 10.2 mm. The impeller was mounted 0.073 m from the tank bottom for both System C1 and C2, so that the ratio of the off-bottom clearance of the impeller to the liquid height was equal to 0.25. The impeller was rotated by the same motor applied in System B at a speed of 159 rpm and 256 rpm, respectively, corresponding to impeller Reynolds Numbers of 2.7×10^4 and 2.4×10^4 for System C1 and C2, respectively. The three-directional traversing apparatus applied in System B was also used here.

4.2 LDV Systems

The LDV apparatus shown in Figure 4-1 was used to experimentally obtain the velocity and turbulence intensity profiles inside the vessel. Two similar LDV systems have been used. One is a 1.5-watt laser (Coherent, Inc.), which has been used for the experimental measurements in System A by our co-investigators at Czech Technical University, Prague, Czech Republic. Another one is a 2-watt laser (Lexel, Inc.), which has been used for the experimental measurements in System B, C1 and C2. Figure 4-1 shows the

general diagram for both LDV systems. The multicolor beam produced by the laser in any of the above two LDV systems passed through the prisms, mirrors, polarization rotator, and beam divider from which only two colored beam (green and blue) emerged. Each of these two beams was split into two parallel beams. The resulting four beams were focused by the beam expander and the final large transmitting lens on a single point 480 mm away from the final lens, i.e., at a distance equal to the focal distance of the final transmitting lens. The focusing point where the beams converge was actually a small control volume (84 μm in diameter) formed by the intersection of the four beams. This point must lie in the fluid contained in the tank under exam to take a velocity measurement.

The water in the mixing vessel was seeded with metal-coated plastic spheres (product of TSI Inc.) capable of scattering light as they traveled through the control volume. These particles, with a density of 1.02 g/cm^3 and mean diameter of 5 μm, follow the trajectories of the fluid elements very closely. When a particle crossed the control volume it scattered the light of the incoming beams. This scattered light produced a light interference pattern that is proportional to the particle velocity. The back-scattering receiving optics collected the scattered light, and the resulting signal was sent to a data acquisition system capable of converting it to two values of the velocity component in two perpendicular directions. The data acquisition system (TSI 1990 A processor) connected to a computer produced on-line measurements of average and fluctuating velocities.

4.3 Experimental Determination of Velocity Distribution

The tridimensional average and fluctuating velocities in the mixing vessel were experimentally obtained at 19 radial distances between the impeller shaft and the vessel wall, and at five different axial levels (Z was equal to 0.053, 0.071, 0.088, 0.160, and 0.233 m, respectively for System A, System C1; Z was equal to 0.080, 0.128, 0.167, 0.235 and 0.315 m, respectively for System B) using a x-y-z traversing apparatus. The tridimensional average and fluctuating velocities at only 7 radial positions in the impeller region at two axial levels (Z was equal to 0.071 and 0.088 m, below and above the impeller, respectively) were experimentally measured for System C2. To obtain all three velocity components, two separate measurements were taken for the same (r,Z) point: one in which the laser axis was oriented perpendicularly to the radius along which the measurement was made (yielding the radial and axial velocity components), and another one in which it was parallel (yielding the tangential and axial velocity components), illustrated by Figure 4-5 (Armenante *et al.*, 1994).

4.4 Power Number

The torque, τ, in System A was experimentally measured with a turntable (Fort *et al.*, 1986), and was used to determine the total power dissipated by the impeller, P, and the power number, N_p, from the equation (Rutherford,1996) :

$$N_p = \frac{2\pi N \tau}{\rho N^3 D^5} = \frac{P}{\rho N^3 D^5} \qquad (4.1)$$

CHAPTER 5

NUMERICAL SIMULATION

A commercial CFD software package (*FLUENT*, Version 2.5 and 4.32; Creare.x, 1990) was used to predict the velocity and turbulent kinetic energy profiles inside the vessels, as well as power dissipation rate and particle trajectories under steady state conditions. Three turbulent models (the k-ε model, algebraic stress model (ASM) and Reynolds stress model (RSM)) were used to account for turbulence effects. Simulations were carried out for all three systems (System A with two agitation speeds 450 and 700 rpm using k-ε model and ASM model; System B with agitation speed of 350 rpm using RSM model; System C1 and C2 with agitation speed of 159 rpm and 256 rpm, respectively, using RSM model).

5.1 Computational Fluid Dynamic Models

CFD programs such as *FLUENT* numerically solve the general equations representing the conservation of mass and momentum. In Cartesian coordinates and at steady state continuity equation can be written as:

$$\nabla \cdot \mathbf{u} = 0 \tag{5.1}$$

and the Momentum conservation equation :

$$\nabla \cdot (\rho \mathbf{u}\mathbf{u}) = \mu \nabla^2 \mathbf{u} - \nabla \bar{p} + \rho \mathbf{g} \tag{5.2}$$

In equation 5.2, the term on left hand side accounts for the convective momentum transport, while the terms on the right hand side represent, respectively, viscous transport, pressure forces, and body forces, such as gravity.

In turbulent flow, the velocity at any point can be taken to be the sum of the mean (time-average) and fluctuating components, i.e.:

$$\mathbf{u} = \overline{\mathbf{u}} + \mathbf{u}' \tag{5.3}$$

Using this equation the continuity equation can be rewritten as:

$$\nabla \cdot \overline{\mathbf{u}} = 0 \tag{5.4}$$

Substitution of equation 5.3 and 5.4 into equation 5.2 yields the ensemble-average momentum equations, which can be used for the prediction of the velocities in turbulent flow:

$$\nabla \cdot \left(\rho \overline{\mathbf{u}}\, \overline{\mathbf{u}}\right) = \mu \nabla^2 \overline{\mathbf{u}} - \nabla \overline{p} + \rho \mathbf{g} - \nabla \cdot \left(\rho \overline{\mathbf{u}'\mathbf{u}'}\right) \tag{5.5}$$

The last term in this equation represents the Reynolds stresses containing the product of the fluctuating velocity components.

Since the Reynolds stresses can not be predicted from first principles they are typically calculated by making some assumptions about their relationship with other variables. A number of different of models are available for this purpose. Software packages using some of these models are also available. One of the most widely used software package is *FLUENT*. *FLUENT* includes three turbulence models which can be used to account for turbulence effects in the simulation. These three models are the k-ε model, the algebraic stress model (ASM) and the Reynolds Stress Model (RSM).

5.1.1 k-ε Model

The k-ε turbulence model is an eddy-viscosity model in which the Reynolds stresses are assumed to be proportional to the mean velocity gradients, with the constant of

proportionality being the turbulent viscosity, μ_t . This assumption, known as the Boussinesq hypothesis, provides the following expression for the Reynolds stresses (Hinze, 1975; Creare.x, Inc., 1991):

$$\overline{u_i' u_j'} = \frac{2}{3}\delta_{ij} k - \frac{\mu_t}{\rho}\left(\frac{\partial \overline{u_i}}{\partial x_j} + \frac{\partial \overline{u_j}}{\partial x_i}\right) \tag{5.6}$$

where δ_{ij} is the Kronecker delta and k is the turbulent kinetic energy defined as:

$$k = \frac{1}{2}(\mathbf{u}' \cdot \mathbf{u}') = \frac{1}{2}\left(\overline{u_x'^2} + \overline{u_y'^2} + \overline{u_z'^2}\right) \tag{5.7}$$

The values of the specific turbulence kinetic energy, k, and the turbulence energy dissipation rate, ε, were obtained from their balance equations:

$$\mathbf{u} \cdot \nabla k = \nabla\left[\left(\frac{\mu_t}{\rho \sigma_k}\right)\nabla k\right] + \frac{G_k}{\rho} - \varepsilon \tag{5.8}$$

$$\mathbf{u} \cdot \nabla \varepsilon = \nabla\left[\left(\frac{\mu_t}{\rho \sigma_\varepsilon}\right)\nabla \varepsilon\right] + C_1 \frac{\varepsilon}{k}\frac{G_k}{\rho} - C_2 \frac{\varepsilon^2}{k} \tag{5.9}$$

where G_k is the generation of k and is given by:

$$G_k = -\rho \overline{\mathbf{u}'\mathbf{u}'} : (\nabla \mathbf{u}) = \mu_t \left(\frac{\partial \overline{u_j}}{\partial x_i} + \frac{\partial \overline{u_i}}{\partial x_j}\right)\frac{\partial \overline{u_j}}{\partial x_i} \tag{5.10}$$

The effective or "turbulent" viscosity, μ_t , is calculated at each point in the flow through the equation (Rodi, 1984, Creare.x, Inc., 1991):

$$\mu_t = \rho C_\mu \frac{k^2}{\varepsilon} \tag{5.11}$$

The values of the constants C_1, C_2, C_μ , σ_k and σ_ε are taken to be equal to 1.44, 1.92, 0.09, 1.0, and 1.3, respectively (Rodi, 1984).

5.1.2 Algebraic Stress Model (ASM)

In complex flows, μ_t may be strongly directional. When this is the case, the isotropic k-ε model may be inadequate. For such flows, we can use Algebraic Stress Model (ASM) or Reynolds Stress Model (RSM). The ASM solves algebraic approximations of the differential transport equations for the Reynolds stresses as (Rodi, 1984; Fluent. Inc., 1995):

$$\overline{u_i' u_j'} = \frac{2}{3}\delta_{ij} k + \frac{C_D}{\frac{Q}{\varepsilon} - 1 + C_3}\frac{k}{\varepsilon}\left(Q_{ij} - \frac{2}{3}Q\delta_{ij}\right) \tag{5.12}$$

where (Creare.x, 1991; Launder and Spalding, 1972):

$$Q = \frac{1}{2}Q_{ii} \tag{5.13}$$

and

$$Q_{ij} = -\overline{u_i' u_\ell'}\frac{\partial \overline{u_j}}{\partial x_\ell} - \overline{u_j' u_\ell'}\frac{\partial \overline{u_i}}{\partial x_\ell} \tag{5.14}$$

The values of the constants C_3, C_D are taken to be 0.55, 0.45 respectively (Rodi, 1984).

5.1.3 Reynolds Stress Model (RSM)

RSM involves solving the individual stresses $\overline{u_i' u_j'}$ in differential transport equations. The following equations are used (Launder, et al., 1975; Launder, 1989; Fluent. Inc., 1995):

$$\overline{u}_k \frac{\partial \overline{u_i' u_j'}}{\partial x_k} = \frac{\partial}{\partial x_k}\left(\frac{\nu_t}{\sigma_k}\frac{\partial \overline{u_i' u_j'}}{\partial x_k}\right) + P_{ij} + \Phi_{ij} - \varepsilon_{ij} + R_{ij} \tag{5.15}$$

where the term on the left hand side is the convective momentum transport. The first term on the right hand side is the diffusive transport, P_{ij} is the stress production rate, Φ_{ij} correlates the pressure/strain, ε_{ij} is the viscous dissipation and R_{ij} is the rotational term, ν_t is the turbulent kinematic viscosity.

5.2 Boundary Conditions

The boundary conditions imposed on the systems are as follows. The boundary conditions at the horizontal top for System A and the vessel wall, baffles, horizontal bottom for all systems were those derived assuming no-slip condition. This implied that the shear stress near the solid surfaces is specified using wall functions and that equilibrium between the generation and dissipation of turbulence energy is assumed (Launder and Spalding, 1974; Ranade *et al.*, 1989). The boundary conditions at the top (free surface) for System B, C1 and C2 are of the zero-gradient, zero-flux type, which is equivalent to a frictionless impenetrable wall. The common symmetry boundary conditions are assumed at the symmetry axis for all systems (Ranade *et al.*, 1989).

The boundary conditions in the impeller region are imposed at two surfaces of the cylinder having the same size of the volume swept by the impeller. The boundary time-averaged velocities in all three directions are directly obtained from LDV data. The turbulent kinetic energies at the same locations are determined from the experimental fluctuating velocities using equation 5.7, whereas ε is calculated from:

$$\varepsilon = \alpha \frac{k^{1.5}}{w} \tag{5.16}$$

where w is the projected blade width (along the vertical axis), and α was taken to be equal to 1.4 (Wu and Patterson, 1989; Armenante *et al.*, 1994). The values of the average velocities, k and ε so obtained were directly used in the simulations as impeller boundary conditions.

For the System A, the average and fluctuating velocities were experimentally determined via LDV at 9 radial locations 2 mm below and 2 mm above the impeller surface (corresponding to Z values equal to 0.071 and 0.088 m, respectively) by our co-investigators Ivan Fort (Faculty of Mechanical Engineering, Czech Technical University, Prague, Czech Republic) and Jaroslav Medek (Faculty of Mechanical Engineering, Technical University, Brno, Czech Republic). For System B, the average and fluctuating velocities were experimentally determined via LDV at 7 radial locations 2 mm below and 2 mm above the impeller surface (corresponding to Z values equal to 0.128 and 0.167 m, respectively) in the Mixing Lab at New Jersey Institute of Technology. For System C1 and C2, 9 points and 7 points, respectively, were experimentally measured at the same two levels as in System A.

5.3 Grid Generation

FLUENT provides a x-window interface for grid generation. According to the research purpose and results requirements, different grid and domain for certain type of mixing systems could be used. For the System A, a repeating 60° domain was selected, and a non-uniform grid composed of 30 radial nodes, 40 axial nodes, and 17 tangential nodes was imposed on this domain. The grid was chosen to be finer (smaller volume of

computational cell) in the region near the impeller. For System B, the entire mixing vessel (360° domain) was chosen, because of the asymmetry characteristic of the flow in the vessel. Cartesian coordinates were used for System B. A non-uniform grid with about 49,000 computational cells was generated for the simulation. For System C1 and C2, a repeating 90° domain was selected because of the cyclic characteristic of flow in the vessel and the presence of four baffles. A non-uniform grid with finer grid (smaller volume of computational cell) near the impeller region was generated. About 40,000 computational cells were applied for this domain during the CFD simulation.

5.4 Power Consumption and Pumping Capacity

The overall power consumption (P) was calculated for System A by numerically integrating the local power consumption (obtained as the product of the numerically determined local ε value and the fluid mass of each cell) over the entire vessel, as:

$$P = \int_m \varepsilon \, dm \cong \sum_{cell\ i} \varepsilon_{cell\ i} \, m_{cell\ i} \tag{5.17}$$

The pumping capacity, Q_c, was obtained by numerical integration of the numerically obtained velocities in the impeller region (Armenante and Chou, 1996), as follows:

$$Q_c = 2\pi \int_0^{D/2} u_z(r)\big|_{Z=Z_b} r\,dr + \pi D \int_{Z_b}^{Z^+} u_r(Z)\big|_{r=\frac{D}{2}} dZ \tag{5.18}$$

The dimensionless flow number, Fl, is defined as the pumping capacity through the impeller zone, Q_c, normalized by ND^3 and then be calculated from:

$$Fl \equiv \frac{Q_c}{N D^3} \tag{5.19}$$

5.5 Local *G* Value Calculation

After the CFD simulation is complete, *FLUENT* can produce the mean velocity components at all three directions, the effective viscosity and the energy dissipation rate in any location throughout the agitated vessel. Using these data we were able to calculate the local G value distribution within the vessel with the rigorous methods described in chapter 3 (the complete definition of local velocity gradient method and the local energy dissipation rate method).

The general procedure to calculate the local G value is as follows. For the complete definition of local velocity gradient method, we downloaded the data output file from *FLUENT* containing the local mean velocity components in all three directions, i.e. the u_t (tangential), u_r (radial) and u_a (axial) velocities for cylindrical coordinates or the u_x, u_y, u_z velocities for cartesian coordinates, as well as the effective viscosity at any position within the vessel. The above data were imported into MS Excel spreadsheets. A macro program (Appendix B) was written using Visual Basic language in order to compute all the differential terms in Eq. 3.21 (for cartesian coordinates) or Eq. 3.22 (for cylindrical coordinates). The derivatives were calculated as the ratios of the differences of the velocities between two adjacent cells to the distances between the same cells. By summing the squared derivative terms according to Eq. 3.21 or Eq. 3.22, and multiplying by the coefficient in these equations (the ratio of effective viscosity to the dynamic viscosity), the local G value at any position was numerically obtained.

For the calculation of the local energy dissipation rate method, we downloaded the data output file from *FLUENT* with the information of local energy dissipation rate

at any position within the vessel. Then the above data file was imported into MS Excel spreadsheets, where the local G value at any position within the vessel was calculated by a macro program (Appendix C) based on the Eq. 3.24. Therefore the local G value distribution was numerically determined.

5.6 Particle Trajectory

FLUENT can determine the trajectory of a dispersed phase particle by integrating the force balance on the particle in a Lagrangian reference frame. This force balance equates the particle inertia with the forces acting on the particle, and can be written (for the x-direction in Cartesian coordinates) as:

$$\frac{du_p}{dt} = F_D + g_x\left(\rho_p - \rho\right)/\rho + F_x \tag{5.20}$$

where $g_x(\rho_p - \rho)/\rho$ is the body force; F_D is the drag force per unit particle mass and:

$$F_D = \frac{18\mu}{\rho_p D_p^2}\frac{C_D\, Re}{24} \tag{5.21}$$

Here, u is the fluid phase velocity, u_p is the particle velocity, μ is the molecular viscosity of the fluid, ρ is the fluid density, ρ_p is the density of the particle, and D_p is the particle diameter. Re stands for the relative Reynolds number, which is defined as:

$$Re = \frac{\rho D_p \left|u_p - u\right|}{\mu} \tag{5.22}$$

The drag coefficient, C_D, is a function of the relative Reynolds number of the following general form:

$$C_D = a_1 + a_2/Re + a_3/Re^2 \tag{5.23}$$

where the a's are constants that apply over several ranges of Re given by Morsi and Alexander (1972).

In equation 5.20, the term F_x represents some additional forces that can be important under special circumstance. The first of these is the "virtual mass" force, the force required to accelerate the fluid surrounding the particle. This force can be written as:

$$F_x = \frac{1}{2}\frac{\rho}{\rho_p}\frac{d}{dt}\left(u - u_p\right) \tag{5.24}$$

and is important when $\rho > \rho_p$.

Another additional force may arise due to the pressure gradient in the fluid:

$$F_x = \left(\frac{\rho}{\rho_p}\right) u \frac{\partial u}{\partial x} \tag{5.25}$$

These forces are optional when using *FLUENT*.

The trajectory equation can be numerically integrated by *FLUENT* to produce the velocity of the particle at each point along the trajectory, where the trajectory itself is obtained through the following equation:

$$u_{pj} = \frac{dx_j}{dt} \tag{5.26}$$

i.e.

$$x_j = \int u_{pj}\, dt \tag{5.27}$$

Therefore, the position of a moving particle at any time can be tracked by simulation method. During the simulation, the density and diameter of the moving particle were chosen to be 1.0 g/cm^3 and 100 μm, repectively.

5.7 Local *G* Value Distribution Along a Particle Trajectory

After certain number of iterations (depending on the total number of computational cells and boundary conditions), *FLUENT* output the converged results including the local mean velocities in three directional components, turbulent kinetic energy, turbulent viscosity and energy dissipation rate at each cell within the entire vessel. By downloading the output file composed of mean velocities of three components and local turbulent dissipation rate from *FLUENT*, importing it into Excel spreadsheet and using Eq. 3.16 or 3.17 for the complete definition of local velocity gradient method (by computing the derivative between two adjacent positions for each term on the right hand side of above equation) or Eq. 3.20 for local energy dissipation rate method, the distribution of local velocity gradient (*G* value) was obtained throughout the entire vessel. Two macro programs, listed in Appendix B and C, were developed to calculate the local velocity gradient through both methods. These macros were written by using Visual Basic language in Microsoft Excel 5.0. When particle trajectory simulation was complete, *FLUENT* produced the trajectory of a dispersed particle with the output of its location (its corresponding x, y, z or radial, tangential, axial values, in cartesian or cylindrical coordinates, respectively), its velocity components in three directions at that position and its corresponding time. The output file from *FLUENT* was downloaded and

then imported into Excel spreadsheet together with the above obtained local G value distribution data. The macro program (attached in Appendix C) can also calculate the corresponding G value at different times (corresponding to different particle positions). Thus the G value distribution along the particle trajectory could be obtained.

5.8 Velocity Gradient-Time Integral

Knowing the particle trajectory, the velocity of particle at each point and the G value distribution along the particle trajectory, it was then possible to calculate the new parameter - the *velocity gradient-time integral* along the particle trajectory - from the following equation:

$$\text{velocity gradient-time integral} = \int_{t_0}^{t} G(x,y,z)dt = \int_{0}^{s} \frac{G(s)}{u_p(s)}ds \qquad (5.28)$$

where the variable s is the linear coordinate along the trajectory and $u_p(s)$ is the particle velocity along the trajectory. A macro program was written to calculate the time interval the moving particle spent at different G value zone and the value for the new parameter velocity gradient-time integral (Appendix C).

CHAPTER 6

RESULTS AND DISCUSSION

6.1 System A

For the unbaffled cylindrical mixing system with both agitation speeds of 450 rpm and 700 rpm, LDV was used to measure both the average and fluctuating velocities in all three directions at 5 different axial levels by our co-investigators at the Czech Technical University, Prague, Czech Republic. Then these experimentally obtained data (via LDV) near the impeller region were used as the boundary conditions when the CFD program *FLUENT* was used to numerically simulate the flow pattern in this mixing vessel. Two turbulence models (k-ε and ASM) were used in the simulation to account for the turbulence effect. The results of both LDV measurements and CFD predictions are presented in the following sections.

6.1.1 LDV Measurements in the Impeller Region

It has been a common procedure to present the standardized local values of mean and fluctuating velocities by relating their original values to the impeller tip speed (πDN). The velocities in these figures, as well as in all other velocities profiles in this work, are presented in a dimensionless form by dividing the actual value by the impeller tip velocity. The turbulent kinetic energy is also presented in a dimensionless form by dividing the actual value by the square of impeller tip velocity.

Figures 6-1a and 6-1b show the velocities in the impeller region obtained via LDV. The tangential velocity profiles show a maximum near the tip of the impeller. This pattern is consistent with that reported for a system similar to that under study

(Armenante *et al.*, 1994) as well as for an unbaffled tank without a lid using a flat-blade paddle (Nagata, 1975), or an eight-blade, flat-blade turbine (Dong *et al.*, 1994a and 1994b). The axial velocities above and below the impeller are all negative, as one would expect for a downward pumping impeller. However, the velocities above the impeller are quite low and uniform, whereas those below the impeller show a strong downward pumping action near the outer edge of the impeller. The radial velocities point slightly inward above the impeller but strongly outward on the lower side of the impeller.

The turbulent kinetic energy profiles for the impeller region are given in Figure 6-1c. k is greatest on the lower side of the impeller near the tip, where the radial velocity is also the greatest. An overall lower distribution of k can be observed on the upper side of the impeller where the average velocities are more uniform.

The values for the velocity components (radial, tangential and axial) and for k shown in the above figures were used as boundary conditions for the numerical simulation resulting in the velocity profiles inside the vessel.

A repeating 60° domain was selected for the CFD simulation, and a non-uniform grid composed of 30 radial nodes, 40 axial nodes, and 17 tangential nodes was imposed on this domain. The grid was chosen to be finer in the region near the impeller to obtain better simulation results. Figure 6-2 and 6-3 show the grid in 2D and 3D view, respectively.

6.1.2 Comparison between LDV Measurements and CFD Predictions

A comparison between the experimental tangential velocities and the results of the CFD simulations is given in Figure 6-4. The results of the simulation based on the ASM model were, in general, superior to those based on the k-ε model. The agreement between the experimental data and the ASM simulation velocities was very good in the planes next to, or lower than, the impeller. Good agreement can be observed also for the velocities on the other two planes above the impeller, but only for radial distances greater than the impeller radius. For $r < D/2$ the agreement in these regions was qualitatively but not quantitatively acceptable.

Figure 6-5 shows that a very good agreement between the numerical and experimental results was also obtained for the axial velocity. Near the vessel bottom the simulation typically overpredicted the experimentally determined velocities. However, it should be remarked that the reproducibility of the LDV velocity results in the region below the impeller was not as good as in the rest of the vessel, most likely because of the lower values of the velocities and the instabilities of the secondary flow pattern (radially inward and axially upward) typically observed just below pitched blade turbines.

The corresponding velocity data in the radial direction are given in Figure 6-6. While the experimental velocities above the impeller are predicted satisfactorily those below the impeller are only qualitatively described by the results of the simulations. Discrepancies exist especially near the center of the vessel, although the curves produced by the simulations show a trend similar to that of the experimental data.

The ultimate test of the appropriateness of the turbulence models used in the simulation is in the agreement between the experimental and predicted turbulent kinetic energy data. This comparison, shown in Figure 6-7, indicates that ASM is clearly superior to the k-ε model. The experimental k values above the impeller are closely matched by the results of the ASM simulation, whereas those based on the k-ε model are significantly off the mark. Significant qualitative agreement exists also for the results below the impeller, but only when the results of the ASM simulation are compared to the experimental data. The inability of results from the simulation with the k-ε model to match the experimental data can be attributed to the local isotropic assumption made in the derivation of this model.

The overall circulation pattern generated by the simulation is captured in Figures 6-8a (in three dimensions) and 6-8b (in a two-dimensional plane through the shaft). The flow pattern in the r-Z plane is dominated by the main flow generated by the impeller, initially strongly directed outward in the radial direction, and to a lesser extent, downward. This flow rapidly becomes horizontal (for $r > T/4$) although the impeller used here is not of the radial type.

Two main recirculation flows, one above and the other below the impeller, can be clearly identified in Figure 6-8b. In general, the magnitudes of the velocity vectors in the r-Z plane outside the impeller stream are small in comparison to those outside this zone, generating large regions in which axial and radial recirculation is limited (such as the upper region for $r > T/4$). In the region just above the impeller the flow in the r-Z plane is mainly directed straight downward, feeding the impeller. In the cylindrical region

immediately adjacent to the shaft the numerically predicted velocity vectors are very small. This is likely to be an artifact of the computer simulation produced by the absence of boundary condition data in the impeller region for $r < 0.075 \cdot T$. The region just below the impeller is nearly completely cut off from the main lower circulation flow. Figure 6-8b shows that the velocity vectors are quite small in both the radial and axial directions.

It is interesting to compare the flow simulation produced here with that reported for the same type of turbine in a baffled system (Armenante and Chou, 1996, their Figure 8). In the baffled system the main flow generated by the impeller had a very strong downward component, resulting in this flow impinging on the bottom of the vessel and then moving upward near the tank wall. In that system the pitched-blade turbine performed as an effective axial impeller (except for the region just below the impeller in which flow reversal can be noticed). A single large recirculation flow in the axial direction was present, which can be expected to provide good top-to-bottom mixing. By contrast in the unbaffled system examined here top-to-bottom recirculation appears to be modest, and the pitched-blade impeller loses most of the axial impeller characteristics that it typically exhibits in baffled systems.

A comparison among Figures 6-4, 6-5, and 6-6 reveals that the tangential velocities in the unbaffled tank are several times greater in magnitude than the corresponding axial and radial velocities. This is not the case for the baffled case for which the velocity vectors have comparable magnitude independently of the direction (Armenante and Chou, 1996). Figure 6-4 also shows that the magnitude of the

tangential velocities is nearly independent of the axial position, indicating the presence of a very strong swirling flow not observed in the baffled system.

In Table 6-1 the power numbers and the flow number for the system are reported. For the 450 rpm case, the power number prediction based on ASM (0.304) could only account for 65.7% of the experimentally obtained power number, whereas that based on the k-ε model (0.482) was very close to the experimental value. The flow number could only be obtained numerically since the velocities at the vertical side of the volume swept by the impeller were not measured. The value so obtained (0.391) compares favorably with the value (0.31) experimentally obtained by Nagata and coworkers (as reported by Gray, 1966) for the case of an 8-blade flat-blade turbine having the same blade-to-diameter ratio as that of the impeller used in this work.

6.1.3 Comparison between Different Agitation Speeds

Experimental results and simulations for the velocity distributions were obtained for the case in which the agitation speed was increased to 700 rpm. The results are reported in Figures 6-9 (boundary conditions in the impeller region), 6-10, 6-11, 6-12 (dimensionless velocity components in three directions), and 6-13 (dimensionless turbulent kinetic energy). The striking feature of all these figures is that they are all nearly superimposable to the corresponding figures obtained at 450 rpm, indicating that the impeller speed plays a minor role in the direction and magnitude of the dimensionless velocities and turbulent kinetic energies at any point (including the region near the impeller). Similar conclusions were reached by Dong *et al.* (1994a) for an

Table 6-1. Power numbers and flow numbers for System A

Agitation Speed (rpm)	Experimentally Determined Power Number	Numerically Determined Power Number (Turbulence Model: ASM)	Numerically Determined Power Number (Turbulence Model: k-ε)	Numerically Determined Flow Number (Turbulence Model: ASM)
450	0.463	0.304	0.482	0.386
700	0.463	0.321	0.447	0.391

open unbaffled system provided with a flat-blade impeller. These results indicate that the potential exists for simple scale-up rules for the velocity distribution and the turbulence intensity in unbaffled tanks. As for the power number and the flow number Table 6-1 shows that both non-dimensional numbers had values very similar to those obtained at 450 rpm.

Although no experiments were conducted here at different scales it is conceivable that non-dimensional velocity and k value profiles nearly identical to those found here would be obtained in a geometrically similar system of a different scale (since the presence of a lid would eliminate any vortex and the scale up problems associated with it). Identical dimensionless conditions in the impeller region are equivalent to identical boundary conditions, and hence identical simulation results. Given the good agreement between the experimental data and the simulation results obtained here with ASM it follows that the flow in the full-scale vessel is likely to be correctly simulated by the figures reported in this work.

6.2 System B

For the baffled rectangular mixing/flocculation system with agitation speed of 350 rpm, tri-dimensional average and fluctuating velocities at 5 different axial levels were experimentally measured via LDV in the Mixing Laboratory at the Department of Chemical Engineering, Chemistry, and Environmental Science, New Jersey Institute of Technology. Then these experimentally obtained data near the impeller region were used as the boundary conditions when the CFD program *FLUENT* was used to produce a

numerical estimate of the velocity distribution, turbulence kinetic energy, the energy dissipation rate, local velocity gradient distribution and particle trajectory in this mixing/flocculation vessel. One turbulence models (RSM) was used in the simulation.

During the CFD simulation process, Cartesian coordinates were used, where the velocities in the three directions were expressed as x, y, z direction velocities. In order to give more intuitive expression of these data (relating them to the tip velocity of the impeller) and make them consistent with the previous results for System A, these data (in Cartesian coordinates) were then transformed into cylindrical coordinate data, where the three directional velocities were expressed as axial, radial and tangential velocities respectively, as shown in the following sections.

6.2.1 LDV Measurements in the Impeller Region

The velocities in the tangential, axial, and radial directions were experimentally determined via LDV for the top and bottom layers (at the vertical plane along the shaft center and the baffle) of the cylindrical region swept by the impeller. These experimentally determined velocities are reported in Figures 6-14a and 6-14b. Each point in these figures represents the average of three measurements. The results of these figures indicate that the flow in the impeller region had a strong radial component across the entire top and bottom surface of the impeller region, and that this velocity had a numerical value approximately in the range 0.16-0.38 of the impeller tip speed (πDN). The radial velocity increased as the distance between the measuring point and the central line of the shaft became larger, and reached its highest value of about 0.38 of the

impeller tip speed at radial position of about (2 *r/D*) = 1.25 at both levels of above and below the impeller.

The axial velocities above the impeller were all negative, indicating downward moving flow near the center above the impeller. The axial velocities below the impeller were all positive, indicating an upward moving flow near the center below the impeller. The absolute value of axial velocity increased as the measuring point moved closer to the centerline of the shaft. This is true for both axial levels above and below the impeller.

The tangential velocities just above the impeller were found to be very close to those just below the impeller. The tangential velocities at both axial levels were positive indicating a outward pumping of the fluid, as one could expected for a paddle type impeller. The values of tangential velocities were very low near the centerline of the shaft, but increased quickly as the measuring points approached the impeller tip.

The fluctuating velocities in all three directions were experimentally determined for the same surfaces in the impeller region and were used to calculate the local turbulence kinetic energy, *k*. The intensity of the turbulent kinetic energy in the same impeller region is shown in Figure 6-14c. A peak of turbulent kinetic energy was found at about (2 *r/D*) = 1.15 for both axial levels. A similar peak were found by other investigators (Ranade and Joshi, 1989; Kresta and Wood, 1993) for other mixing systems. The value of the turbulent kinetic energy at the axial level above the impeller was slightly higher than that of its corresponding position at the axial level below the impeller.

The values for the velocity components (radial, tangential and axial) and for *k* shown in the above figures were used as boundary conditions when *FLUENT* was used

to predict the velocity and velocity gradient distribution as well as the trajectory of a particle moving in this vessel.

When generating the grid, the entire mixing vessel (360° domain) was chosen, because of the asymmetry characteristic of the flow in the vessel. A non-uniform grid with 49,000 computational cells was generated for the simulation, shown in Figure 6-15(2*D* view) and Figure 6-16 (3*D* view).

6.2.2 Comparison between LDV Measurements and CFD Predictions

The results of the numerical simulation, as well as the values of the three experimentally determined velocity components in the bulk of the fluid obtained at five vertical levels (at the vertical plane along the shaft and the baffle) are presented in Figures 6-17, 6-18, and 6-19. Figure 6-17 shows a comparison between the experimental data for the tangential velocities at different positions inside the vessel and the corresponding values obtained from the numerical simulation by using *FLUENT* RSM model. One can see that the agreement is quite good for all the cases examined here (i.e., all the different *Z/H* values). A peak of the tangential velocity was found near the impeller tip for both axial levels above and below impeller, with the value of 0.28 impeller tip velocity. The tangential velocities were found to be higher near the impeller and its adjacent region than the other regions within the vessel. The much lower values of the tangential velocities at the bottom level (Z=80 mm) and top level (Z=315 mm) indicate that almost no swirl flow exists at both the top and bottom of the vessel.

A comparison between experimental and simulation results is also provided for the axial velocity component for the same *Z/H* values (Figure 6-18). Significant agreement was obtained for all levels. This figure shows that below the impeller near the vessel wall, the axial velocity is directed downwards and near the vessel center, the axial velocity is directed upwards, indicating a main recirculation exist below the impeller. It also shows that above the impeller near the vessel wall, the axial velocity is directed upwards and near the shaft center, the axial velocity is directed downwards, indicating another main recirculation exist above the impeller.

A very good agreement between the experimentally determined radial velocities and the values obtained through *FLUENT* simulation at the same 5 *Z/H* levels is shown in Figure 6-19. Positive peak values were observed for the axial levels just above and below the impeller. The highest radial velocity with the value of about 0.4 impeller tip velocity was found at about (2 *r/T*) = 0.28 on both levels of above and below the impeller. The negative values of radial velocity at the other three axial levels indicating an inwards moving flow both near the bottom and top of the vessel.

Figure 6-20 presents a comparison between the experimental dimensionless turbulent kinetic energies and the corresponding values produced using *FLUENT*. It is seen that the predictions fit the experimental measurements quite well. The values of turbulent kinetic energies near the impellers are much higher than those at the rest of the vessel. A peak was found near the impeller tip.

Figure 6-21 shows a bidimensional cross-sectional view of the velocity profiles on a plane passing through the impeller shaft obtained via simulation. A tridimensional

view of the same velocities is also depicted in Figure 6-22. Two large recirculation patterns both above and below the impeller were found. Fluid were first ejected by the impeller and moved outward. Before they reached the wall, part of them changed their direction to upward and moved up the vessel till certain height, then moved inward to the center of the vessel and finally fell down to the impeller region and be ejected again by the impeller for another cycle; part of the ejected fluid changed their direction to downward and moved down near the wall, then moved inward to the center of the vessel before hitting the bottom of the vessel and finally moved upward reaching the impeller again and thus formed another recirculation flow below the impeller. A similar flow pattern produced by a paddle type impeller was reported by Bertrand (1994).

Top views of the flow pattern in this system were captured in Figure 6-23, 6-24 and 6-25 for different axial levels of *Z/H* equal to 0.18, 0.37 and 0.70, respectively. At *Z/H* equal to 0.18, a small swirling zone at the center of the vessel was observed with fluid moving upward towards the impeller. The flow pattern at *Z/H* equal to 0.70 shows a similar swirling zone at the center of the vessel, with the difference of downward movement of the liquid. Figure 6-24 shows that fluids were almost uniformly ejected outward by the impeller. A repeated flow pattern at each 90° domain of the vessel can be easily seen.

6.2.3 Velocity Gradient Distribution

Figure 6-26 shows the velocity gradient distribution in the *r-Z* plane at the center of the rectangular vessel. The values of the local velocity gradients shown in this figure were

obtained through the method of complete definition of local velocity gradient. The labels of the contour curves in this figure are the G values in the form of $\log_{10}G$. It is clear that significant variations in the local velocity gradient exist in the vessel. The velocity gradient values near the vessel wall were very low, only around 10 s^{-1}. They increase as the interested position moves close to the impeller. The closer the position to the impeller, the higher the G value. The highest values were found just near the impeller. It is obvious that the velocity gradient distribution within a agitated vessel is far from uniform.

Figure 6-27 maps the local velocity gradient distribution, obtained through the local energy dissipation rate, in the r-Z plane at the center of the rectangular vessel in the same agitated vessel as in Figure 6-26. Comparing Figure 6-26 and Figure 6-27, one will find that the values obtained by these two different methods at corresponding position within the vessel were of the same magnitude. The relatively small value differences existed here were brought from the numerical calculation process, as one could expect. In general, they provide the same information about the distribution of local velocity gradient in the turbulent mixing/flocculation process. This convinced us of the validity of the second method (by local energy dissipation rate), derived from a modified Camp and Stein (1943) approach to G determination.

Similarly to what it was found in this work, Geisler and Forschner (1996) found that "Maximum values of ε are always in the discharge region of the impeller" when they studied the local turbulent shear stress for different mixing tanks. Stanley and Smith (1995) also found that "the local dissipation rate in the impeller zone is 4-6 times higher

than the vessel average dissipation rate" when the turbulent flow was studied in a standard jar test. All these information convinced us that using the average G value, obtained by the conventional method throughout the entire vessel, as a key parameter for flocculation process modeling is inadequate.

6.2.4 Particle Trajectory

The trajectory of a virtual particle with physical properties similar to that of a floc particle moving in a typical flocculation process was numerical predicted by using *FLUENT*. This particle was assumed to be initially put in a position 75 mm away from the shaft center along the diagonal line on the top surface of the rectangular tank, where the coagulant is usually added to the solution being treated in flocculation process. Figure 6-28 and 6-29 show the particle trajectory at time equal to 2000 and 10000 seconds, respectively. The particle tended to visit some zones of the vessel more often than other zones. It never visited certain kind of zone such as the upper corners of the vessel. It is clear that the time intervals spent by the particle at different positions of the flocculation vessel were quite different by looking at the particle trajectory intensities in these figures. Such a non-uniform movement of the particle within the vessel was also found by Bakker *et al* (1996) when the effects of flow pattern on the solids distribution in a stirred tank was investigated.

In order to better understand and model the flocculation process, it would be advantageous to find the time a moving particle spend in different zone of the vessel with different intensity of velocity gradient. Therefore, we proposed a new parameter, the

velocity gradient-time integral, which accounts for both the local velocity gradient distribution and the time a particle spend in each of those zones with certain G value.

6.2.5 Velocity Gradient-Time Integral along the Particle Trajectory

By knowing the local velocity gradient distribution within the entire mixing/flocculation vessel and the trajectory of a particle moving in this vessel, we were able to calculate the proposed new parameter, the velocity gradient-time integral along the particle trajectory.

Using the macro program attached in appendix C, the local G value at each point the particle went through during the flocculation process was obtained. The result is shown in Figure 6-30, where the x coordinate represents the time a moving particle spent in the vessel and the y coordinate represents the local G value the moving particle experienced. It is clear that the G value experienced by the particle as it moves through the vessel is extremely non-uniform. Very high peaks were calculated (when the particle moved through the impeller region), followed by long periods during which the G values were extremely low. The dotted line shown in Figure 6-30 is the average G value obtained through the conventional method for the entire flocculation vessel. Obviously, the use of average G value throughout the entire vessel by the conventional method is a very crude estimation of the actual flocculation characteristics.

Besides the distribution of the local velocity gradient in flocculation vessel it is of great interest to pay attention to the maximum values of the local velocity gradient the particle experienced. In this flocculation system the maximum value of the local velocity gradient the particle experienced is about 920 s^{-1}, as shown in Figure 6-30. If the

maximum value of the local velocity gradient that the particle experienced is higher than the value at which a floc breakup occurs, then certain adjustment need taken to reduce this maximum local G value. Otherwise it will lead to the floc breakup and, as a consequence, to a reduction of the process efficiency, although the time the particle spent in these zones with maximum local G value is much less than the time the particle spent in other zones. Stanley and Smith (1995) also pointed out that: "As the circulation time in a small vessel, such as a jar test apparatus, is in the order of seconds and normal flocculation time is in the order of 5-30 minutes, many of the floc characteristics (especially floc size) are probably governed by hydrodynamic conditions found in the impeller zone. With the circulation time being much smaller than the flocculation time, the flocs will pass through the impeller zone numerous time during the time the flocculation test is run. Because floc size is dependent on the forces applied to it, this area of increased turbulence will tend to govern the equilibrium floc size."

In order to better characterize the local G value the moving particle experienced, the G value distribution was analyzed. Using the macro program attached in appendix C, the time the particle spent in those zones with the same local G value throughout the entire vessel was obtained. Figure 6-31 shows the G value distribution curve along the particle trajectory. The x coordinate represents the local G value and its corresponding y coordinate value represents the time the moving particle spent in those cells with the same local G value. A peak value of time equals to 320 seconds was found at G value about 30 s^{-1}. This value dropped quickly after the peak value. The time the moving particle spent in zones with G value larger than 200 s^{-1} is very small. The higher the G

value, the shorter the time the moving particle spent in those zones. It is quite evident that the local residence time or, vice versa, the residence probability of a particle is much smaller in zones of high velocity gradient (near the impeller region) than in zones far away from the impeller blades, because the local fluid velocities differ greatly between the direct discharge area and zones far away from the impeller blades.

The cumulative G value distribution along the particle trajectory was also obtained and is presented in Figure 6-32. At the beginning, the cumulative time spent by the moving particle increase dramatically as G value increase. It slowed down when the G value reached about 60 s^{-1} and almost kept a stable value after G value is larger than 200 s^{-1}. This again indicates that the time the particle spent in those zones with high G value was much less than the other zones with low G value.

Knowing the distribution of local G value the particle experienced along its trajectory, the new parameter proposed in this work was calculated. Multiplying the local G value by the time the moving particle spent in a cell and integrating this value as a function of time produces the numerical value of this new parameter. Figure 6-33 shows the numerical integration of this new parameter vs. the time the particle spent in the entire vessel. As the time added up, the value of this integration increased steeply at the first 100 seconds and then slowly. The moving average of the G value along the particle trajectory is presented in Figure 6-34 as a function of time. This average G value was obtained by dividing the previously obtained velocity gradient-time integral by the time spent by the particle up to that point. This average G value fluctuated at the beginning of the process when the total time was less than 400 seconds and then reached

an almost constant value of 29 s^{-1}, indicating the possibility that this new parameter could give a stable representation of flocculation process after certain length of running time.

A comparison between the average and maximum G value calculated with the conventional method and obtained with the rigorous method (complete definition of local velocity gradient method) proposed in this work is presented in Table 6-2. The average G value along the particle trajectory obtained through this work was found to be much lower than the one obtained by conventional method for the entire vessel.

6.3 System C1

For the baffled cylindrical mixing/flocculation System C1, tri-dimensional average and fluctuating velocities at 5 different axial levels were experimentally measured via LDV in the Mixing Laboratory at the Department of Chemical Engineering, Chemistry, and Environmental Science, New Jersey Institute of Technology. A 101.6 mm pitched-blade turbine rotating at 159 rpm was studied. The experimentally obtained data near the impeller region were used as the boundary conditions when the CFD program *FLUENT* was launched to produce numerical estimates of the velocity distribution, turbulence kinetic energy, energy dissipation rate, local velocity gradient distribution and particle trajectory in this mixing/flocculation vessel. One turbulence model (RSM) was used in the simulation. The results of both LDV measurements and CFD predictions are presented below.

Table 6-2. Comparison of G average value between two methods for different systems

Mixing / Flocculation System	**Average G Value** For the entire tank **(Conventional Method)**	**Average G Value** Along the particle trajectory **(This Work)**	**Maximum G Value** experienced by a moving particle **(This Work)**
System B	131.1	29.5	920
System C1	131.1	24.9	640
System C2	131.1	43.8	1390

* G values were expressed in s^{-1}

During the CFD simulation process, cylindrical coordinates were used, and the velocities in the three directions (r, θ, z) were expressed as radial, tangential and axial velocities.

6.3.1 LDV Measurements in the Impeller Region

LDV was used to experimentally measure the velocity components in all three directions (i.e., tangential, axial, and radial velocities) for the top and bottom layers of the cylindrical region swept by the impeller. These experimentally determined velocities are reported in Figures 6-35a and 6-35b. Each point in these figures represents the average of three measurements. As usual, these figures are presented in dimensionless form.

The tangential velocity profiles show a maximum near the tip of the impeller. This pattern is consistent with that reported in System A of this work.

The axial velocities, with negative values for both axial levels 2 mm above and below impeller surfaces (indicating downward flow) were found to be much higher than the velocities in the other two components as one could expect for a downward pumping impeller.

The radial velocities were low at the axial level above the impeller, but at the axial level below the impeller they had almost the same magnitude to that of the corresponding tangential velocities.

The turbulent kinetic energy profiles for the impeller region are presented in Figure 6-35c. The turbulent kinetic energy was found to be high near the impeller tip both above and below the impeller, with the highest value on the lower level of the

impeller near the tip where the radial velocity was also the greatest. These profiles are different from those observed in the unbaffled system (System A).

The values for the velocity components (radial, tangential and axial) and for k shown in the above figures were used as boundary conditions for the numerical simulation using *FLUENT*.

A repeating 90° domain was selected for the CFD simulation, and a non-uniform grid composed of 30 radial nodes, 48 axial nodes, and 26 tangential nodes was imposed on this domain. The grid was chosen to be finer in the region near the impeller to obtain better simulation results. Figure 6-36 and 6-37 show the grid in 2D and 3D view, respectively.

6.3.2 Comparison between LDV Measurements and CFD Predictions

Figures 6-38, 6-39, and 6-40 show the results of the numerical simulation, as well as the values of the three experimentally determined velocity components in the bulk of the fluid at five axial levels.

Figure 6-38 presents a comparison between the experimental data for the tangential velocities at different positions inside the vessel and the corresponding values obtained from the numerical simulation by using *FLUENT* RSM model. Excellent agreement between the LDV data and the CFD predictions was obtained. A peak for the tangential velocity $u_t/u_{tip} = 0.29$ was found below the impeller near the impeller tip (at 2 $r/T = 0.32$). A similar pattern was found for System A in the results presented by Ranade and Joshi (1989). A peak for the tangential velocity $u_t/u_{tip} = 0.23$ was found

above the impeller between the shaft and the impeller tip (at 2 $r/T = 0.25$). The velocity peak at axial level $Z = 53$ mm was shifted to the right of the impeller tip (at 2 $r/T = 0.38$), where the tangential velocity value was equal to 0.18 of the impeller tip velocity. The tangential velocities in the top region of the vessel were found to be much lower, indicating much less movement of the fluid in that region.

Figure 6-39 shows a comparison between the LDV axial velocity measurements and the CFD predictions. Good agreement was observed. A very strong downward movement at the center of the vessel and a small upward movement near the vessel wall were observed. The maximum axial velocity was found in the impeller discharge stream, giving a value equal to about 0.46 u_{tip} at (2 r/T) = 0.34. This maximum value and the profiles in the discharge stream are in good agreement with the results reported by Fort (1986), and by Ranade and Joshi (1989). The maximum value of axial velocity in the upward stream near the vessel wall was found to be 0.18 u_{tip}. Very low values were found at the top level ($Z = 233$ mm), indicating very little movement of the fluid in this region.

Figure 6-40 compares the radial velocities at 5 different axial levels obtained through the LDV measurements and the CFD predictions. Again, very good agreement could be observed. An intensive radial circulation was observed only in the discharge stream ($Z = 71$ mm) and at level $Z = 53$ mm. The maximum value of the radial velocity was found to be 0.24 u_{tip} at 2 $r/T = 0.34$ and $Z = 71$ mm. The negative radial velocities at $Z = 160$ mm indicate inward flow at that axial level. Almost zero velocities were found at the top axial level ($Z = 233$ mm).

Figure 6-41 shows a comparison between the experimentally obtained turbulent kinetic energies at 5 different axial levels and their corresponding values predicted by simulation. Significant agreement was obtained. The turbulent kinetic energies at the impeller discharge area were found to be much higher than those at the rest of the vessel. This is consistent with the results observed in System A in this work. The maximum value was found to be about 0.15 u^2_{tip} below the impeller at 2 $r/T = 0.34$. A peak for k was also found at axial levels equal to Z =53 mm and Z =88 mm.

The general flow pattern in this agitated vessel, as obtained by simulation is depicted in Figure 6-42 and Figure 6-43 in 2D and 3D view, respectively. It is clear that the main flow generated by the impeller had a very strong downward component, resulting in this flow impinging on the bottom of the vessel and then moving upward near the tank wall. This illustrates that the pitched-blade turbine effectively functions as an axial impeller. A single large recirculation flow in the axial direction was observed, which can be expected to provide good top-to-bottom mixing. This is consistent with the previous results obtained by this researching group (Armenante and Chou, 1996). Below the impeller hub, a reversal flow with low intensity, expanding conically towards the vessel bottom was observed. This reserval flow was also reported by Fort (1986).

6.3.3 Velocity Gradient Distribution

The velocity gradient distribution in the r-Z plane at the center of the rectangular vessel is shown in Figure 6-44. This contour plot was drawn by using Standford Graphics version 3.0b. The values of local velocity gradients shown in this figure were obtained

through the method of complete definition of local velocity gradient (by using the macro program attached in appendix B). The reason we only chose one rigorous method here to calculate the local velocity gradient is that both rigorous methods, i.e. the complete definition of local velocity gradient method and the local energy dissipation rate method, have been tested and found to be valid for turbulent flocculation process and could provide similar information about the local G value distribution, a result for System B. The labels of the contour curves in this figure are the G values in the form of $\log_{10}G$. The local velocity gradient varies from position to position within the vessel, as found in System B. The values of the local velocity gradients near the impeller region were found to be much higher than those in the area near the vessel wall.

6.3.4 Particle Trajectory

The trajectory of a virtual floc particle moving within the agitated vessel was tracked through *FLUENT*. The results are depicted in Figure 6-45 and Figure 6-46 at time equal to 2,000 seconds and 10,000 seconds, respectively. It can be clearly observed that the floc particle tended to move only in the conical area, from the position at 9/10 of the vessel height and near the shaft surface as the cone pinnacle to the vessel bottom as the cone base. It never reached the places beyond this conical area, similar to the case found in System B. However, the ratio of the volume the floc particle never reached to the entire vessel volume is even larger than that in System B.

6.3.5 Velocity Gradient-Time Integral along the Particle Trajectory

Using the same macro program attached in appendix C, the local *G* value at each point the floc particle experienced along its movement trajectory during the flocculation process was numerically obtained. The results are shown in Figure 6-47, where the x coordinate represents the time a moving particle spent in the vessel and the y coordinate represents the local *G* value the moving particle experienced. As in System B it was found that the local *G* value experienced by the particle as it moved through the vessel is extremely non-uniform. Very high peaks were observed (when the particle moved through the impeller region), followed by long periods during which the *G* values were very low. The dotted line shown in the above figure is the average *G* value obtained with the conventional method for the entire flocculation vessel. Clearly this average *G* value throughout the entire vessel by the conventional method can not characterize the real effect of the local *G* value on the floc particle.

The maximum value of the local velocity gradient the particle experienced in this system is about 640 s^{-1} as shown in Figure 6-47. This value is much lower than the one experienced by the particle in System B, indicating that for certain flocculation process with a maximum local *G* value of 640 s^{-1}, which will lead to floc breakup, the System B is not suitable while the System C1 may be suitable to use.

The *G* value distribution along the particle trajectory was also analyzed. Using the macro program attached in appendix C, the time the particle spent in those zones with the same local *G* value throughout the entire vessel was obtained. The results were presented in Figure 6-48. The x coordinate in this figure represents the local *G* value,

and the y coordinate represents the time the moving particle spent in those cells having the same local G value. A peak was found at G value about 20 s^{-1}($t \approx 365$ s). The time the moving particle spent in those zones with G value larger than 200 s^{-1} was very small, as also found in System B. The higher the G value, the less the time the moving particle spent in those zones. One can clearly see that the local residence time or vice versa, the residence probability of a particle is much smaller in zones of high velocity gradient (near the impeller discharge region) than in zones far away from the impeller blades.

Figure 6-49 shows the cumulative G value distribution along the particle trajectory.

With a knowledge of the local G value the particle experienced along its trajectory and the time the particle spent in those zones within the vessel, the new parameter, velocity gradient-time integral, proposed in this work was then numerically obtained. Multiplying the local G value by the time the moving particle spent in a cell and integrating this value as a function of time produces the numerical value of this new parameter. Figure 6-50 presents the numerical integration of this new parameter vs. The time the particle spent in the entire vessel. During the first 150 seconds, this new parameter increased quickly and then it slowed down till reached the value of 20,000 at t = 800 s.

Figure 6-51 shows the moving average of the G value along the particle trajectory as a function of time. This average G value was obtained by dividing the previously obtained velocity gradient-time integral by the time spent by the particle up to this point. This average G value steeply increased from 10 s^{-1} at the beginning to 45 s^{-1}

at time 60 seconds. It then fluctuated for a while until it reached a peak value of about 50 s^{-1} at time 140 seconds, and then started to drop. For $t > 300$ seconds, this average G value changed very slightly. A almost stable value of 25 s^{-1} was found when time went up to 800 seconds.

A comparison between the average and maximum G values calculated with the conventional method and that obtained with the rigorous method (complete definition of local velocity gradient) proposed in this work is presented in Table 6-2. The average G value along the particle trajectory obtained through this work was found to be much lower than the one obtained by conventional method for the entire vessel, as found for System B.

6.4 System C2

System C2 had a configuration identical to System C1 with the only exception of different size of the same type of impeller (76.2 mm instead of 101.6 mm). Since very significant agreement between the LDV measurements and CFD predictions for the velocity components and the turbulent kinetic energy had been obtained in both System B and System C1, we felt quite confident about the predictions of the results obtained with the CFD simulation. Therefore for System C2, only the tri-dimensional average and fluctuating velocities in the impeller region were experimentally measured via LDV. The impeller agitation speed was 256 rpm in this case. As before, the experimentally obtained data in the impeller region were used as the boundary conditions when the CFD program *FLUENT* was used to produce a numerical estimate of the velocity distribution,

turbulence kinetic energy, energy dissipation rate, local velocity gradient distribution and particle trajectory in this mixing/flocculation vessel. One turbulence model (RSM) was used in the simulation. The results of both LDV measurements and CFD predictions are presented below.

During the CFD simulation process, cylindrical coordinates were used, and the velocities in the three directions (r, θ, z) were expressed as radial, tangential and axial velocities.

The computational grid was the same used in System C1 (Figure 6-36 and Figure 6-37) except for the radial size of the region swept by the impeller. In System C2, there were 7 radial cells above and below the impeller surfaces that were defined as input boundary area, while in System C1, there were 9 radial cells above and below the impeller surfaces that were defined as input boundary area.

6.4.1 LDV Measurements in the Impeller Region

LDV was used to experimentally measure the velocities components in all three directions (i.e., tangential, axial, and radial velocities) for the top and bottom layers of the cylindrical region swept by the impeller. Figure 6-52a and 6-52b show these experimentally determined mean velocities. Each point in these figures represents the average of three measurements.

The tangential velocity profiles show a maximum value near the tip of the impeller. This pattern is consistent with that reported for System A and C1 in this work. A very strong downward flow at the center of the vessel was clearly observed as

indicated by the negative values of the axial velocities for both axial levels. The axial velocities were found to be dominating over the other two velocity components as in System C1. The radial velocities below the impeller were found to be close to the tangential components and have a maximum value near the tip of the impeller, whereas the radial velocities above the impeller had very small values and fluctuated around zero.

Figure 6-52c presents the turbulent kinetic energy profiles in the impeller region. A peak of the turbulent kinetic energy was found near the impeller tip, showing the high intensity of turbulence near the impeller region. The same observation was made for System A and System C1.

The experimental values for the mean velocity components (radial, tangential and axial) and for k shown in the above figures were used as boundary conditions during the CFD simulation.

6.4.2 Numerical Predicted Velocity Distribution

The velocity distribution in System C2 predicted via CFD is shown in Figure 6-53 and Figure 6-54 (2D and 3D views, respectively). A flow pattern very similar to that reported for System C1 was observed. The main flow generated by the impeller had a very strong downward component, indicating a very effective axial impeller. A single large recirculation flow in the axial direction was observed. Similar results were found for System C1 and in the work previously conducted by this research group (Armenante and Chou, 1996). Below the impeller hub, a low intensity reversal flow, expanding conically towards the vessel bottom was observed, as in System C1. However, the size

of this cone differed from that for System C1 because of the different impeller sizes used in these two cases.

6.4.3 Velocity Gradient Distribution

The local velocity gradient distribution in System C1 is shown in Figure 6-55. The values of the local velocity gradients shown in this figure were obtained through the method of complete definition of local velocity gradient, with the same reason to choose just one rigorous method for System C1. Again, the labels of the contour curves in this figure are the G values in the form of $\log_{10}G$. The local velocity gradient varies from position to position within the vessel, similarly to System B and System C1. The values of the local velocity gradients near the wall were very low around 10 s^{-1}. This value increased as the position moved closer to the impeller. Values in the impeller region (around 1000 s^{-1}) were much higher than those in the rest of the vessel.

6.4.4 Particle Trajectory

FLUENT was also used to determine the trajectory of a virtual floc particle moving within the agitated vessel. The results are depicted in Figure 6-56 and Figure 6-57 at time equal to 2,000 seconds and 10,000 seconds, respectively. These two figures look very similar to Figure 6-45 and Figure 6-46 obtained for System C1. The main difference is in the height of the conical area the particle often visited. The volume of the conical area the particle often visited is even less than that in System C1. About half of the vessel volume never was visited by the moving particle.

6.4.5 Velocity Gradient-Time Integral along the Particle Trajectory

The local G value experienced by the floc particle as it moved in the vessel was numerically obtained using the same macro program attached in appendix C. The results are shown in Figure 6-58, where the x coordinate represents the time a moving particle spent in the vessel and the y coordinate represents the local G value the moving particle experienced. The local G value experienced by the particle as it moved through the vessel is extremely non-uniform, similarly to System B and C1. The particle spent most of the time in the cells with low G values, while the time it spent in the cells with high G values was extremely short.

The maximum value of the local velocity gradient the particle experienced in this system is about 1390 s^{-1} as shown in the above figure. This value is much higher than the one experienced by the particle in System C1 and higher than the one in System B, indicating that System C2 would be more likely to produce floc breakup than System B or System C1.

Figure 6-59 presents the G value distribution along the particle trajectory for System C2 (see macro program attached in appendix C). A peak value of time about 330 seconds was found at G value about 40 s^{-1}. The time the moving particle spent in those zones with G value larger than 200 s^{-1} was very small, as in System B and System C1. The higher the G value, the less the time the moving particle spent in those zones.

The cumulative G value distribution along the particle trajectory is shown in Figure 6-60. The cumulative time spent by the moving particle increased abruptly before G reached 100 s^{-1} and then remained constant for G values larger than 100 s^{-1}.

The velocity gradient-time integral was also numerically obtained. Multiplying the local G value by the time the moving particle spent in a cell and integrating this value as a function of time produces the numerical value of this new parameter. Figure 6-61 shows the numerical integration of this new parameter vs. the time the particle spent in the entire vessel.

Figure 6-62 shows the moving average of the G value along the particle trajectory as a function of time. This average G value was obtained by dividing the previously obtained numerical velocity gradient-time integral by the time spent by the particle up to this point. This average G value increased quickly with t, reached a peak G value of 75 s^{-1} at time about 130 seconds, then decreased gradually, and finally reached a almost stable G value of 44 s^{-1} when time was larger than 550 seconds, a same trend (with different final G values) observed in both System B and C1.

A comparison between the average and maximum G value calculated with the conventional method and obtained with the rigorous method (complete definition of local velocity gradient method) proposed in this work is shown in Table 6-2. The average G value along the particle trajectory obtained through this work was found to be much lower than the one obtained by conventional method for the entire vessel, as found for System B and System C1. From Table 6-2, one can see that the conventional method to obtained average G value throughout the entire vessel produced the same average G value for three quite different mixing/flocculation systems, which have quite different local G value distribution and floc particle trajectory, and hence potentially significantly different effects on flocculation performance. Although we cannot, at the present time,

produce a trend about the new parameter and the average G value along the particle trajectory, nor to correlate them to the flocculation process, much more information and better understanding to this process was obtained through this work.

6.5 Future Work

This dissertation work is the first of many steps leading to the general goal of elucidating the fundamental aspects of flocculation, as well as producing design specifications for equipment that can be used commercially to improve the water purification and wastewater treatment processes through flocculation and efficient floc removal. The major emphasis of this work was to develop a new method to calculate the actual local velocity gradient, to propose a new parameter, the velocity gradient-time integral, which can better characterize the flocculation process than those used currently in the flocculation process modeling, and to develop a rigorous approach to quantify this new parameter for certain flocculation processes.

To accomplish the general goal stated above, much work needs to be carried out in the future such as:

- Investigate other flocculator configurations and compare the results in terms of local velocity gradient distribution, particle trajectory and velocity gradient-time integral;
- Transfer the above information to co-investigators at Queen's university so that experimental data for these flocculator configurations can be obtained;

- Correlate the velocity gradient-time integral with the results of actual flocculation processes;
- Provide design specifications for equipment that can be used commercially to improve the flocculation process.

CHAPTER 7

CONCLUSIONS

In this work two advanced technologies, LDV and CFD, have been used to investigate the turbulence effects in a number of mixing/flocculation systems. The Laser-Doppler Velocimetry (LDV) was used to experimentally measure the mean and fluctuating velocities in all three directions in mechanically agitated vessels. A computational fluid dynamic (CFD) software, *FLUENT*, was used to numerically predict the velocity distribution, fluctuating velocities, power consumption, local energy dissipation rate and particle trajectory, using different turbulent model such as k-ε model, algebraic stress model (ASM) and Reynolds Stress Model (RSM). The experimentally obtained mean velocities and turbulent kinetic energies on the top and bottom horizontal surfaces of the region swept by the impeller were used as boundary conditions in the simulations.

A novel approach to numerically calculate the local velocity gradient in turbulent flocculation was developed. The distributions of local velocity gradients in three systems were mapped in the entire mixing/flocculation vessels using the numerically obtained local mean velocity and local turbulent viscosity, as well as by using the numerically obtained local energy dissipation rate. The distribution of velocity gradient along a particle trajectory provided quantitative information on the time an individual floc particle spends in different zones of the tank while being exposed to velocity gradients of different intensities. A new parameter, the velocity gradient-time integral along the particle trajectory, was proposed to better characterize the shear experienced by a floc particle during a flocculation process instead of the conventional average

velocity gradient obtained by measuring the average power consumption throughout the entire vessel.

The main results for an unbaffled cylindrical tank with no headspace and provided with a pitched blade turbine (System A) can be summarized as follows:

- Throughout the tank the velocities in the tangential direction were experimentally found to be significantly higher than the other two velocity components.
- In the r-Z plane a strong radially oriented flow was observed to emerge from the impeller, producing two main recirculation flows, one above and the other below the impeller. When used in an unbaffled tank pitched-blade turbines appear to lose most of the axial flow-generating characteristics observed in baffled vessels.
- The numerical predictions were typically found to be in substantial agreement with the experimental data. However, predictions based on ASM were always superior to those based on the k-e model.
- The turbulent kinetic energy was found to be much higher in the impeller region and, to a limited extent, in the region below the impeller, than anywhere else in the vessel.
- The dimensionless velocity and turbulent kinetic energy profiles were nearly identically at two different agitation speeds, indicating that such profiles are independent of agitation intensity. In addition, the power numbers and the flow numbers were also very similar at the same two agitation speeds.

The main observations for a baffled square tank provided with a paddle impeller (System B) and for baffled cylindrical tanks provided with a pitched blade turbine (System C1 and C2) are as follows:

- Two main recirculation flows, one above and the other below the impeller were observed in System B. One single large recirculation flow in the axial direction and a small reversal flow in the conical area below the impeller hub were observed in both System C1 and System C2,
- The turbulent kinetic energies were found to be much higher in the impeller region than anywhere else in the vessel for all three systems.
- Significant agreement between the experimental data and the numerical predictions was obtained for the velocity profiles and turbulent kinetic energies for all three cases.
- The two new methods to calculate local velocity gradient proposed in this work, i.e., the complete definition of local velocity gradient method and the local energy dissipation rate method, were tested to be both valid for turbulent mixing/flocculation applications and exchangeable, provided that accurate local values are available.
- The local velocity gradient distribution was mapped throughout the entire agitated vessel. The local velocity gradients near the impeller region were found to be much higher than those in the rest of the tank for all three systems.
- The trajectory of a virtual particle with physical properties similar to that of a floc particle moving in each one of above three systems was obtained by simulation.

The particle tended to visit some zones more often than the others, and it never moved through certain places such as the top corner of the agitated vessel.

- The local G values experienced by the particle as it moved through the vessel were extremely non-uniform. Very high peaks (when the particle moved through the impeller region), followed by long periods during which the G values were extremely low, were observed in all three systems, except that the maximum G value and its corresponding time the particle visited, as well as the low value were different for each system.
- A newly defined parameter, the velocity gradient-time integral along the particle trajectory, was numerically obtained for all three systems. This information will be eventually incorporated into new flocculation models to be developed in the future.
- The average G values along the particle trajectory obtained for three systems studied here were found to be different, while the average G values obtained by conventional method throughout the entire vessel for these three systems were the same.
- A rigorous approach to obtain the above information was successfully developed and used in all these systems.

The above results confirm the validity of the general simulation approach used in this work and provide some new information, both qualitative and quantitative, of importance for fluid dynamic modeling of mixing and flocculation vessels.

APPENDIX A

FIGURES FOR SYSTEM CONFIGURATIONS AND RESULTS

This appendix includes the figures showing the impeller and vessel configurations, boundary conditions in the impeller region and the comparison between the LDV experimental data and CFD simulation results for System A, System B, System C1 and System C2, as well as the particle trajectory, local velocity gradient distribution and velocity gradient-time integral along the particle trajectory for System B, System C1 and System C2.

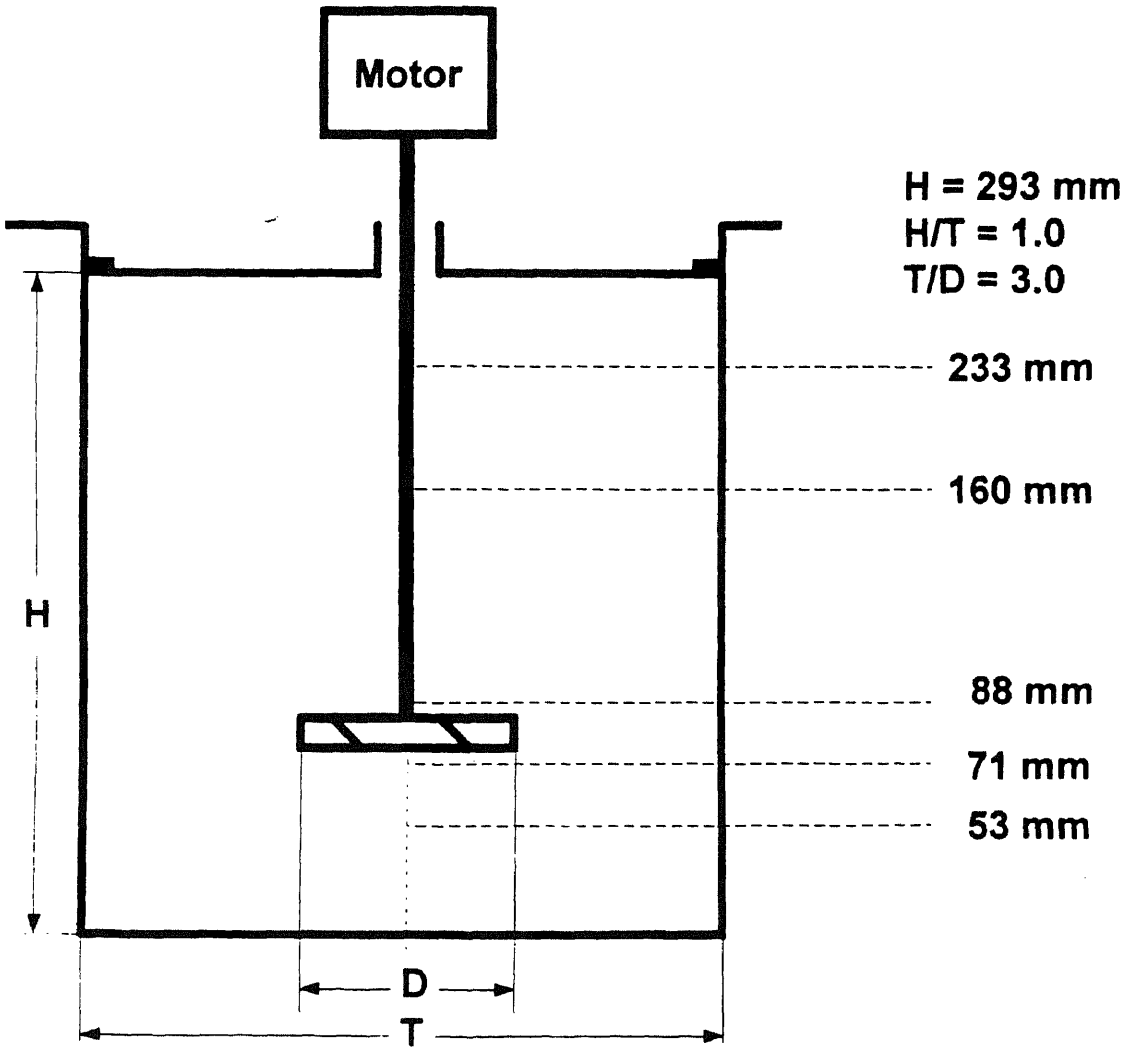

Figure 4-2 Configuration of unbaffled cylindrical tank (System A)

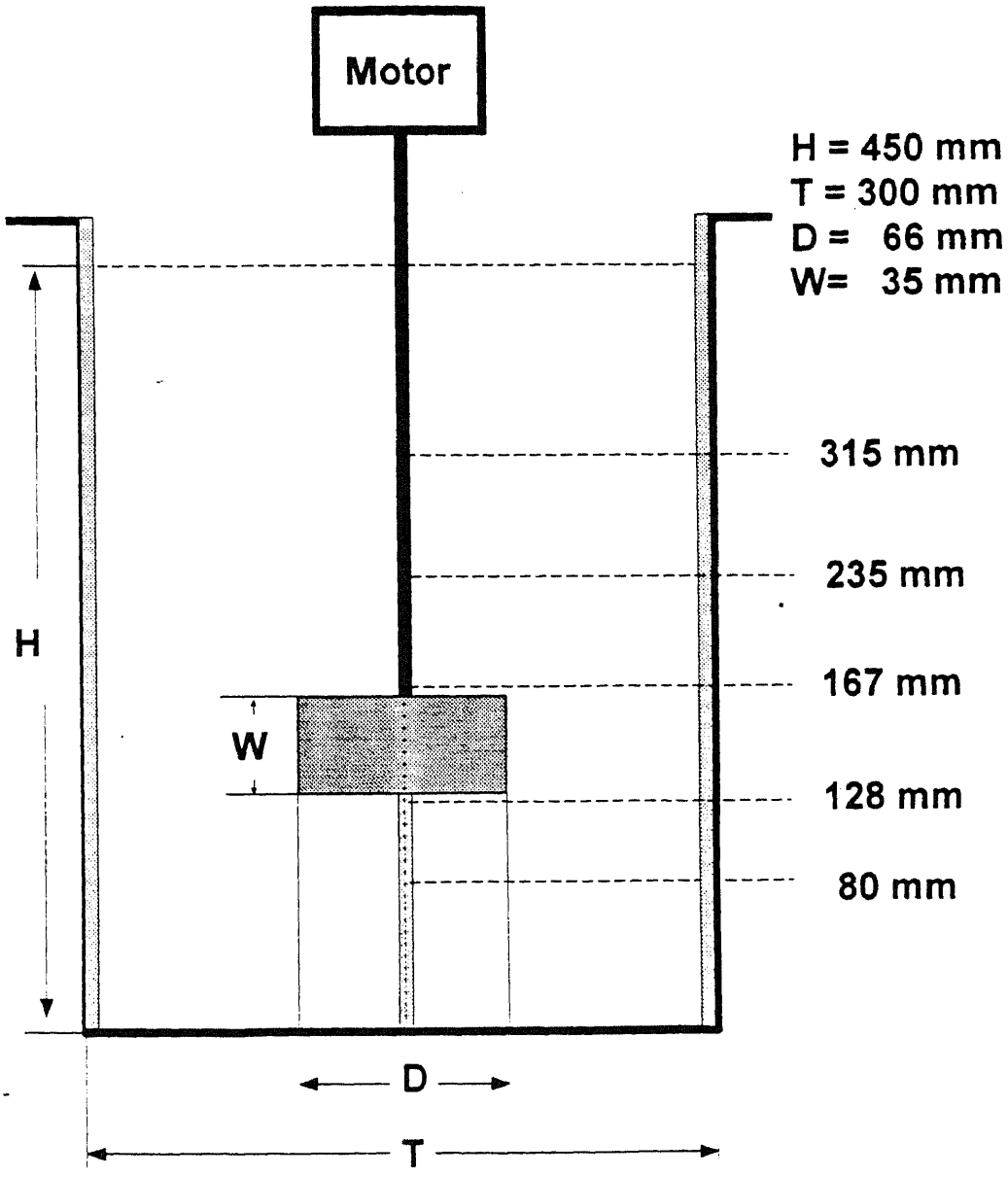

Figure 4-3 Configuration of baffled rectangular tank (System B)

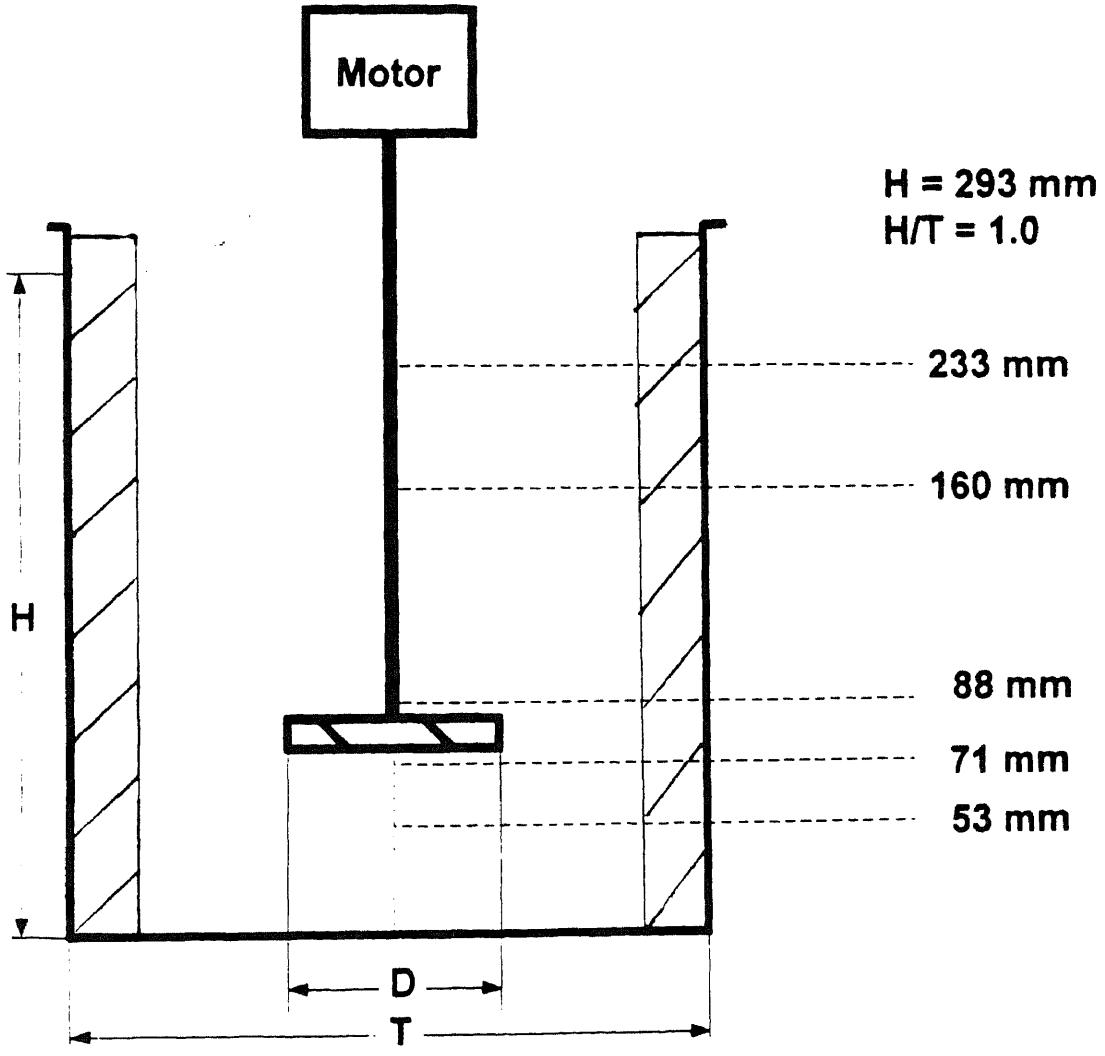

Figure 4-4 Configuration of baffled cylindrical tank (System C1 and C2)

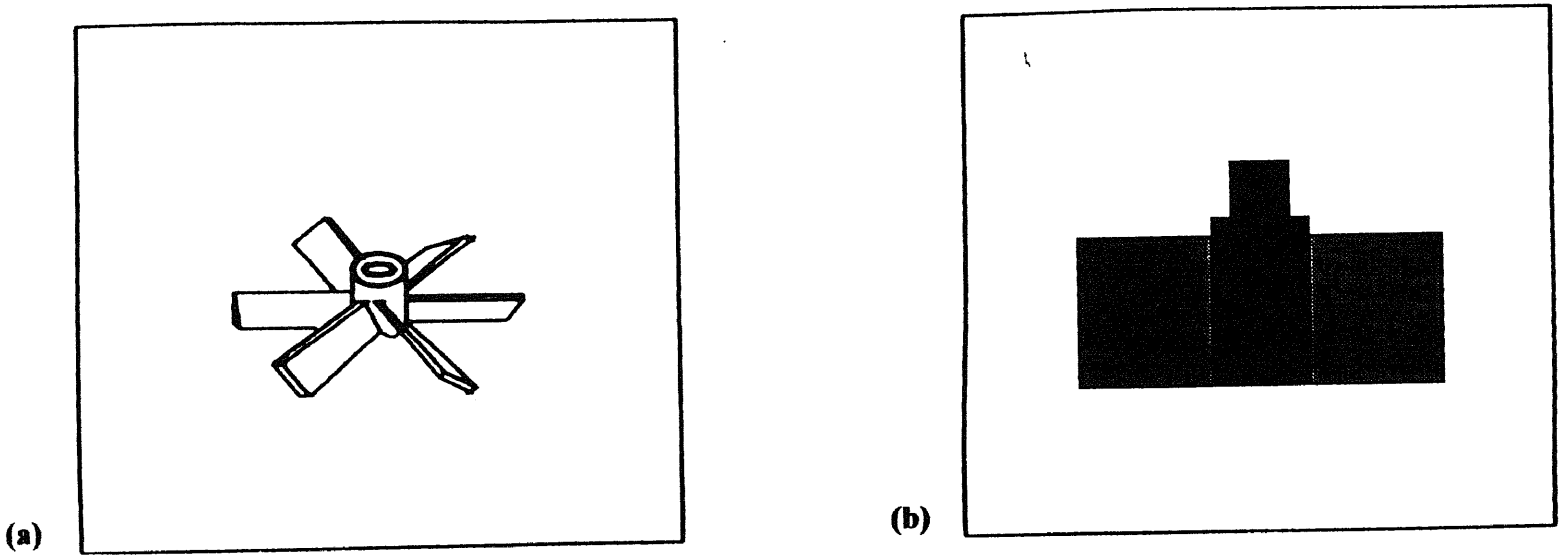

Figure 4-5 Outline of impellers: (a) 6-blade pitched bladed impeller, (b) 2-blade paddle type impeller

Axial and radial velocity measurement

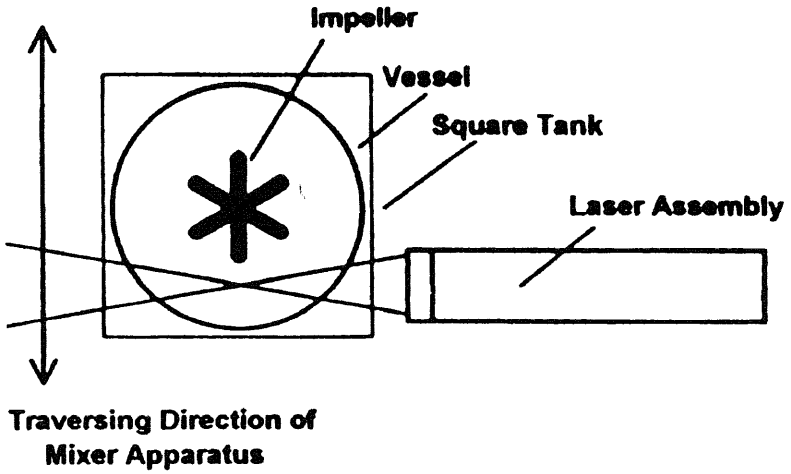

Axial and tangential velocity measurement

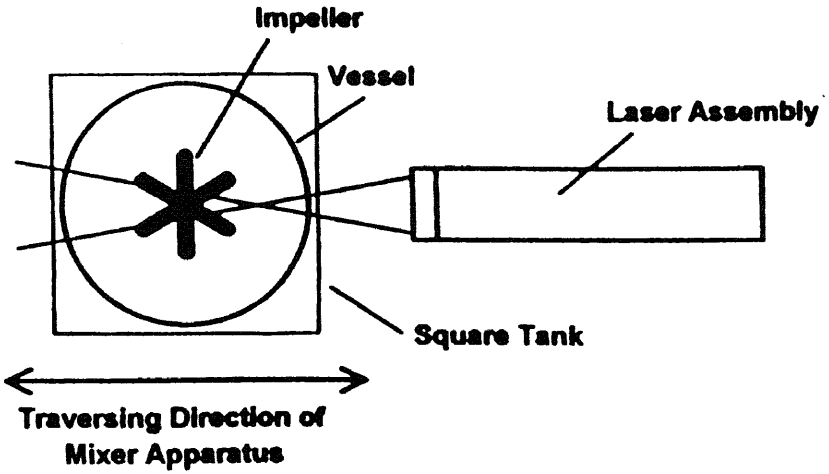

Figure 4-6 Measurement methods used in determining three velocity components

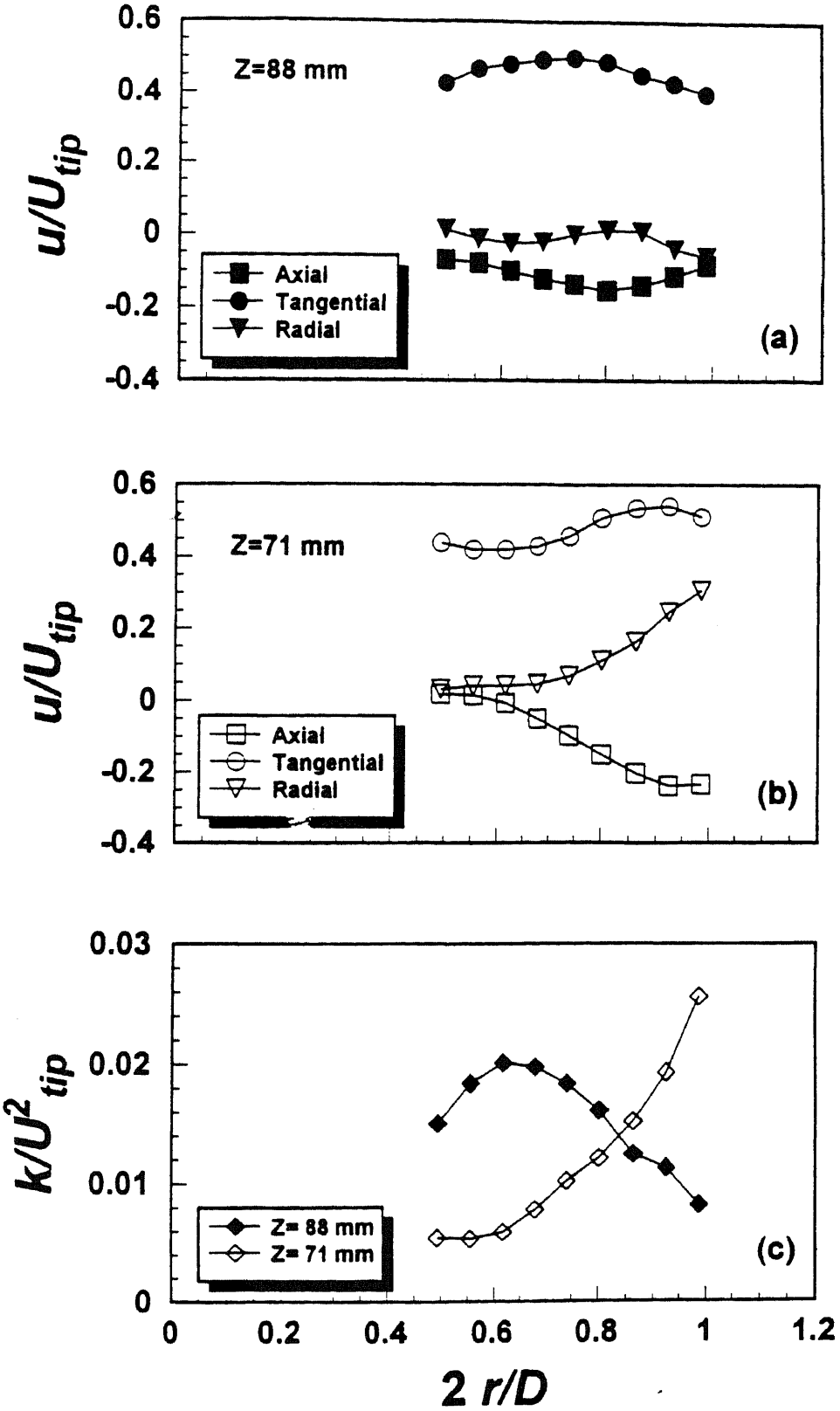

Figure 6-1 Experimentally determined (via LDV) dimensionless velocities and turbulent kinetic energies in the impeller region (System A, $N = 450$ rpm)

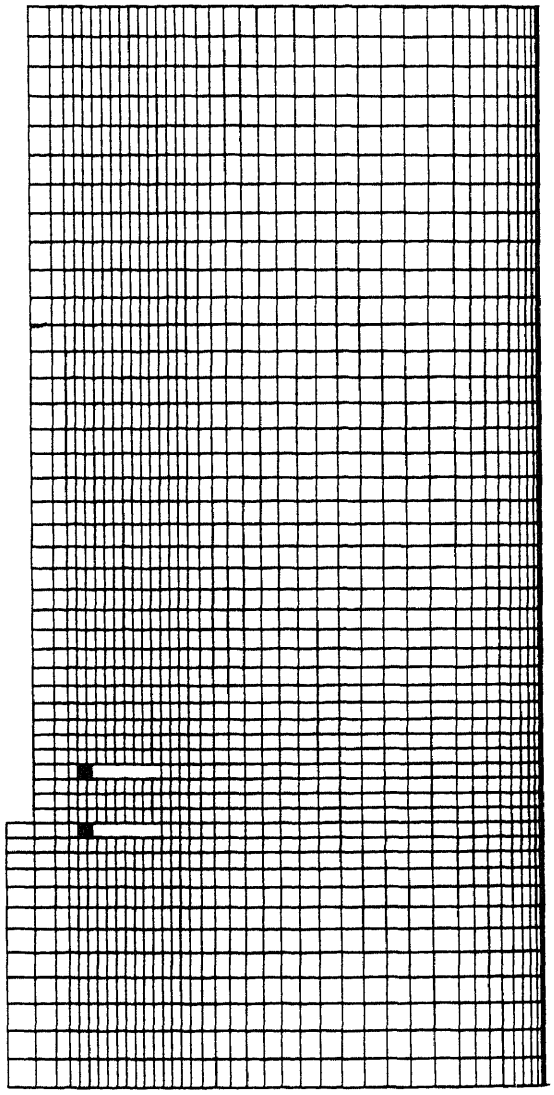

Figure 6-2 Grid used in the CFD simulation for System A (2*D* view)

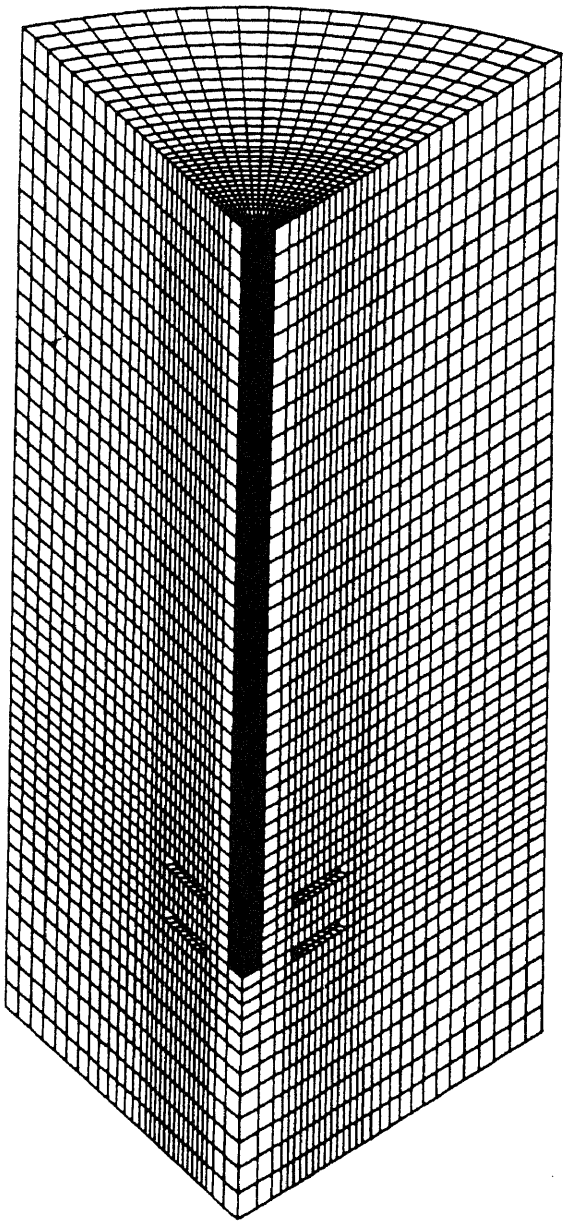

Figure 6-3 Grid used in the CFD simulation for System A (3*D* view)

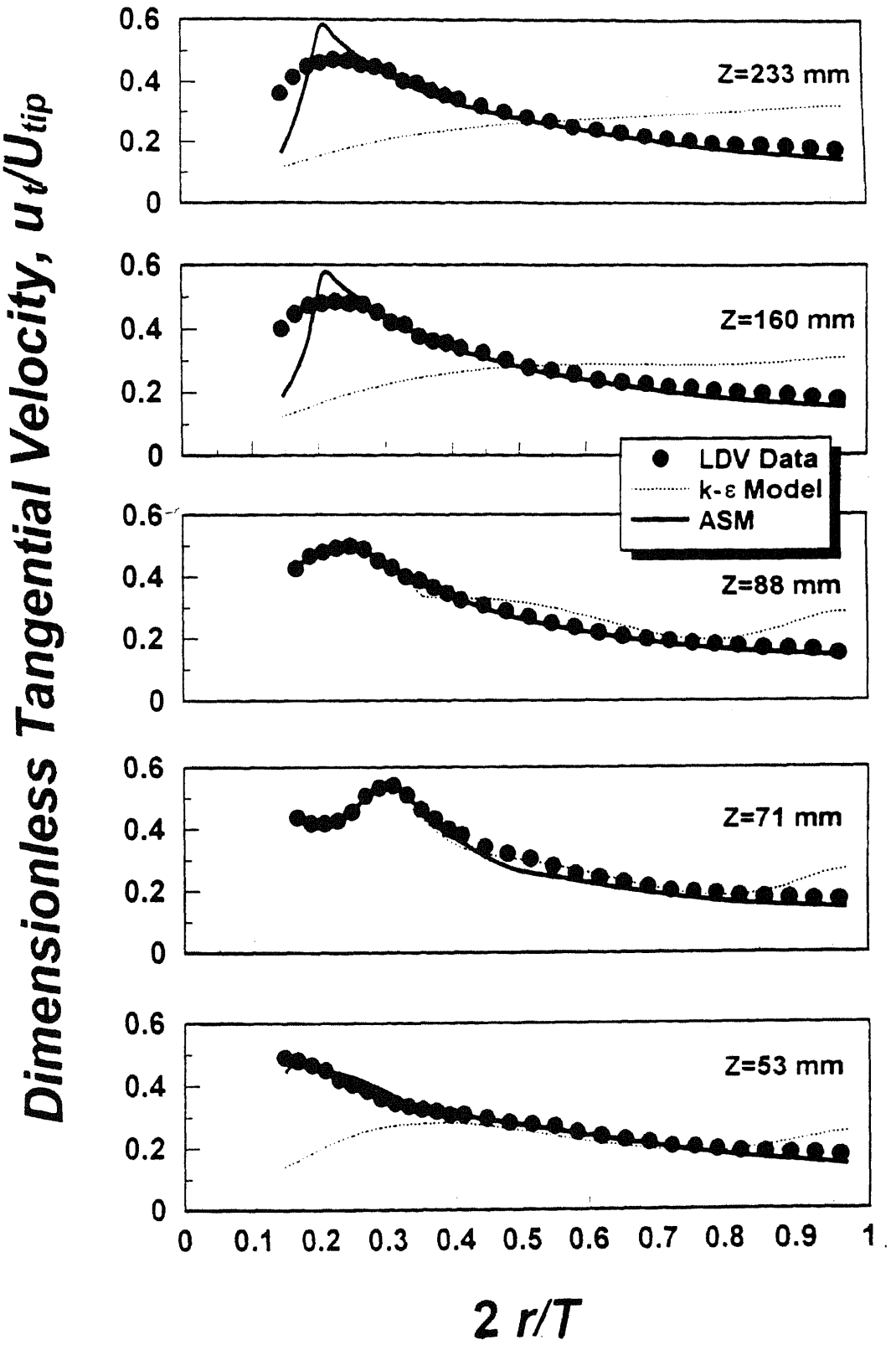

Figure 6-4 Comparison between experimental tangential velocity measurements (via LDV) and numerical predictions (via CFD) (System A, N = 450 rpm)

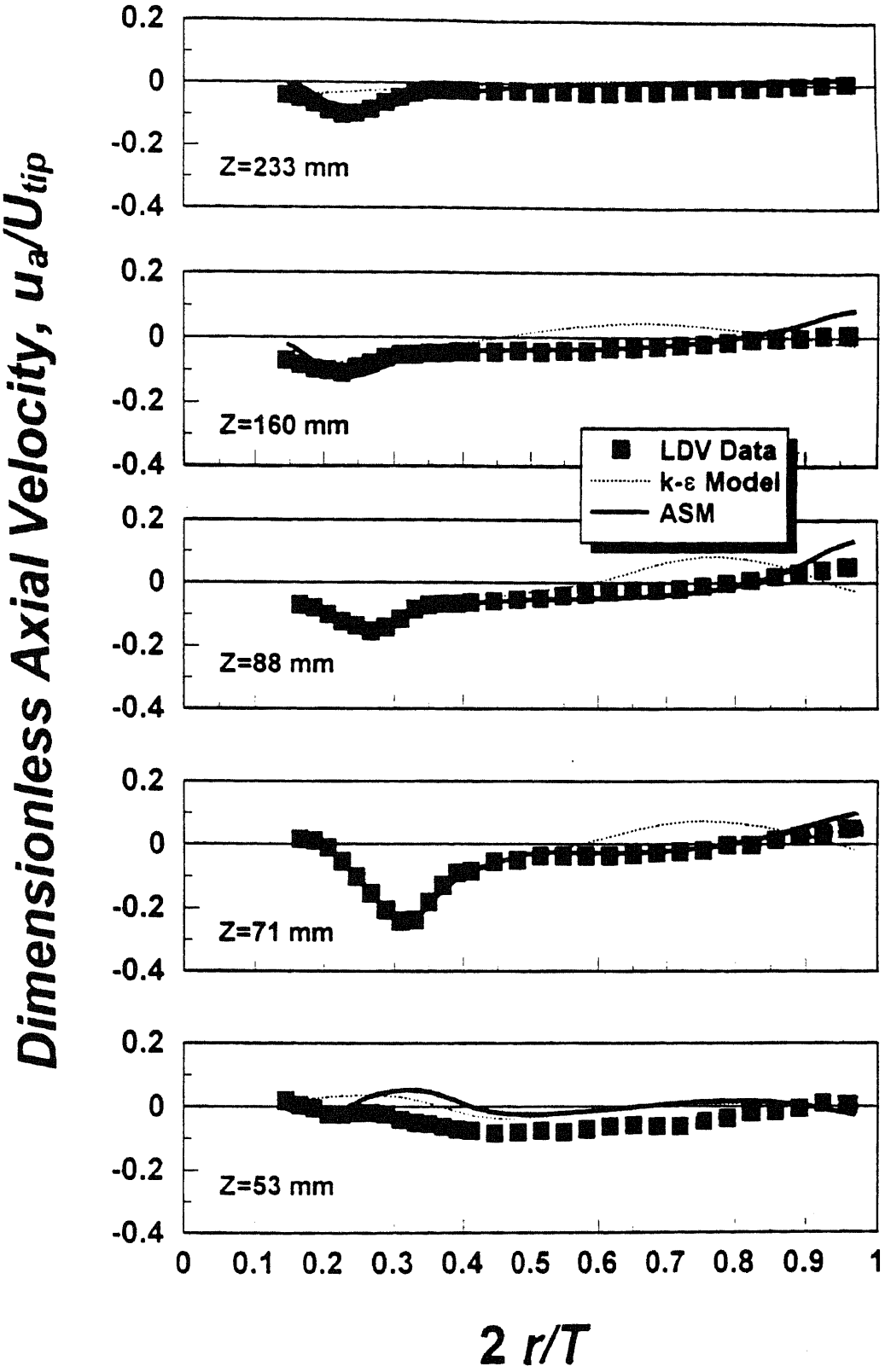

Figure 6-5 Comparison between experimental axial velocity measurements and numerical predictions (System A, N = 450 rpm)

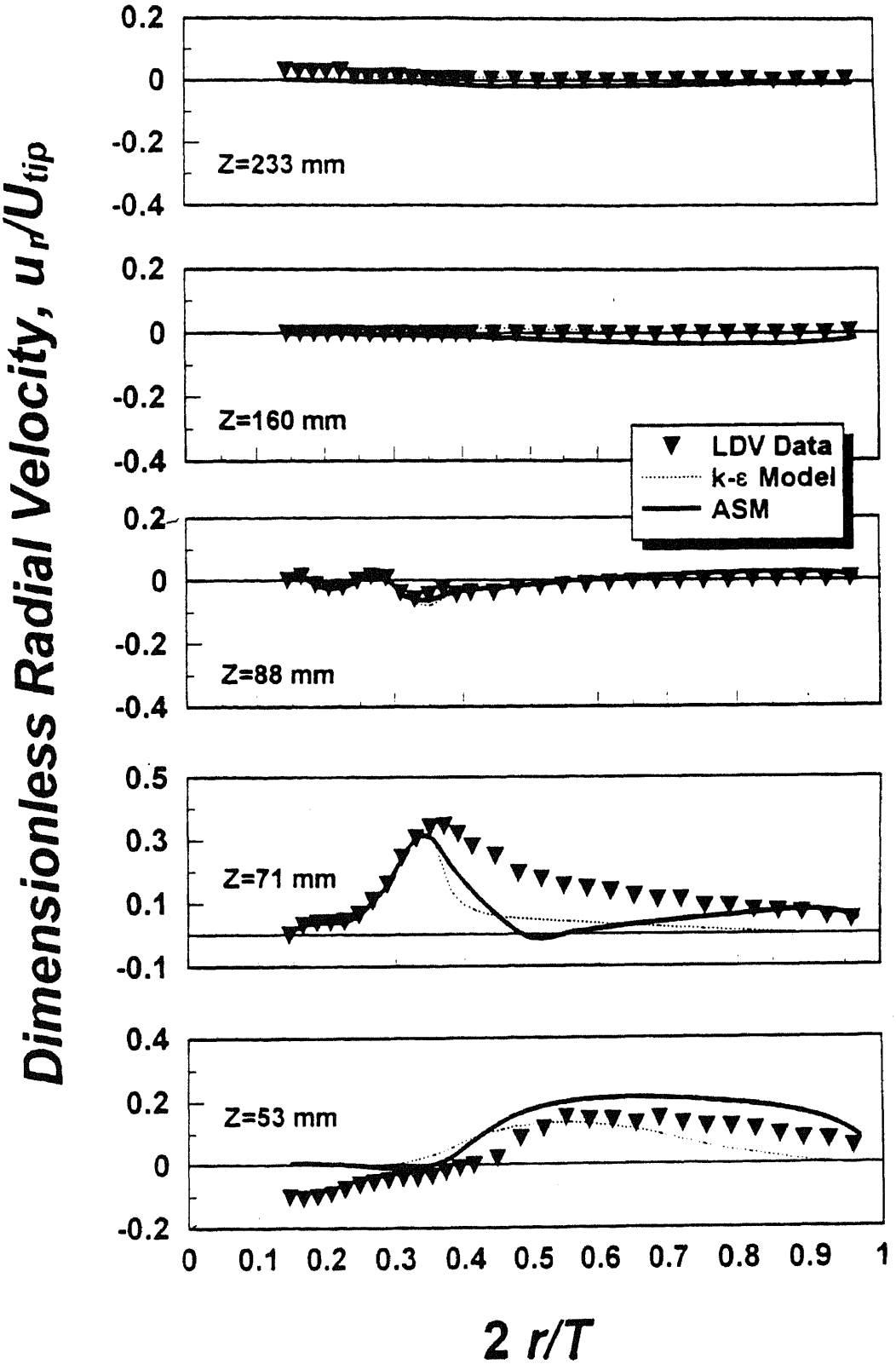

Figure 6-6 Comparison between experimental radial velocity measurements and numerical predictions (System A, N = 450 rpm)

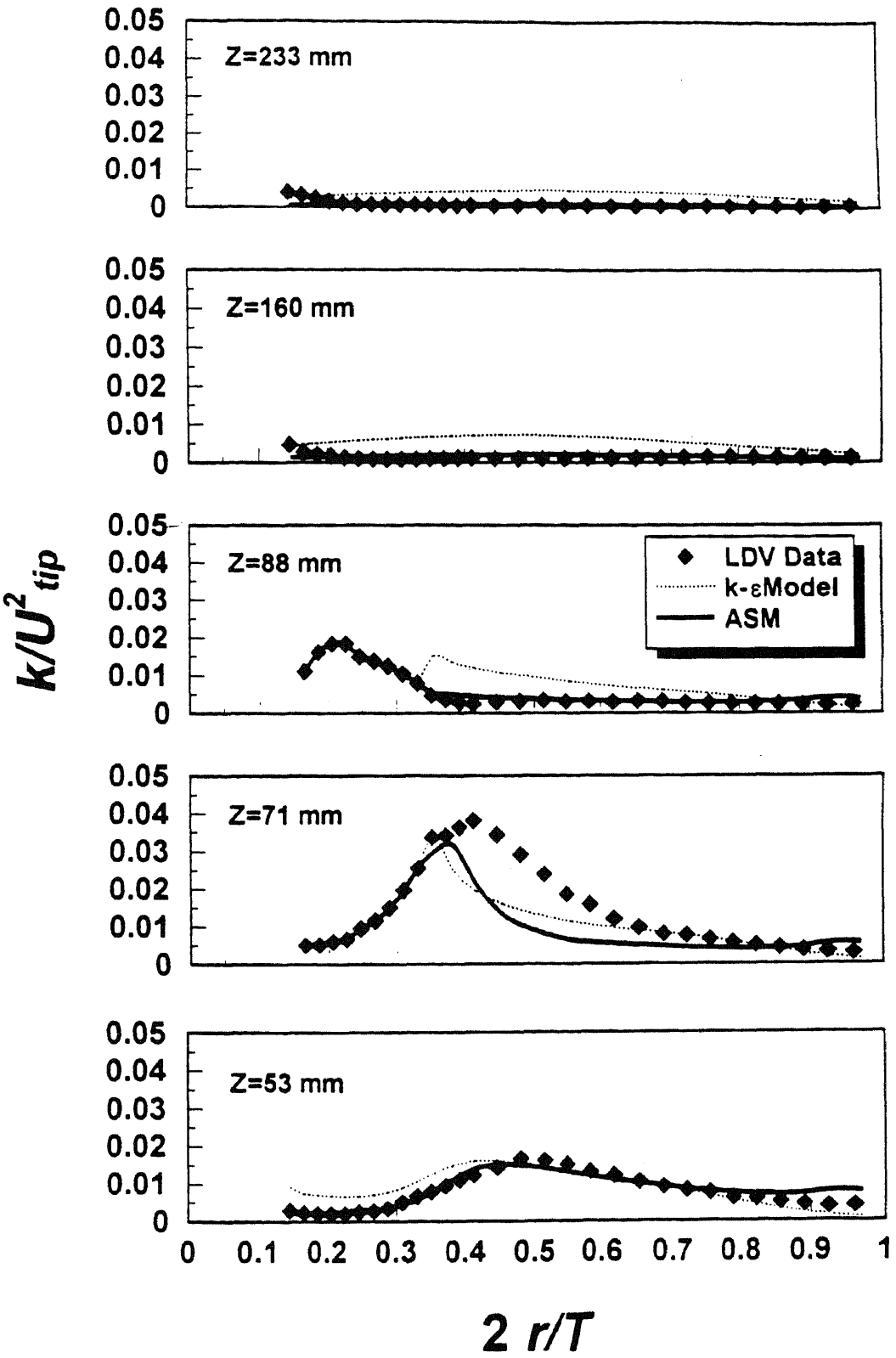

Figure 6-7 Comparison between experimental and numerically predicted turbulent kinetic energies (System A, N = 450 rpm)

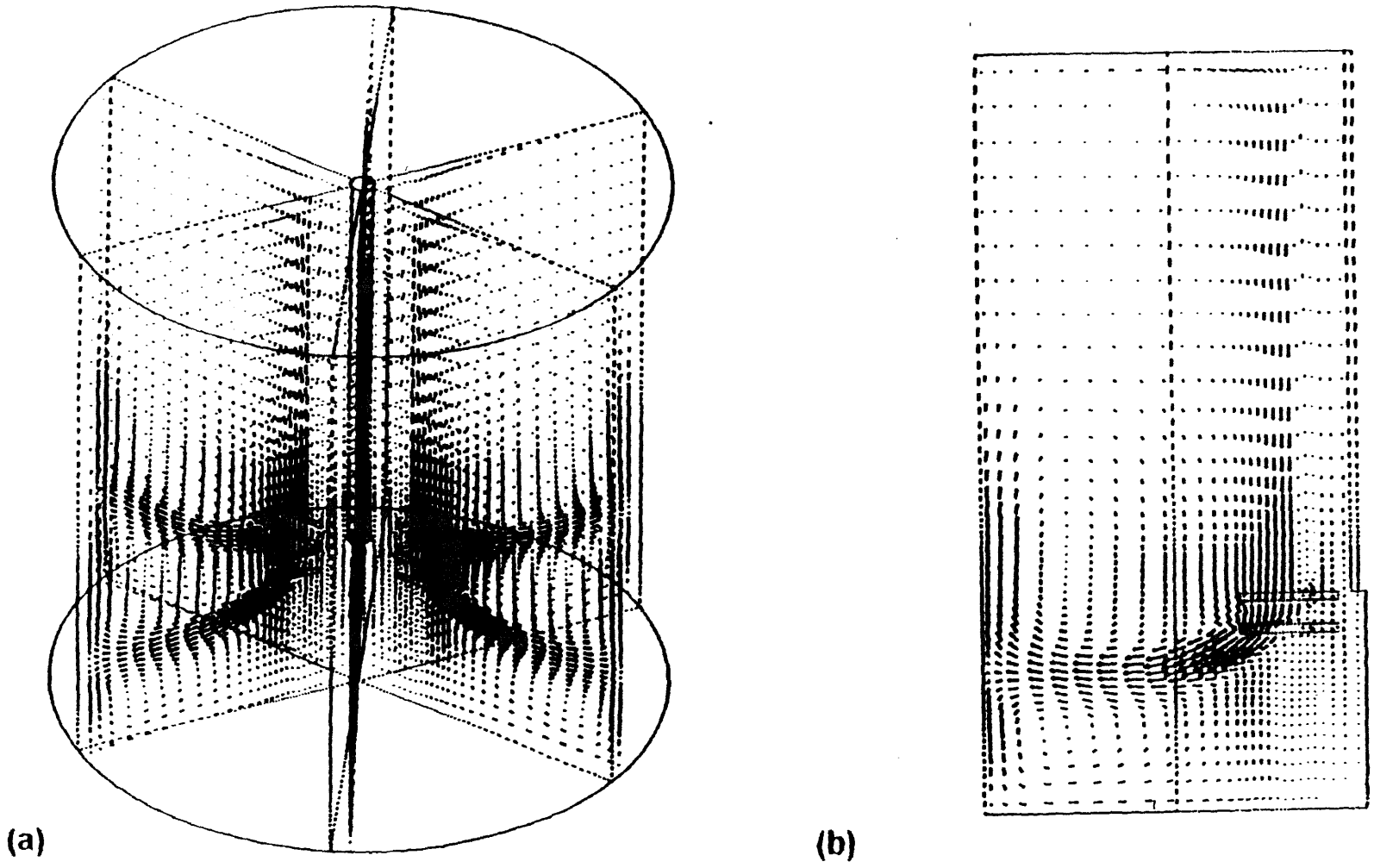

Figure 6-8 CFD prediction of velocity distribution in system A (N = 450 rpm) (a): 3D view; (b) 2D view

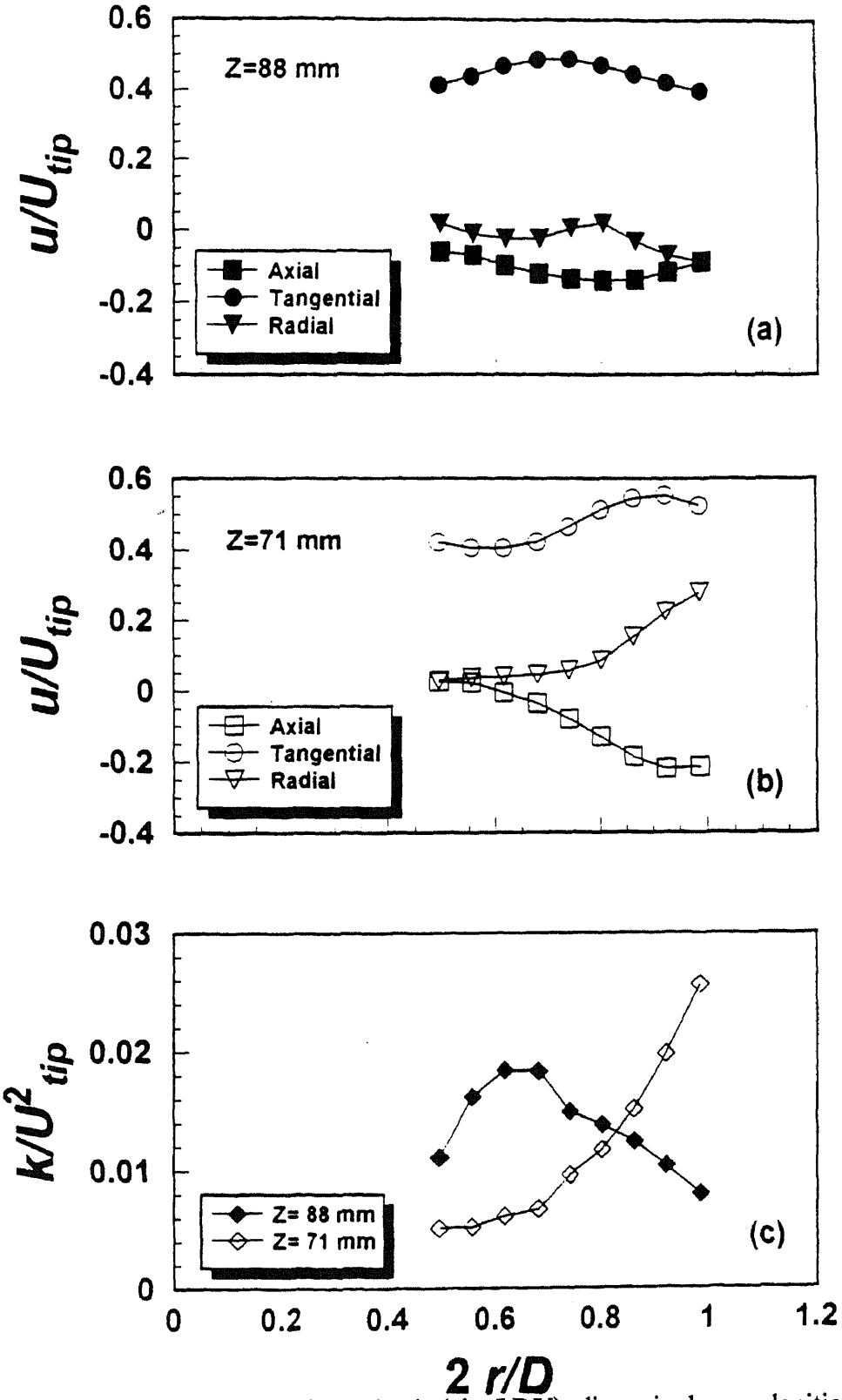

Figure 6-9 Experimentally determined (via LDV) dimensionless velocities and turbulent kinetic energies in the impeller region (System A, $N = 700$ rpm)

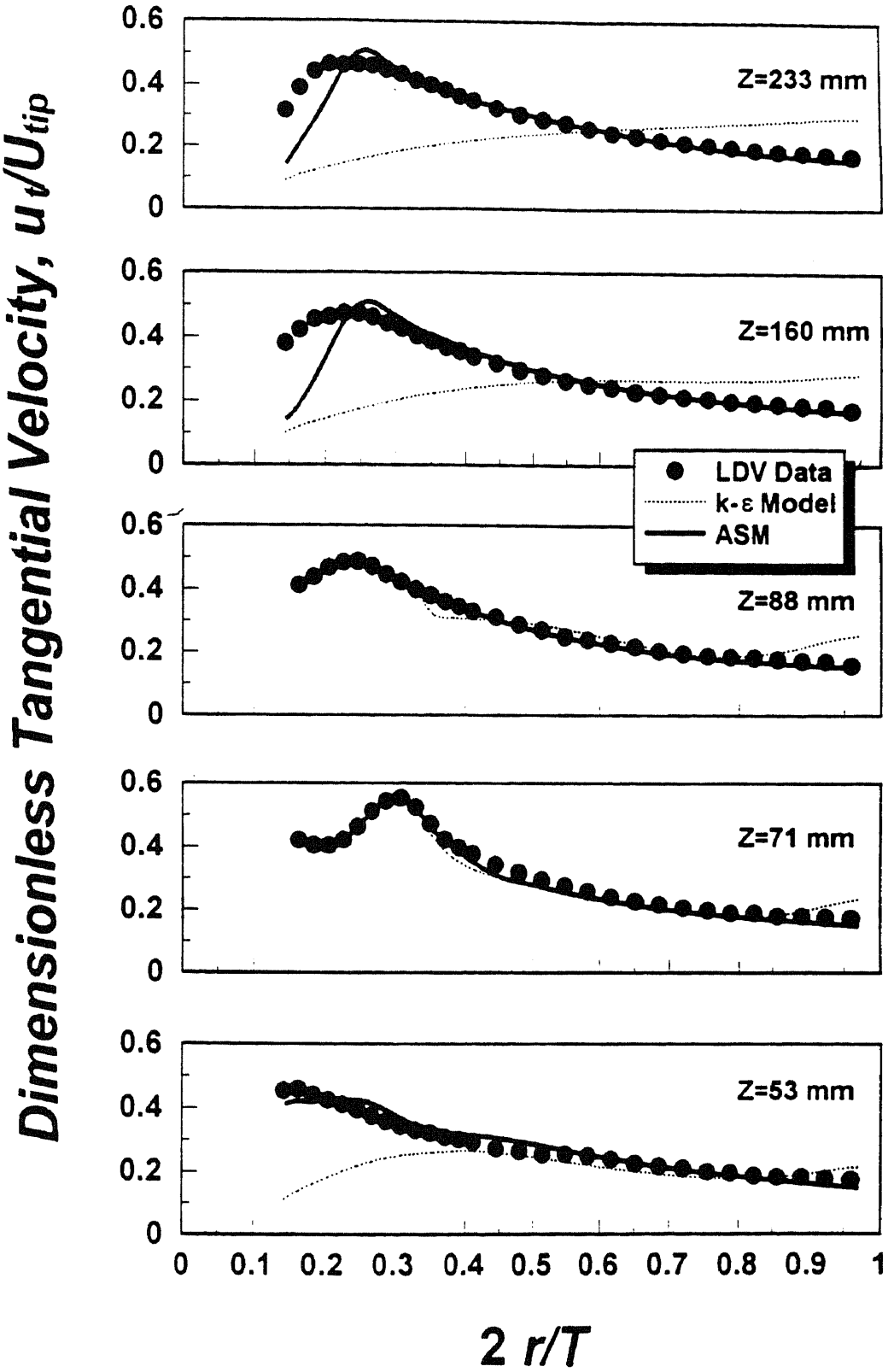

Figure 6-10 Comparison between experimental tangential velocity measurements (via LDV) and numerical predictions (via CFD) (System A, N = 700 rpm)

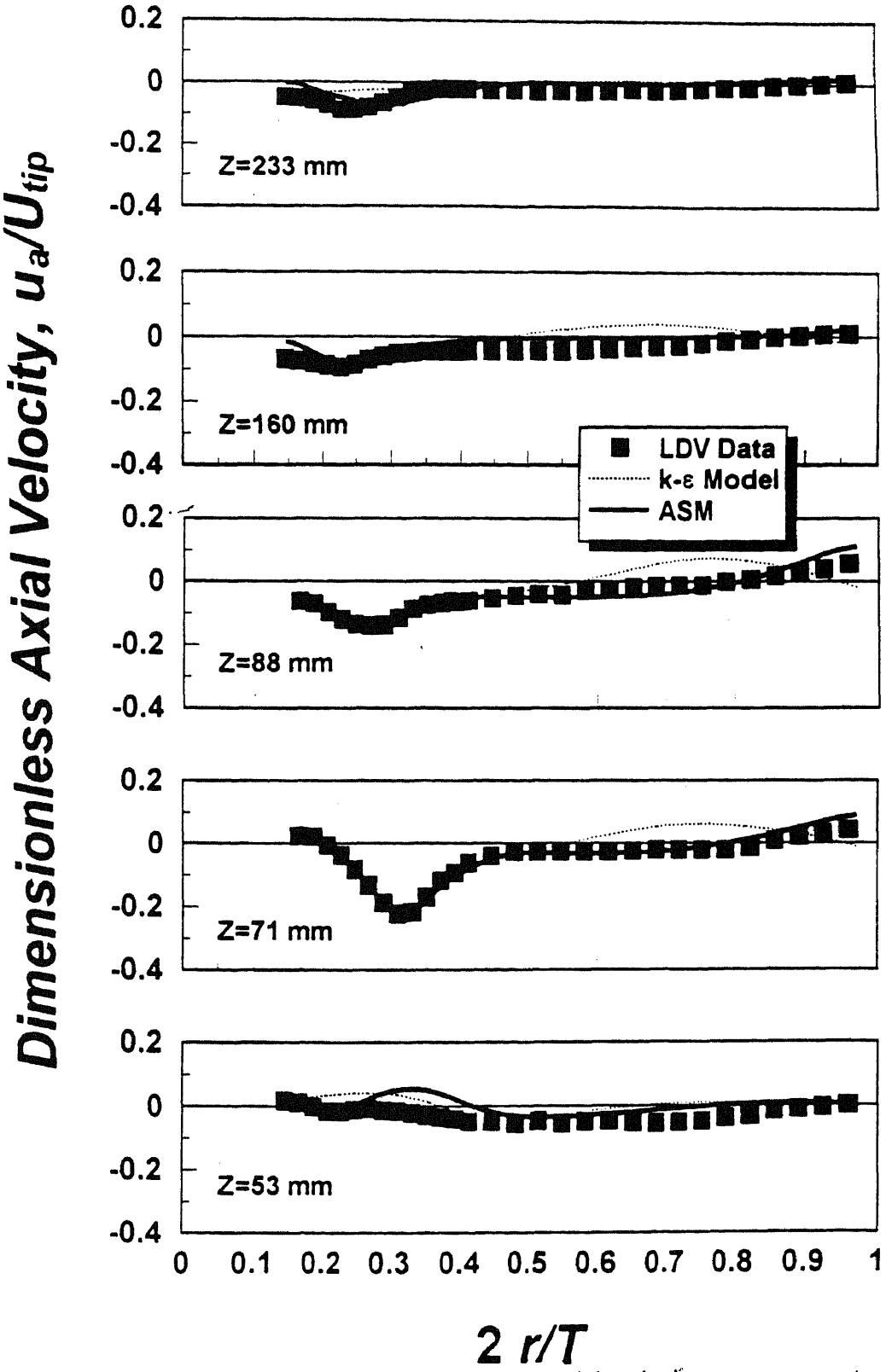

Figure 6-11 Comparison between experimental axial velocity measurements and numerical predictions (System A, N = 700 rpm)

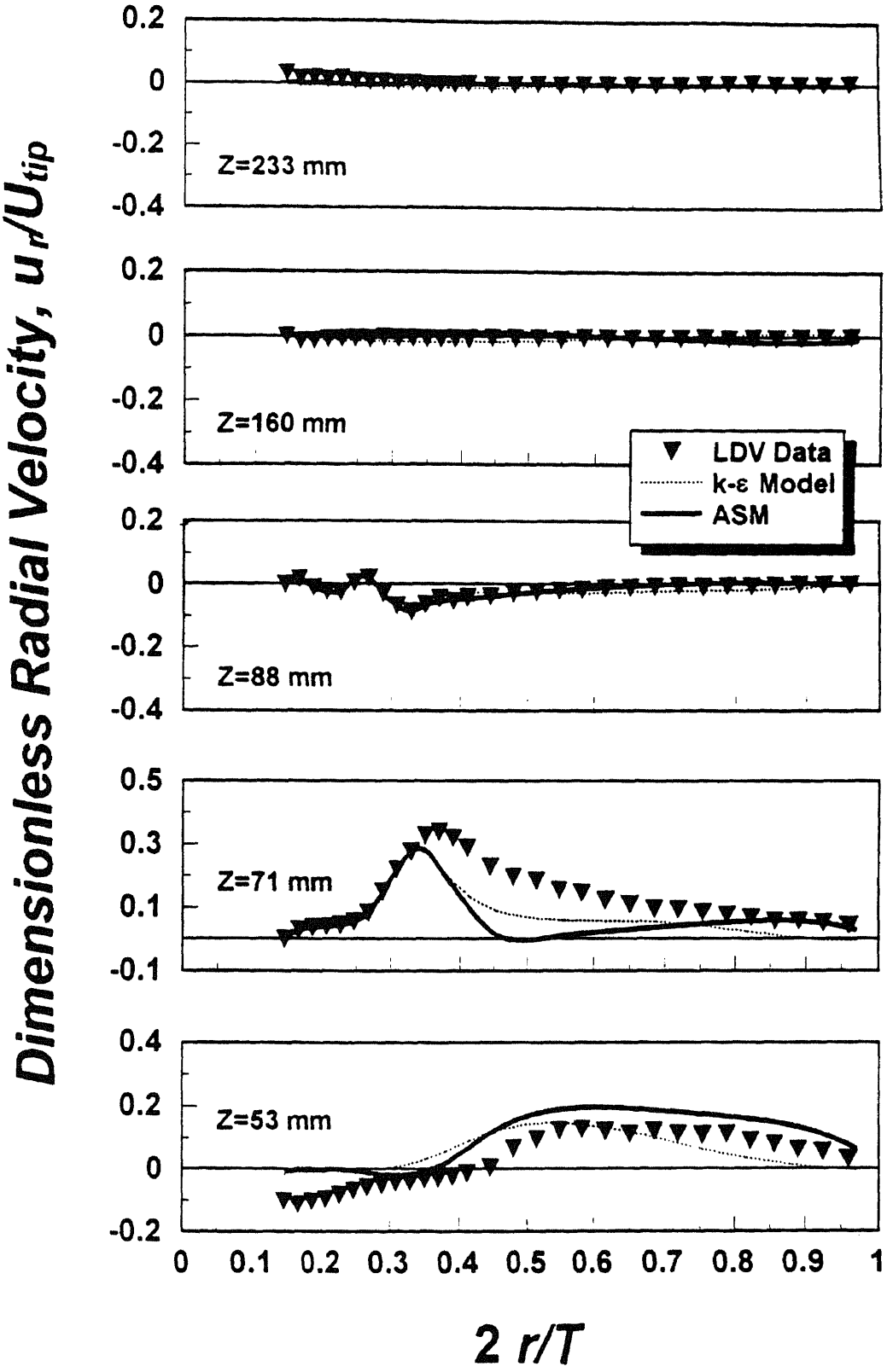

Figure 6-12 Comparison between experimental radial velocity measurements and numerical predictions (System A, N = 700 rpm)

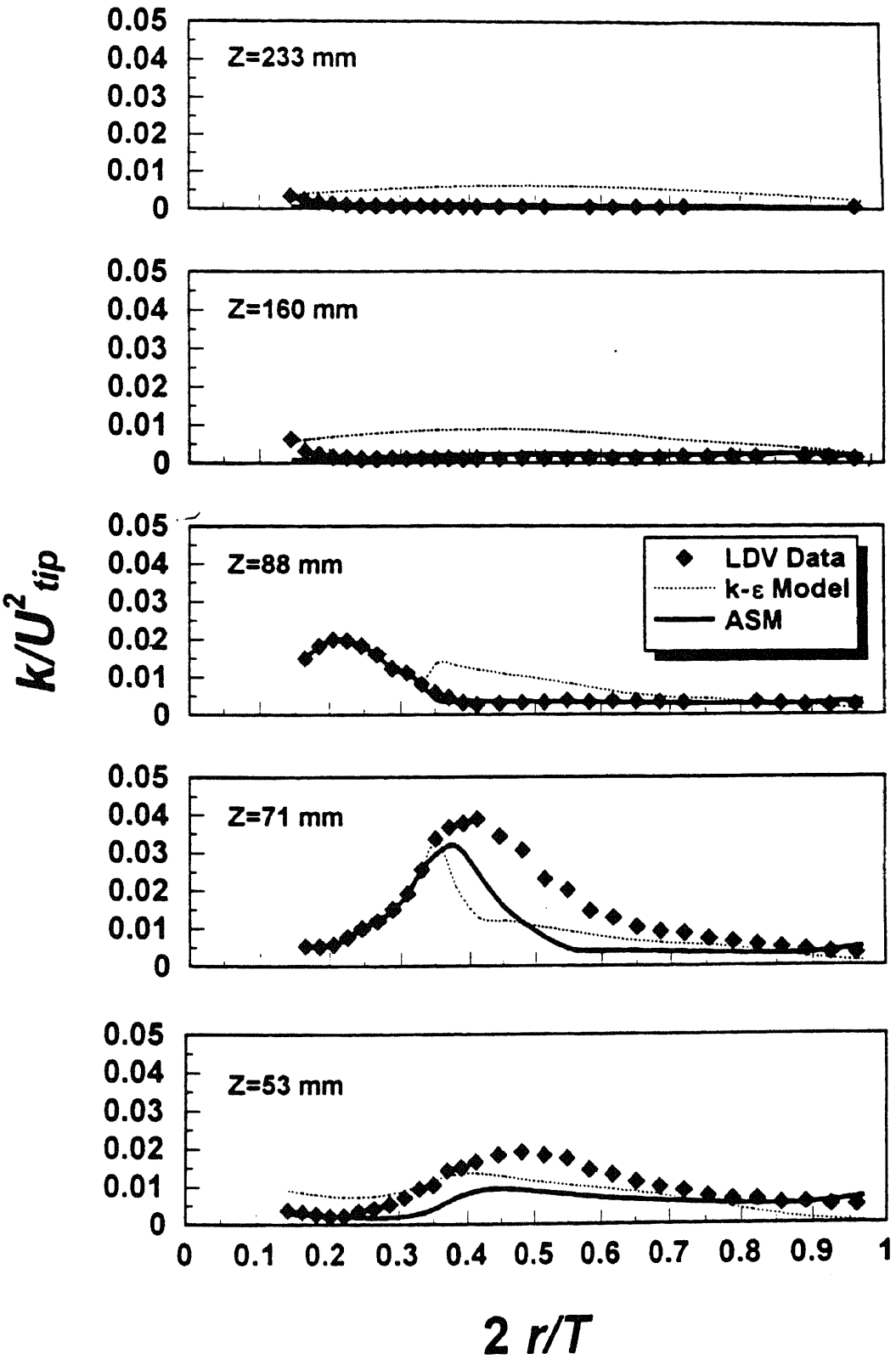

Figure 6-13 Comparison between experimental and numerically predicted turbulent kinetic energies (System A, N = 700 rpm)

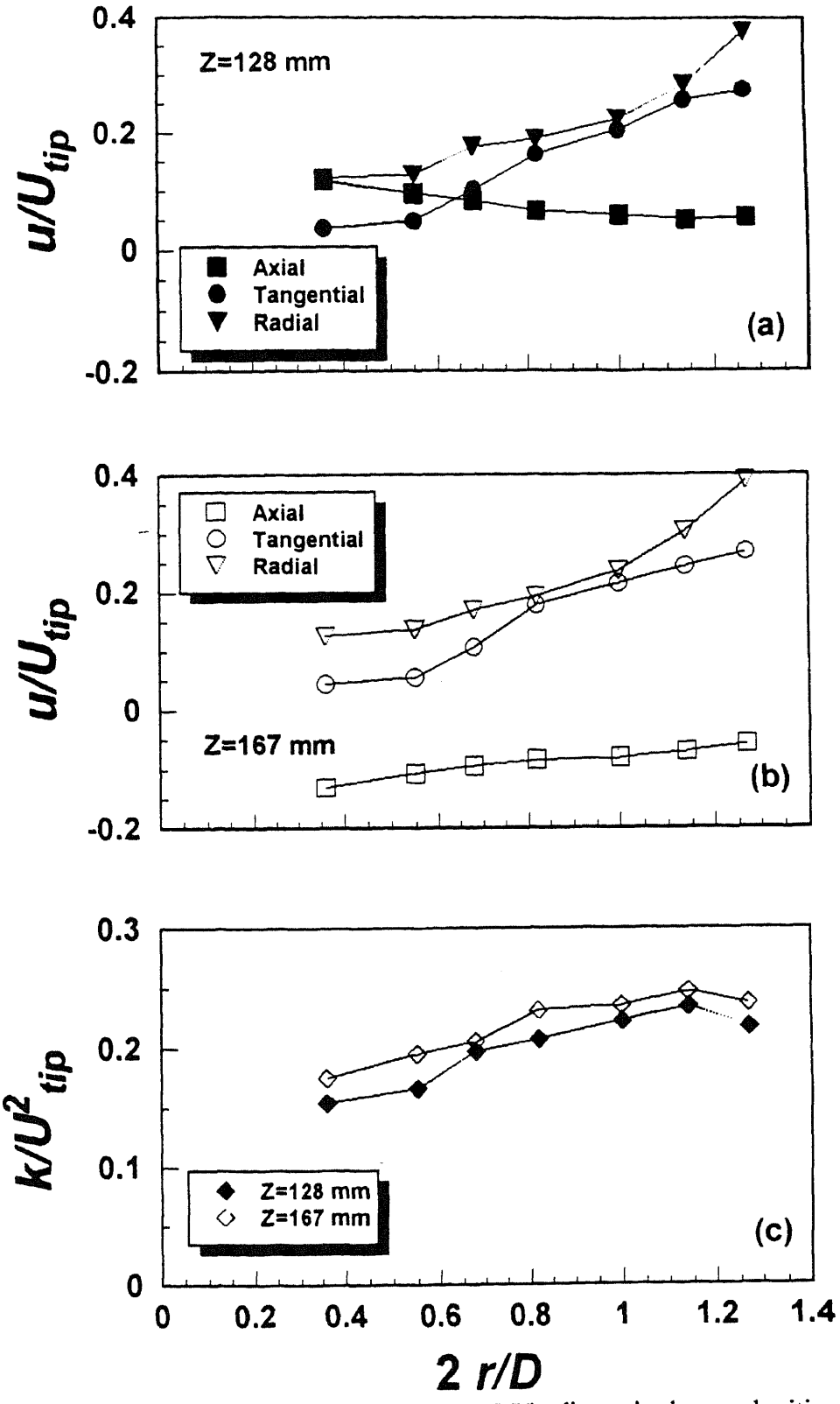

Figure 6-14 Experimentally determined (via LDV) dimensionless velocities and turbulent kinetic energies in the impeller region (System B, $N = 350$ rpm)

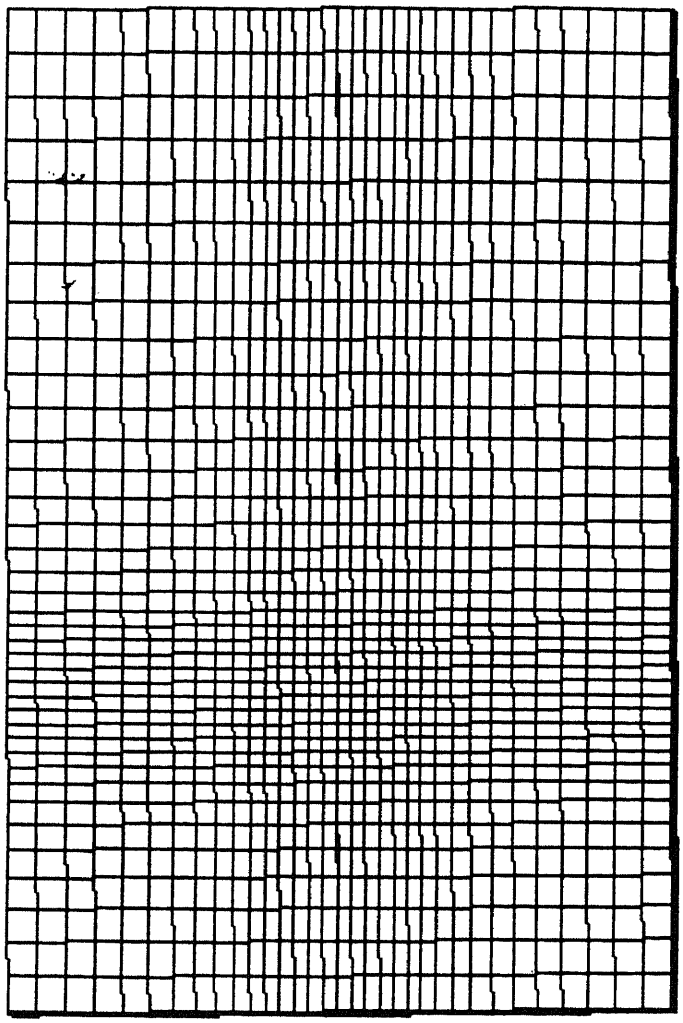

Figure 6-15 Grid used in the CFD simulation for System B (2*D* view)

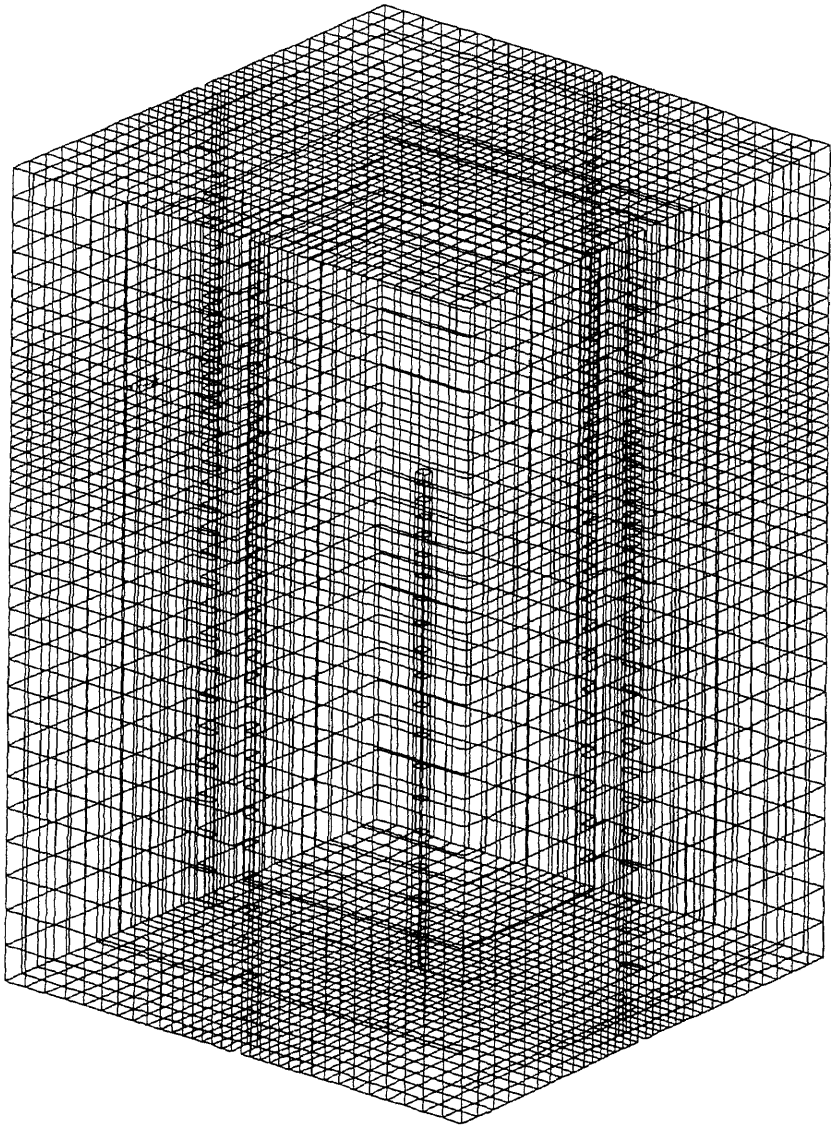

Figure 6-16 Grid used in the CFD simulation for System B (3*D* view)

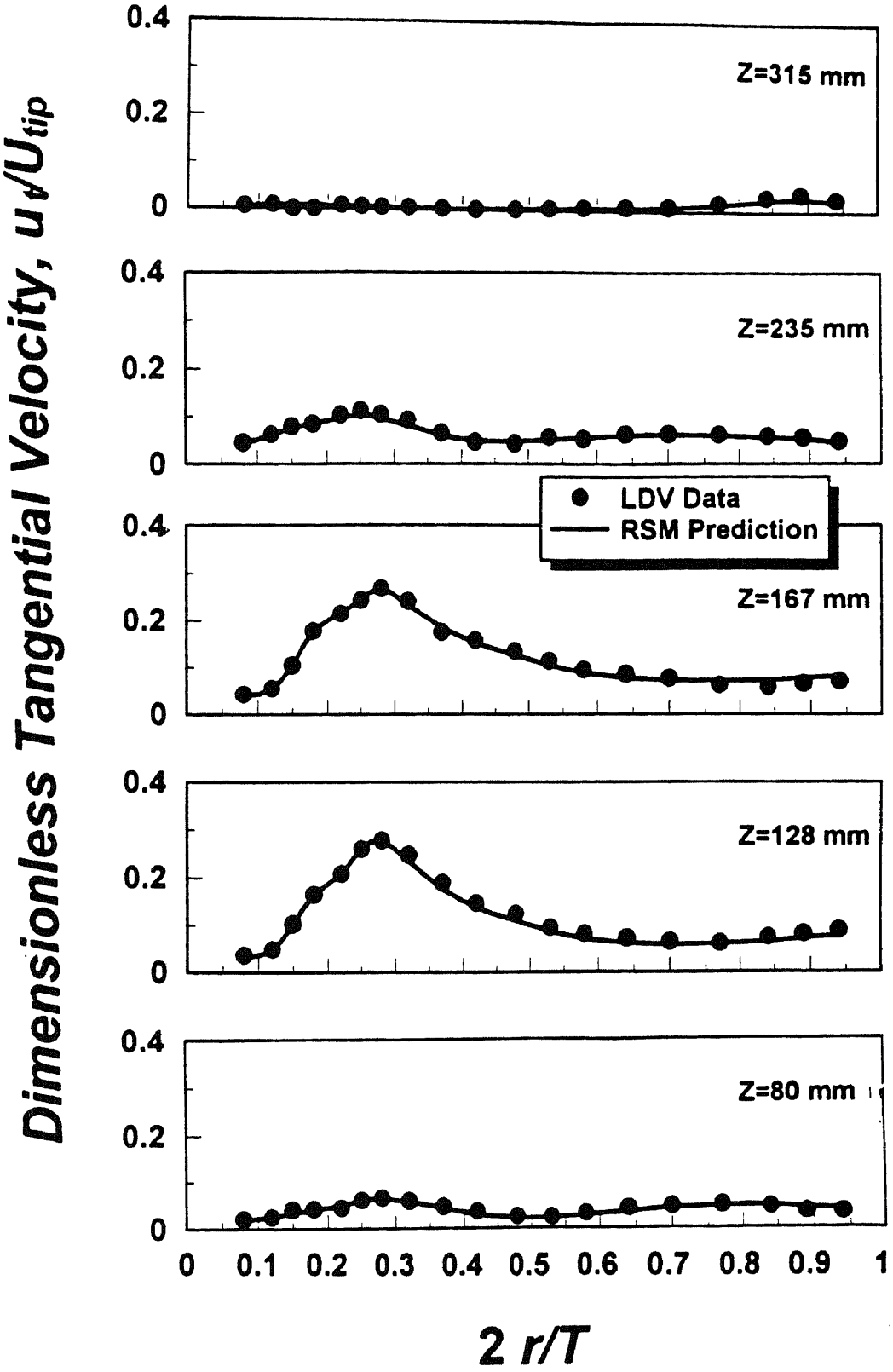

Figure 6-17 Comparison between LDV measurements and CFD predictions: tangential velocity (System B, N = 350 rpm)

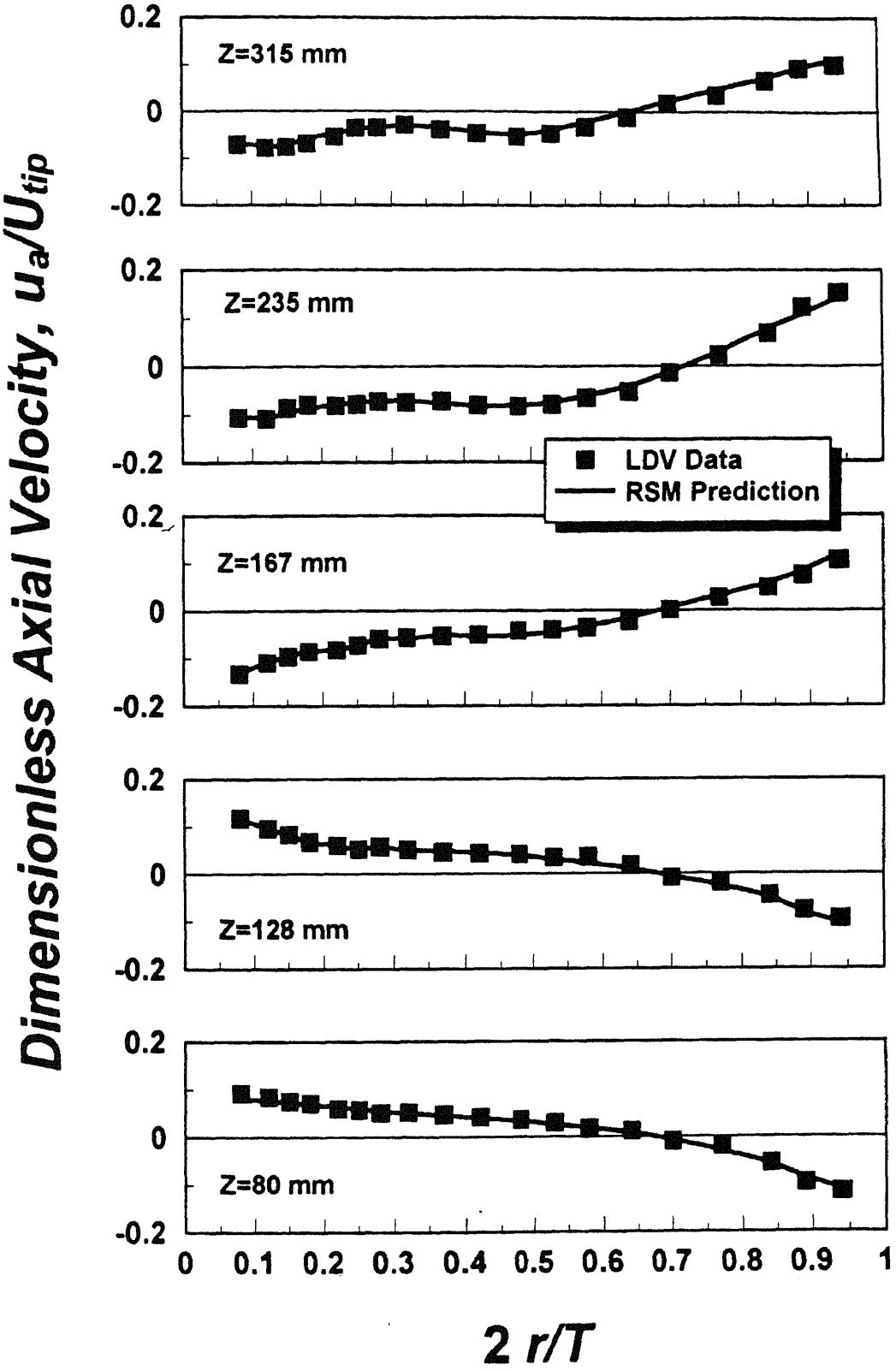

Figure 6-18 Comparison between LDV measurements and CFD predictions: axial velocity (System B, N = 350 rpm)

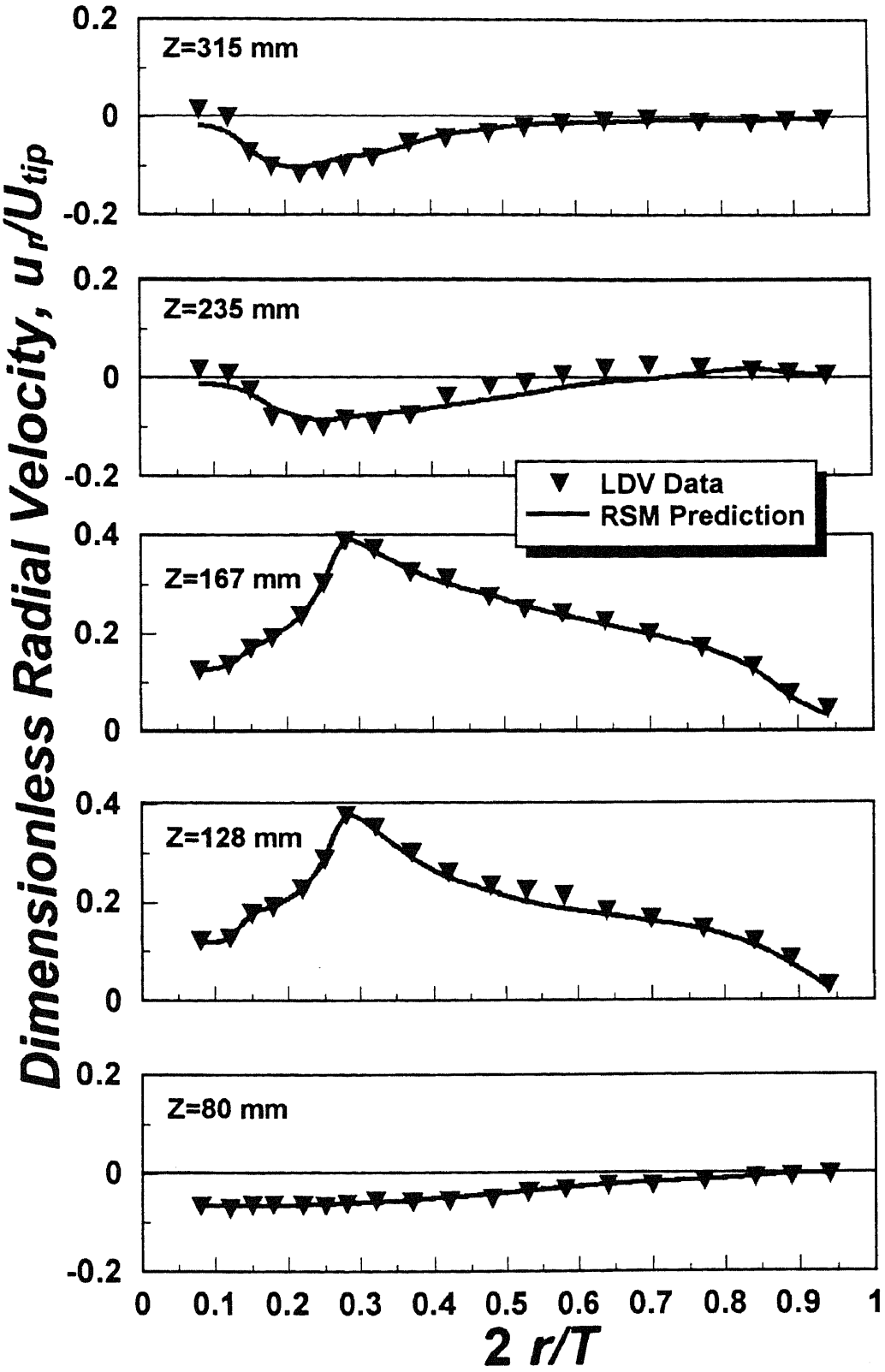

Figure 6-19 Comparison between LDV measurements and CFD predictions: radial velocity (System B, N = 350 rpm)

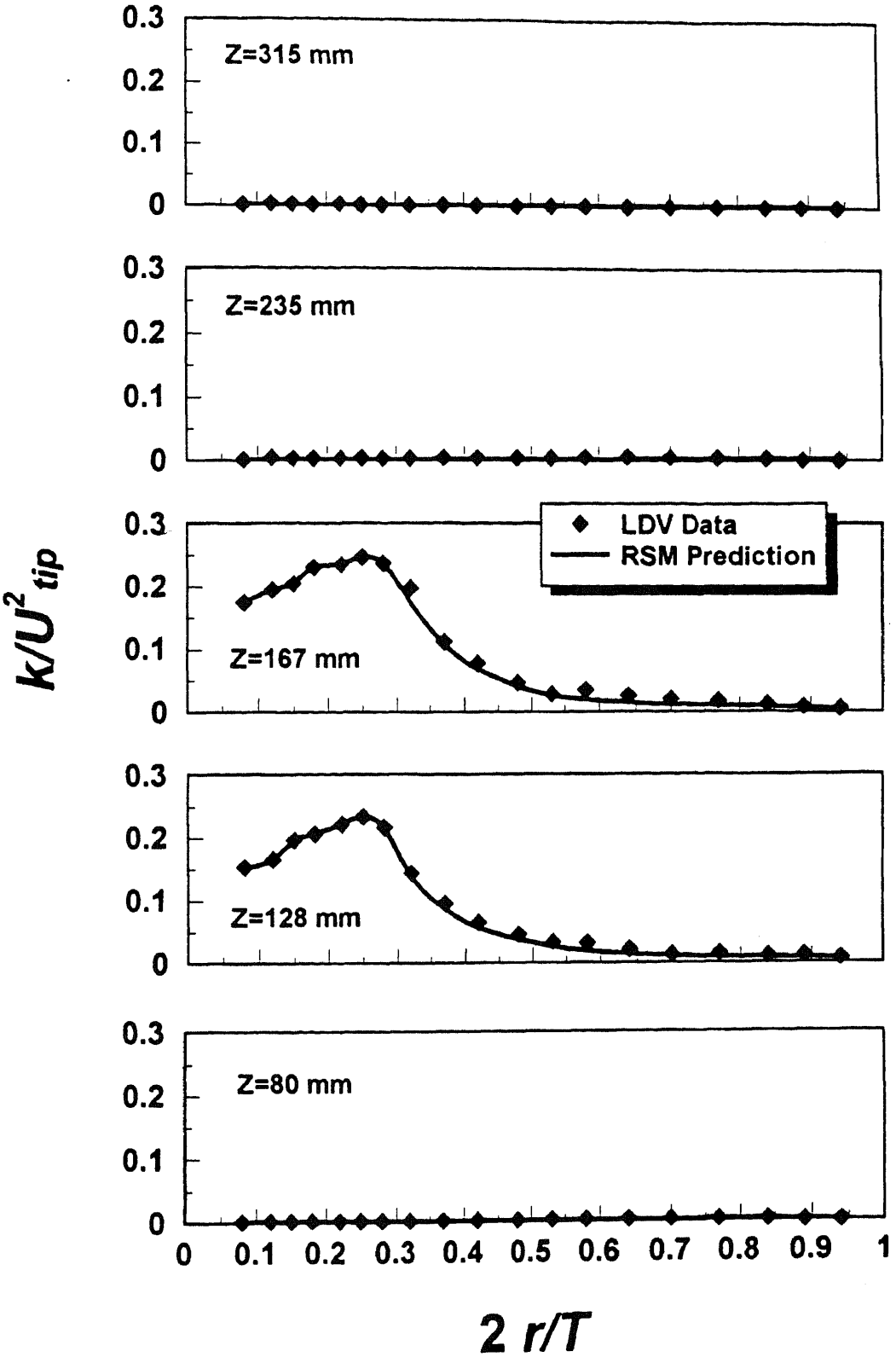

Figure 6-20 Comparison between LDV measurements and CFD predictions: turbulent kinetic energy (System B, N = 350 rpm)

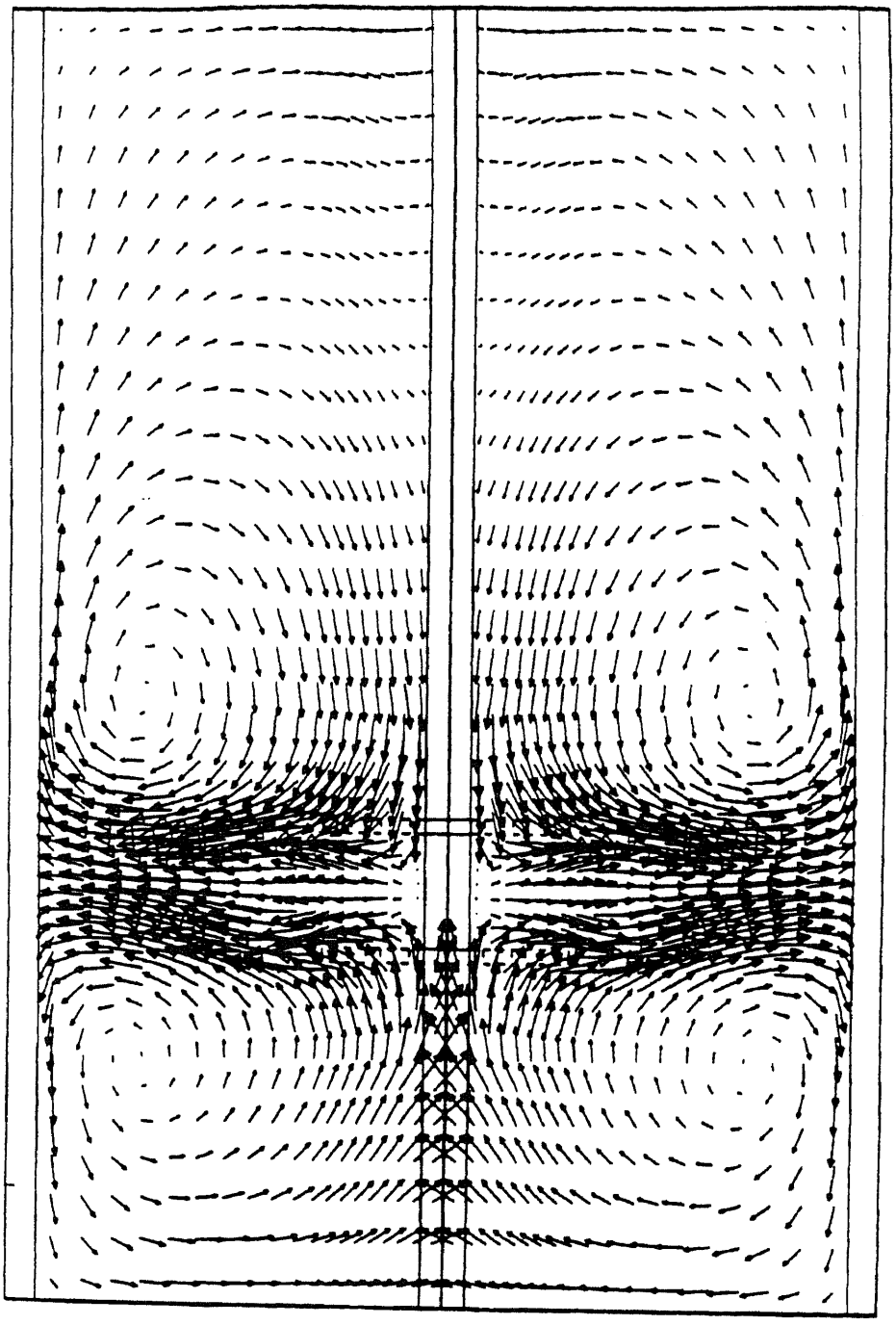

Figure 6-21 CFD prediction of velocity distribution in System B (2*D* view)

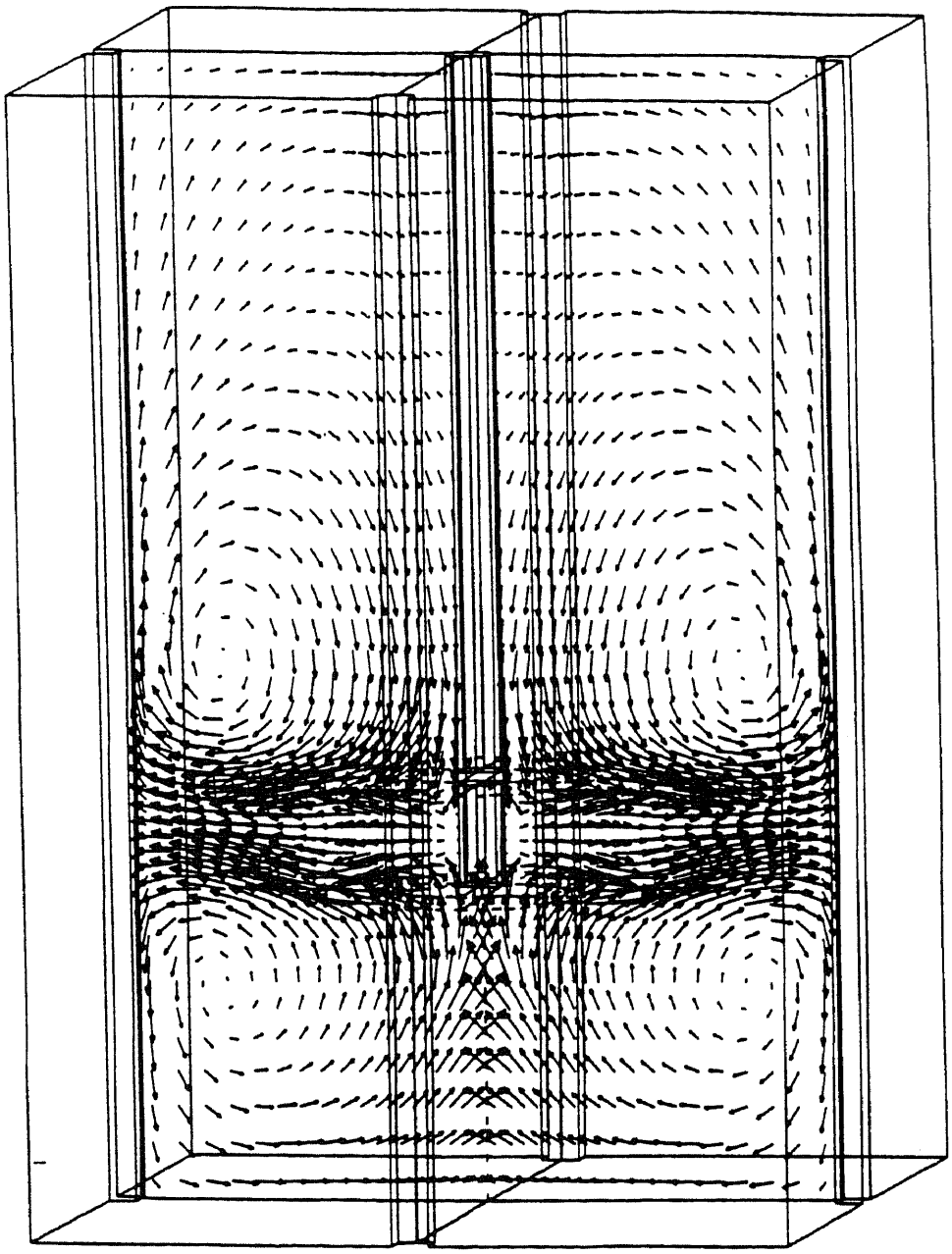

Figure 6-22 CFD prediction of velocity distribution in System B (3*D* view)

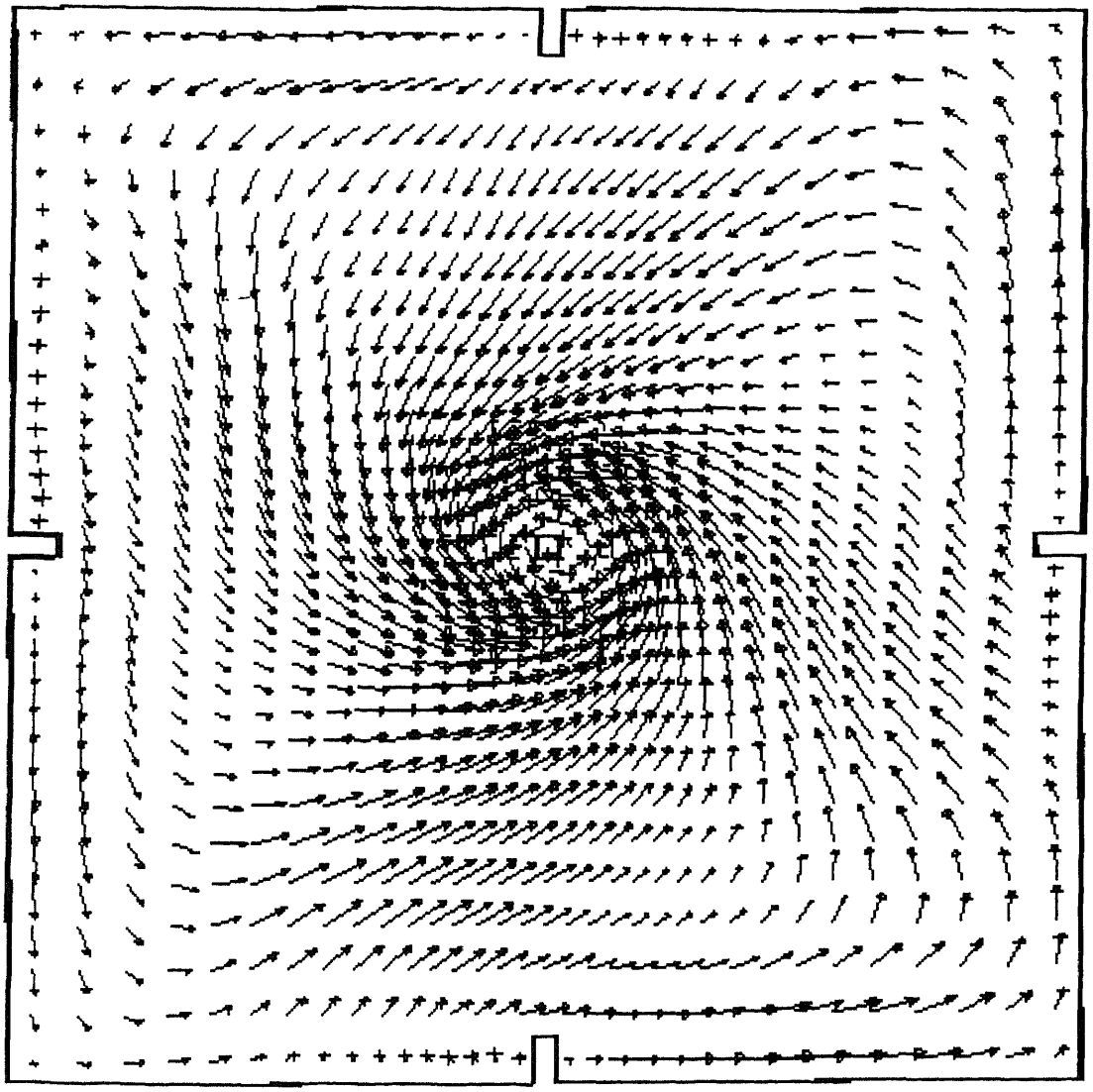

Figure 6-23 CFD prediction of velocity distribution in System B (top view: Z/H = 0.18)

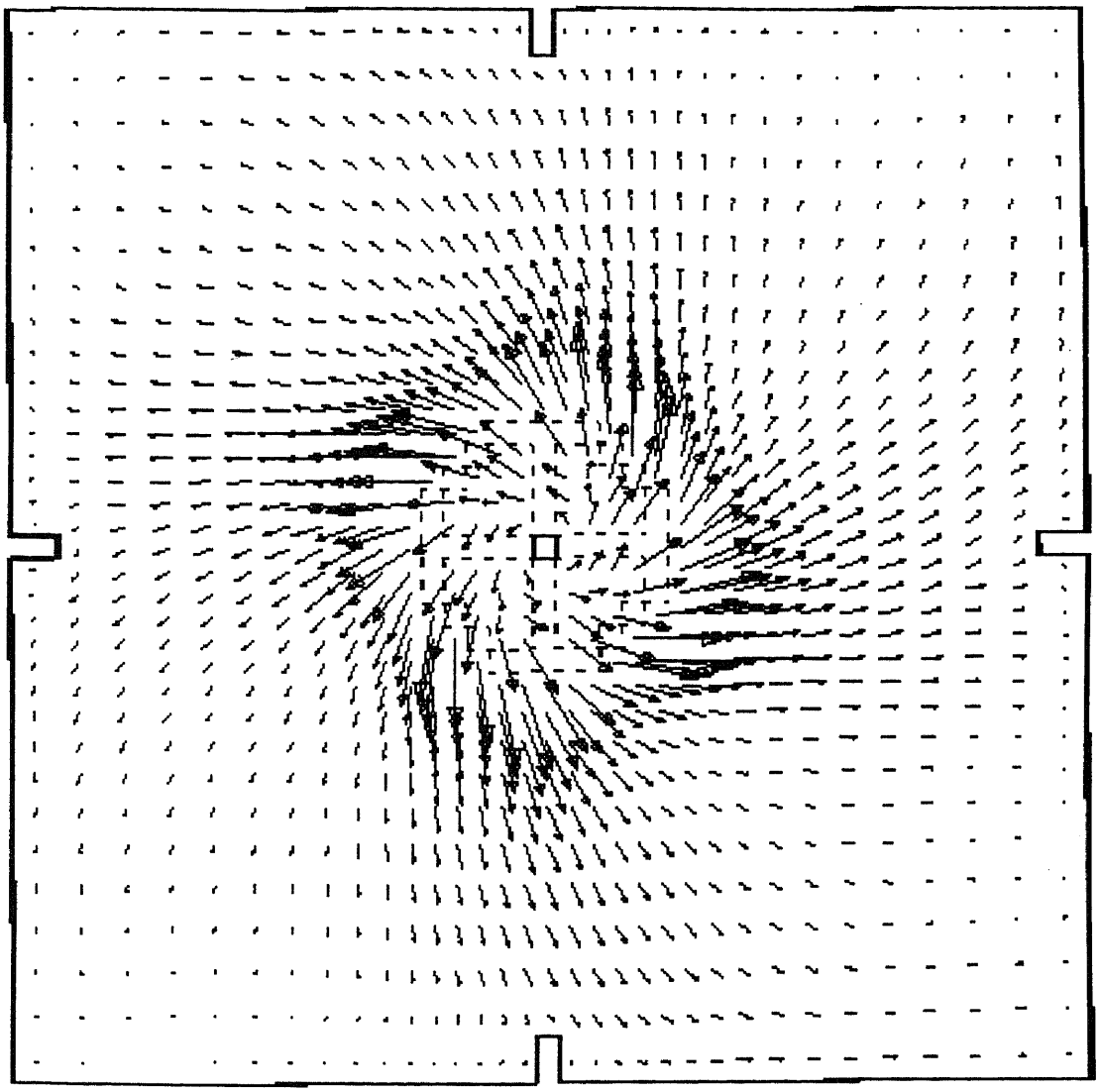

Figure 6-24 CFD prediction of velocity distribution in System B (top view: Z/H = 0.37)

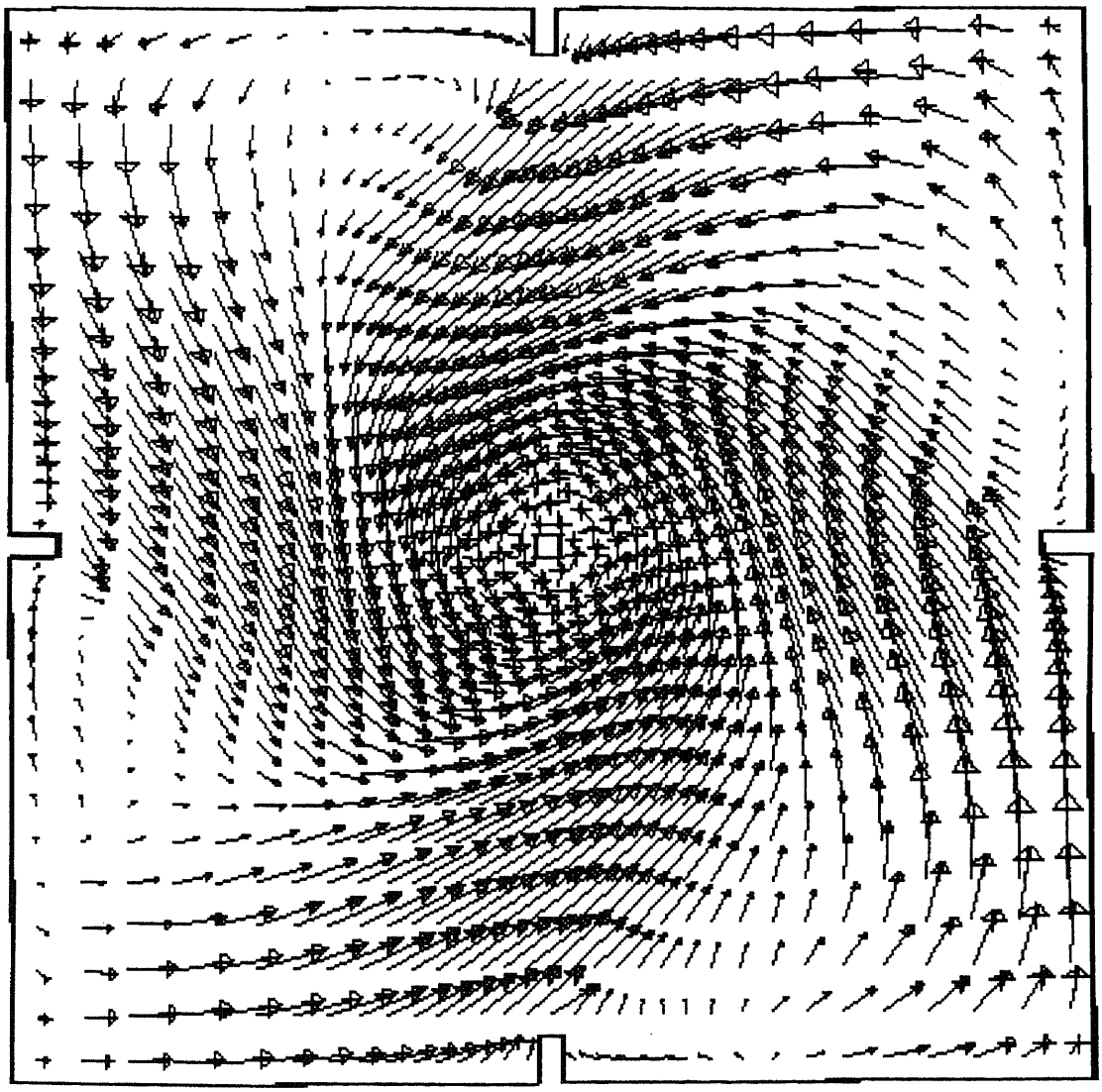

Figure 6-25 CFD prediction of velocity distribution in System B (top view: Z/H = 0.70)

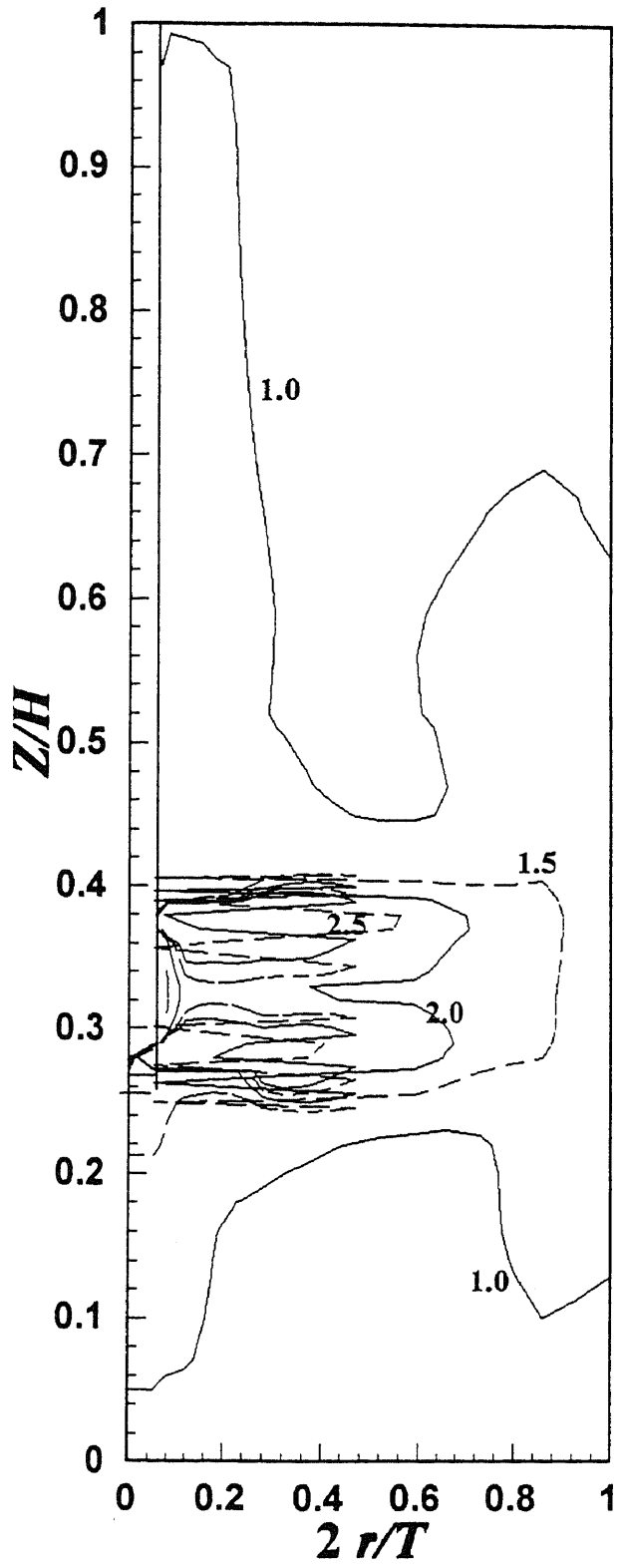

Figure 6-26 CFD prediction of velocity gradient distribution in System B (by complete definition of local velocity gradient, curve labels give the value of $\log_{10}G$)

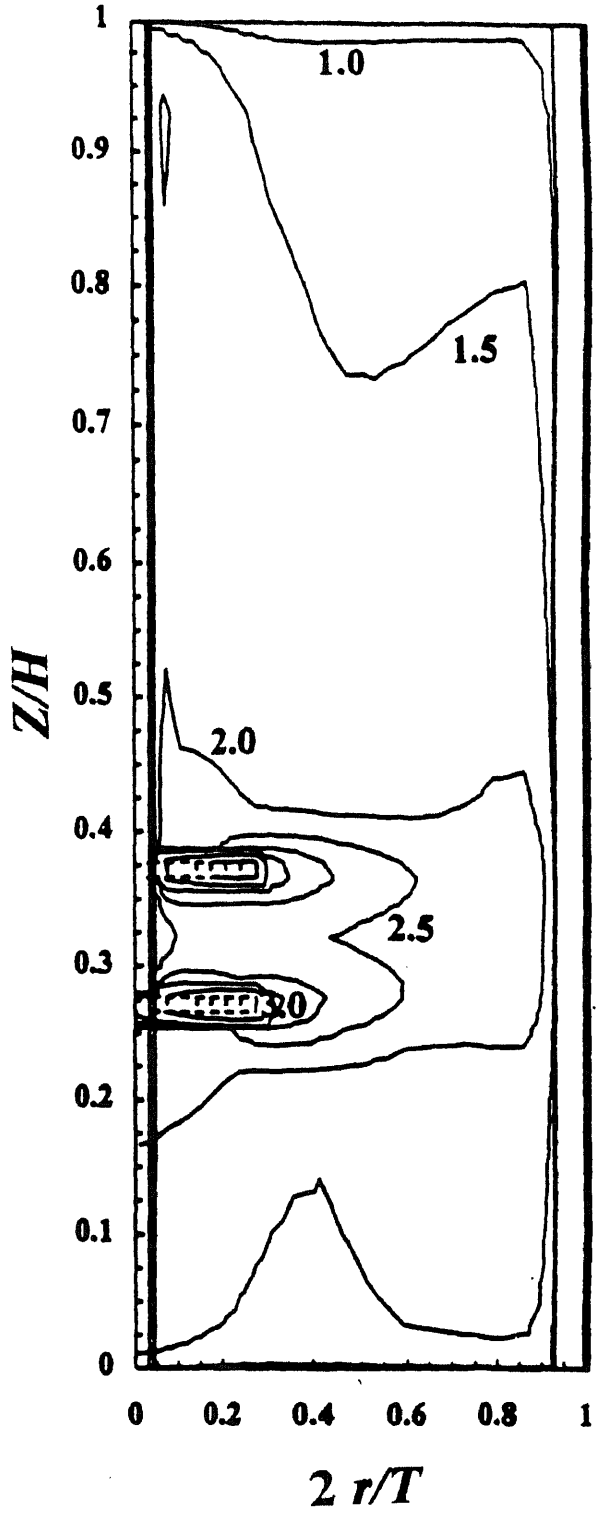

Figure 6-27 CFD prediction of velocity gradient distribution in System B (by local energy dissipation method, curve labels give the value of $\log_{10}G$)

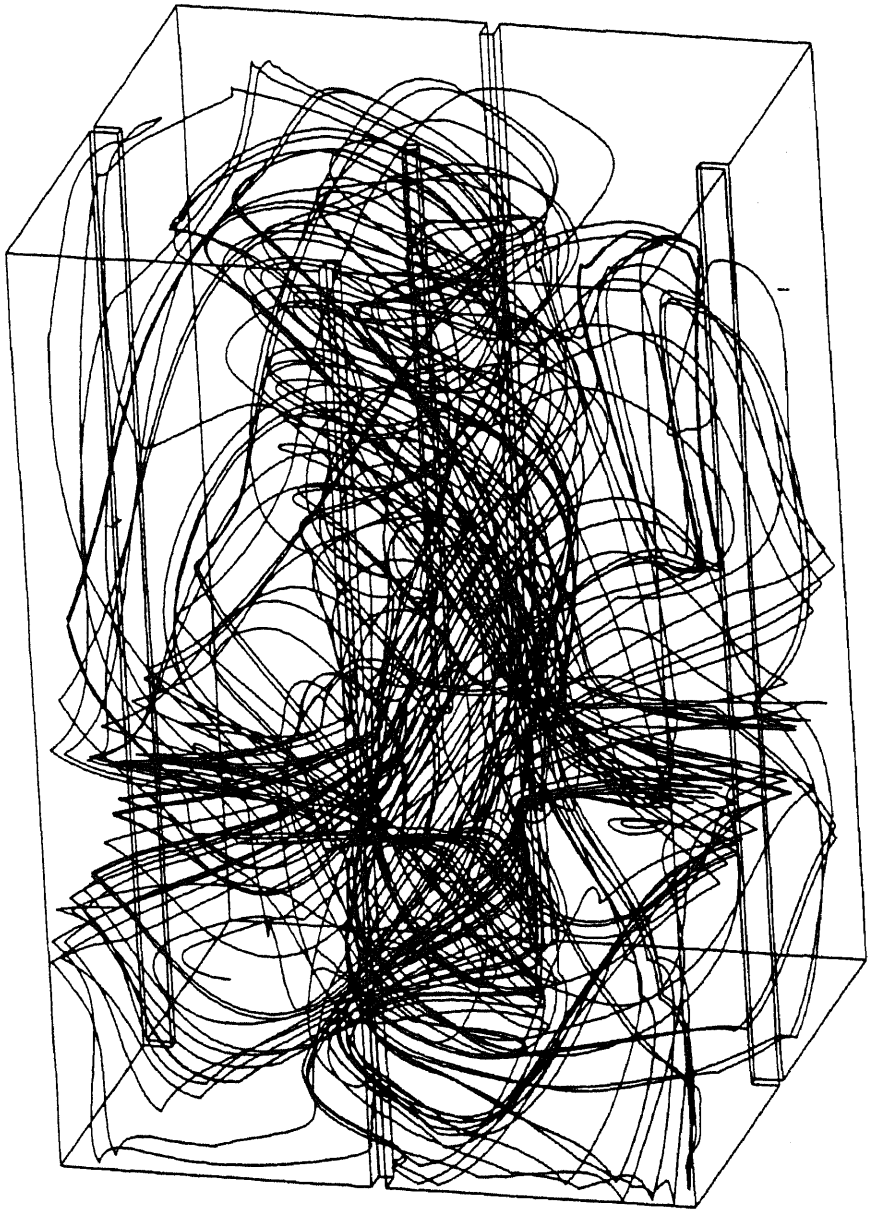

Figure 6-28 CFD prediction of particle trajectory in System B (t = 2,000 s)

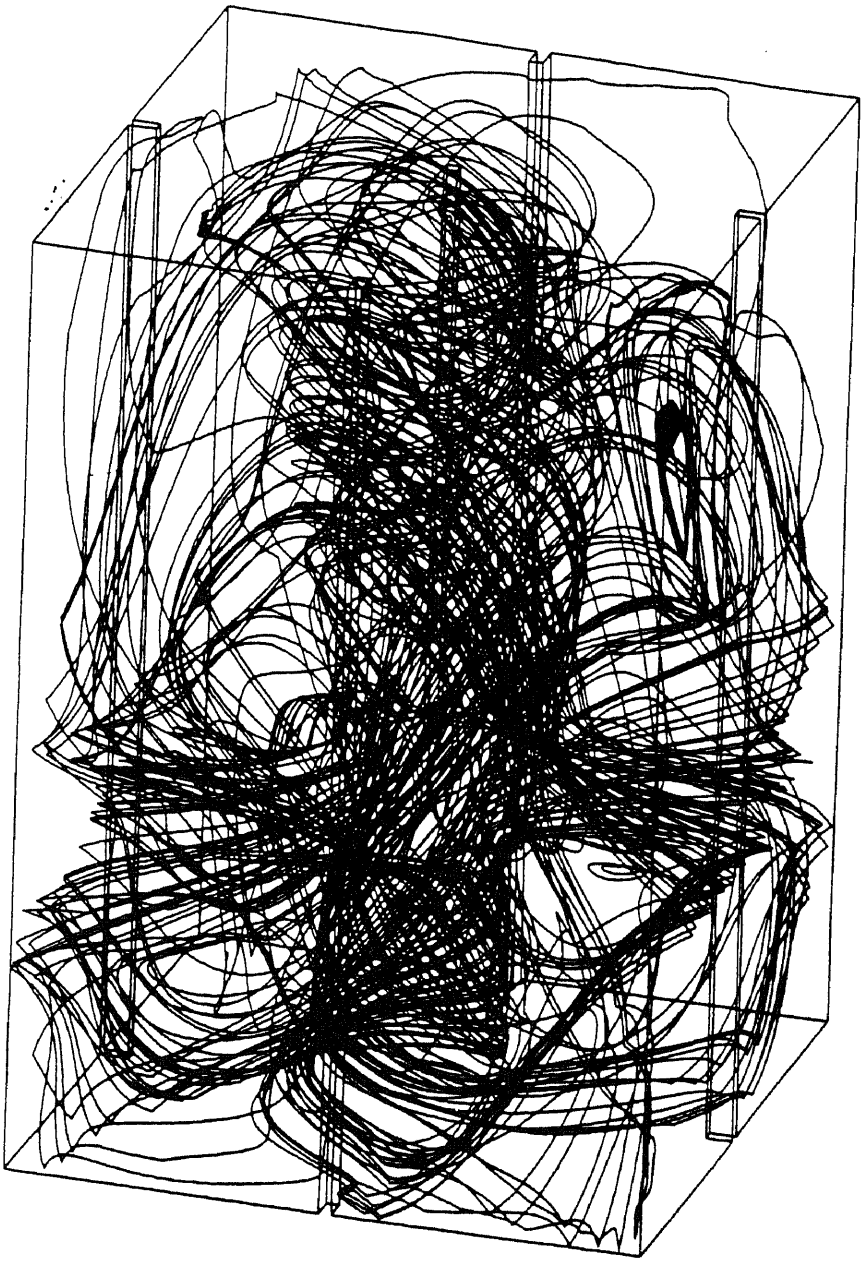

Figure 6-29 CFD prediction of particle trajectory in System B (t = 10,000 s)

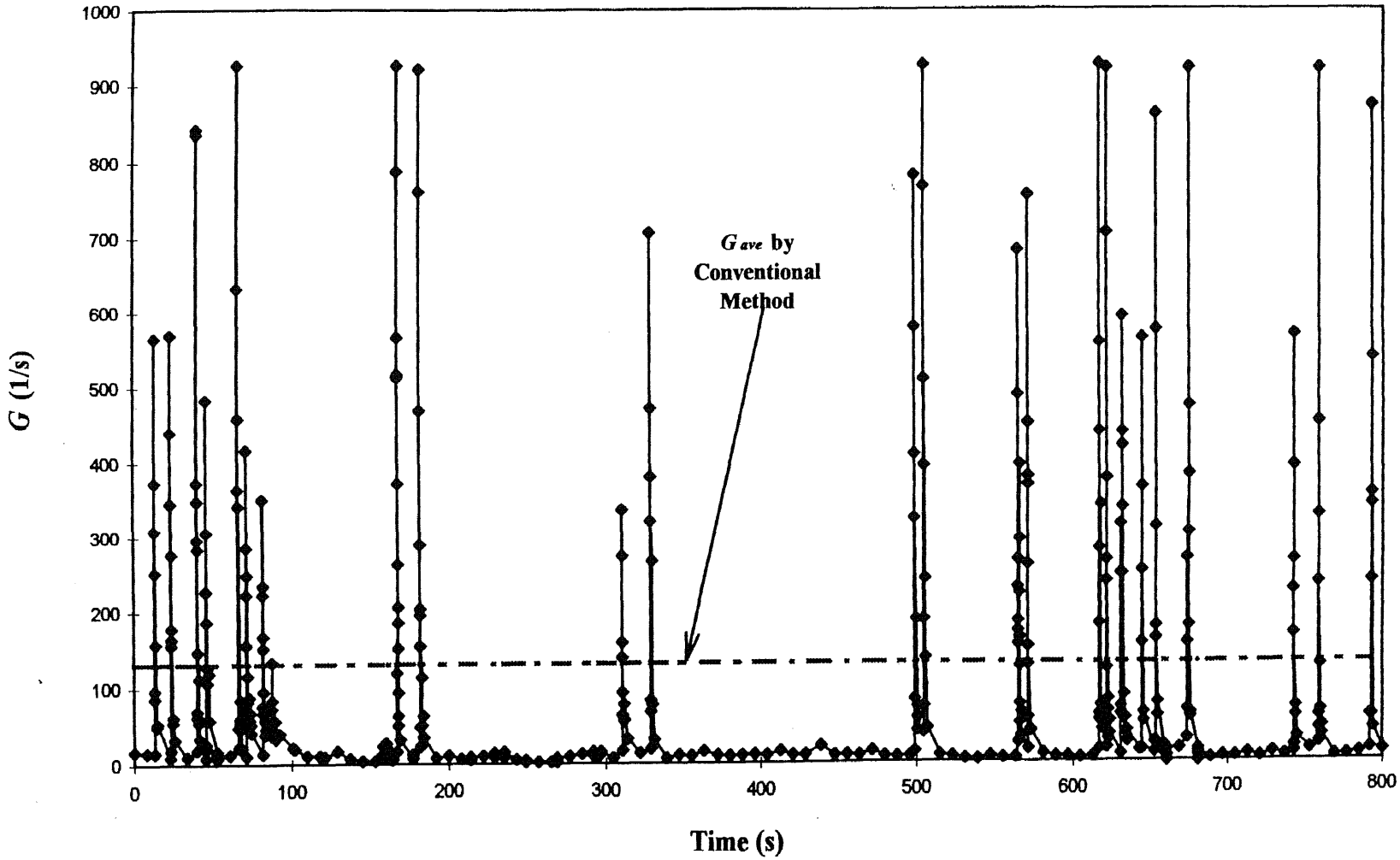

Figure 6-30 G value along the particle trajectory in System B

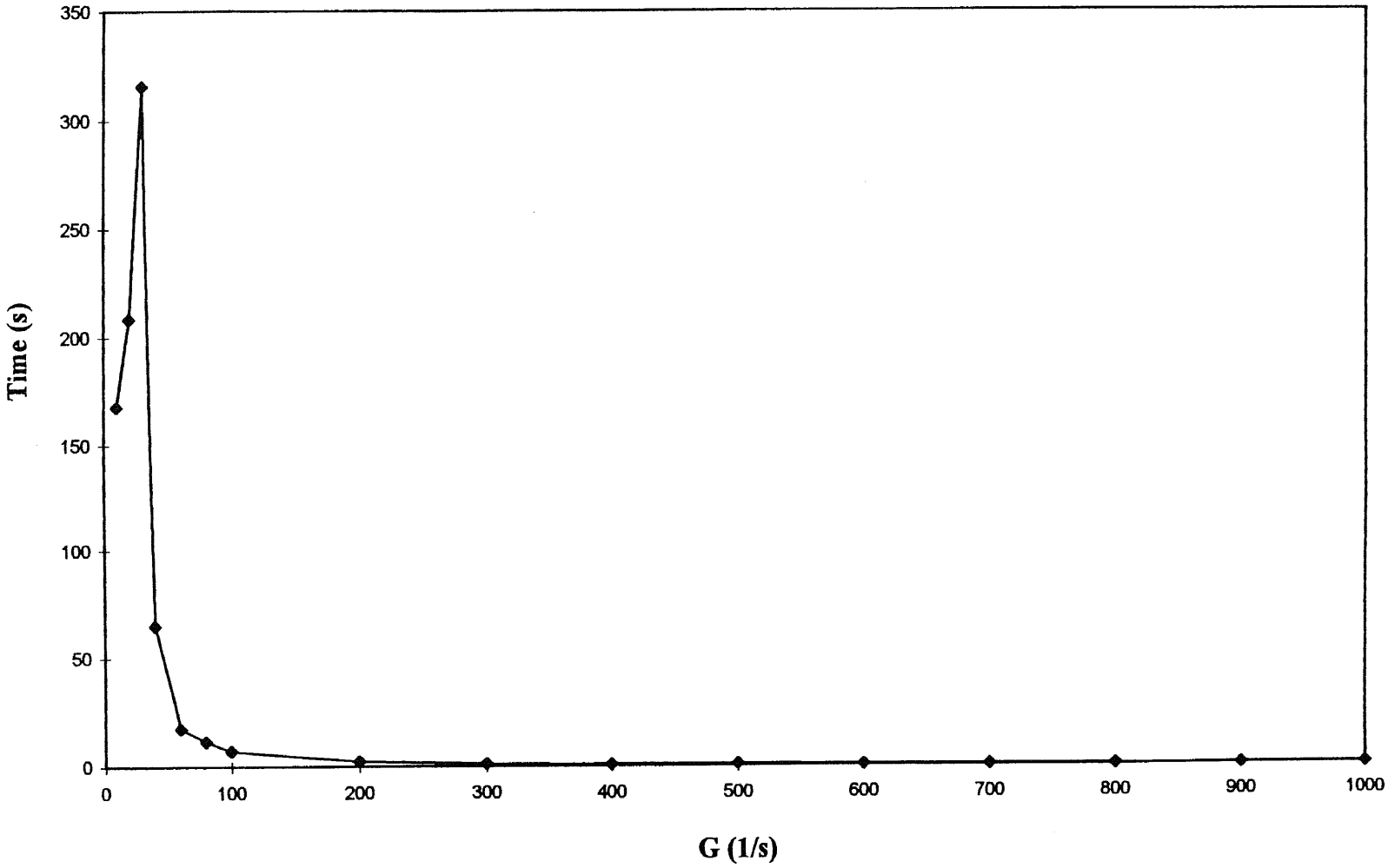

Figure 6-31 *G* value distribution curve along the particle trajectory in System B

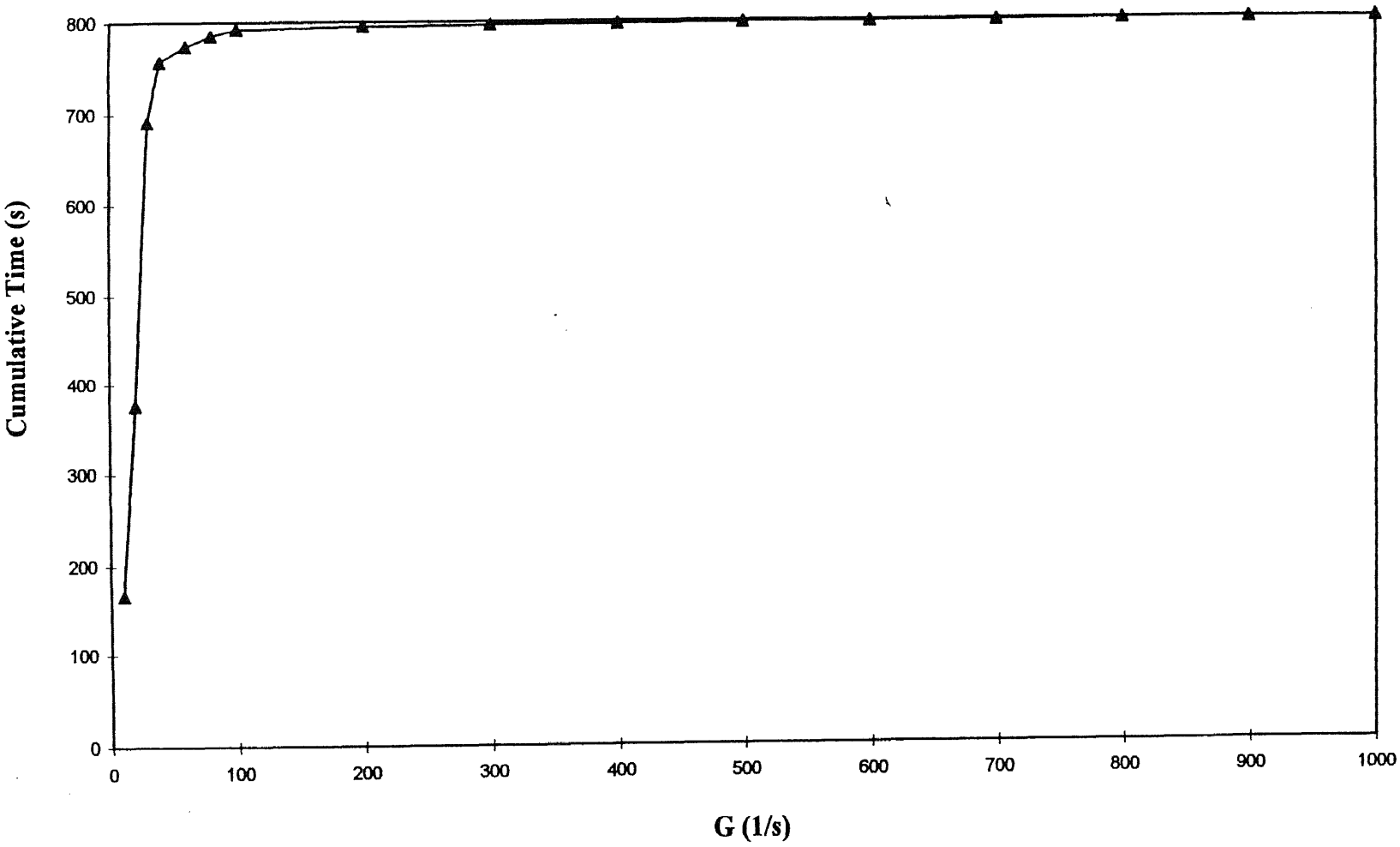

Figure 6-32 Cumulative G value distribution curve along the particle trajectory in System B

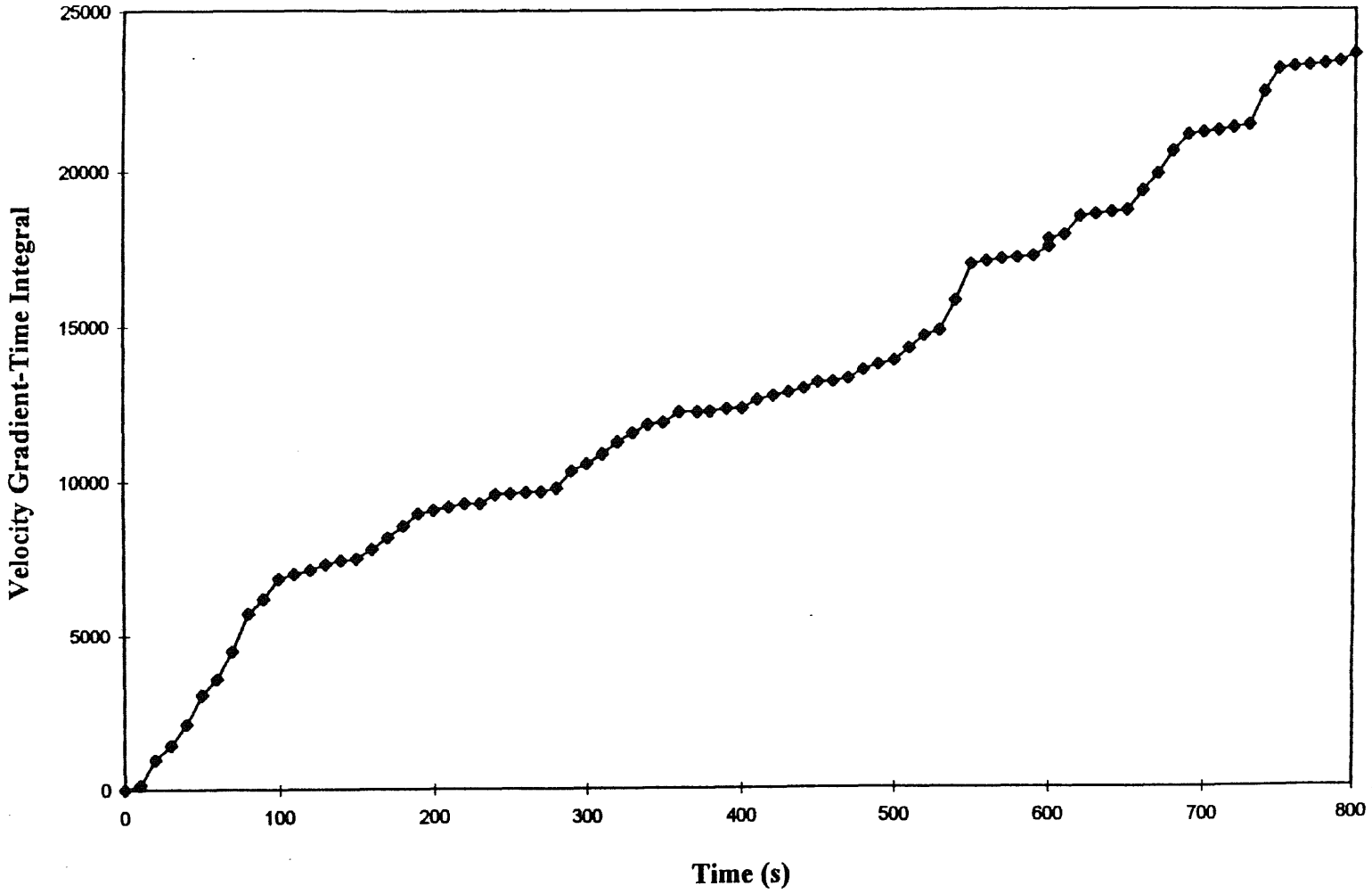

Figure 6-33 Numerical integration of (t * G) vs. time (along the particle trajectory) in System B

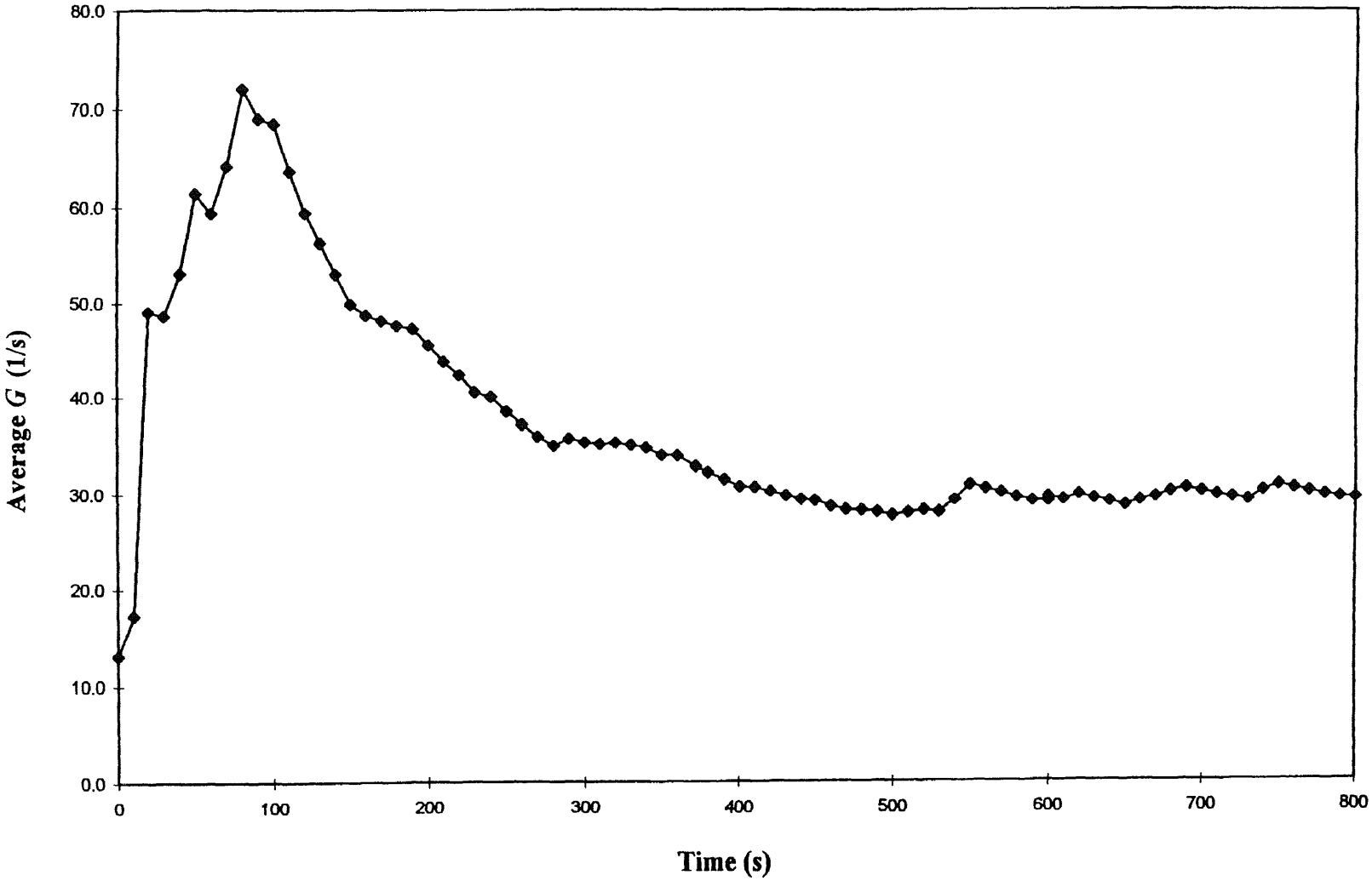

Figure 6-34 Average G value vs. time (along the particle trajectory) in System B

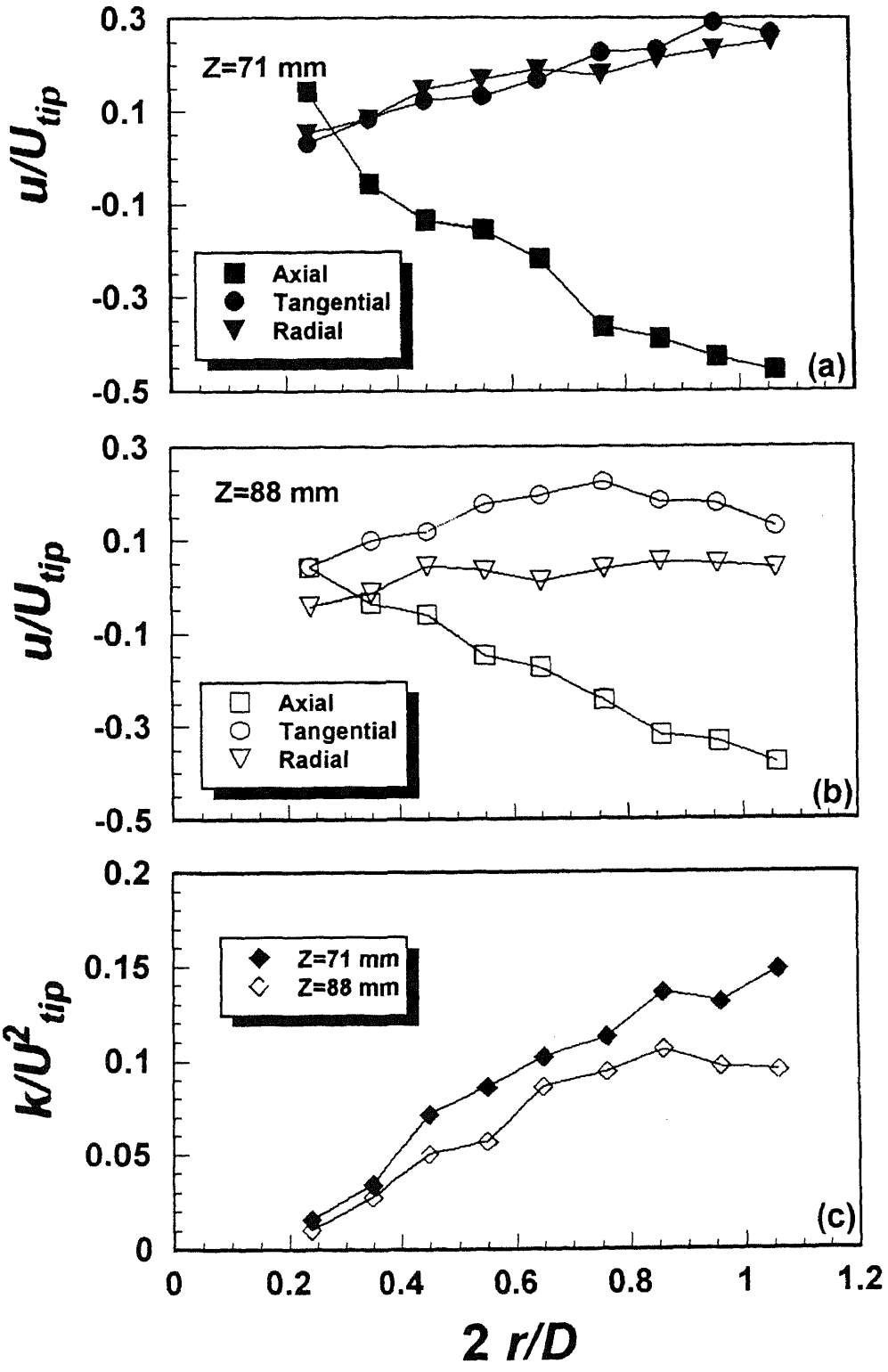

Figure 6-35 Experimentally determined (via LDV) dimensionless velocities and turbulent kinetic energies in the impeller region (System C1, $N = 159$ rpm)

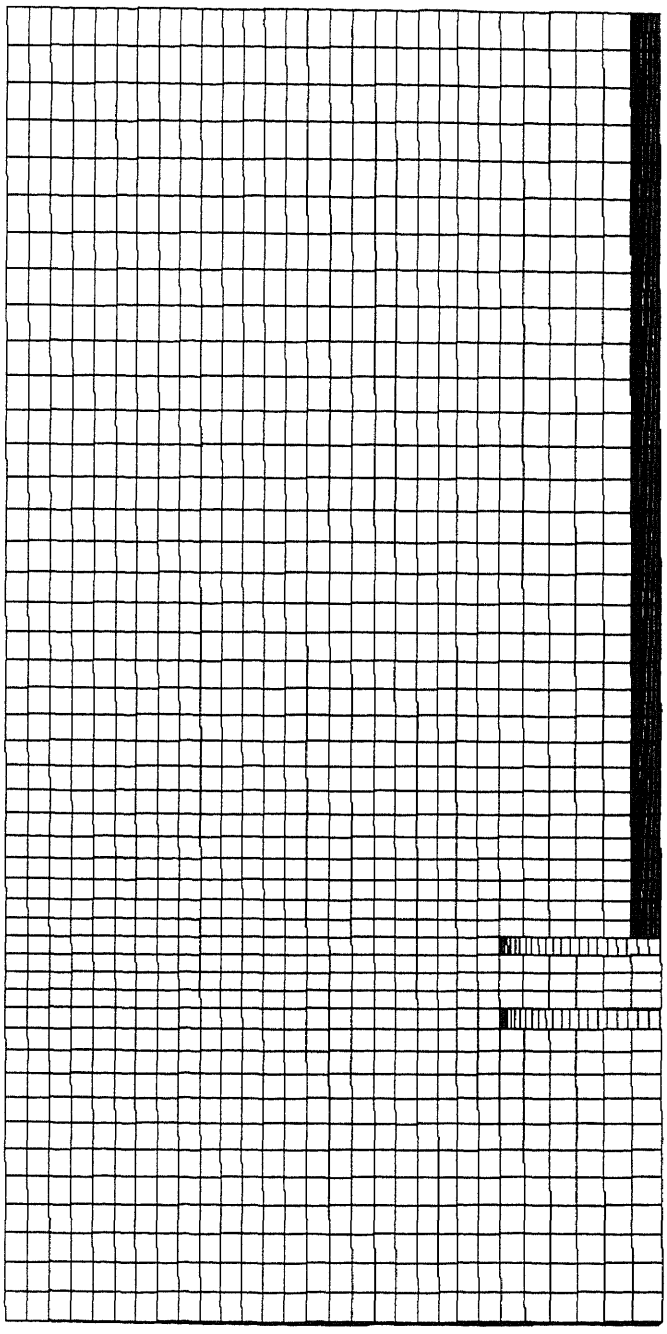

Figure 6-36 Grid used in the CFD simulation for System C1 and C2 (2*D* view)

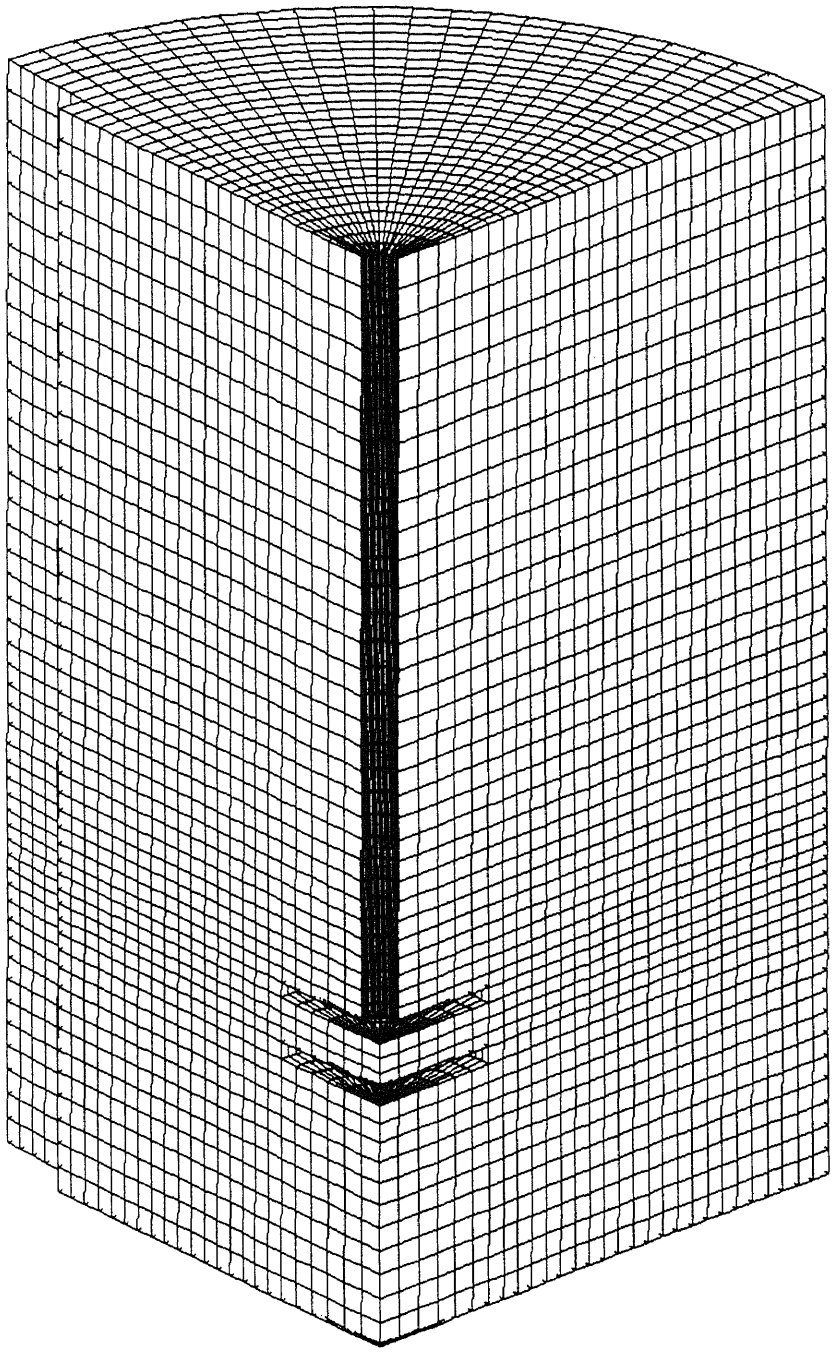

Figure 6-37 Grid used in the CFD simulation for System C1 and C2 (3*D* view)

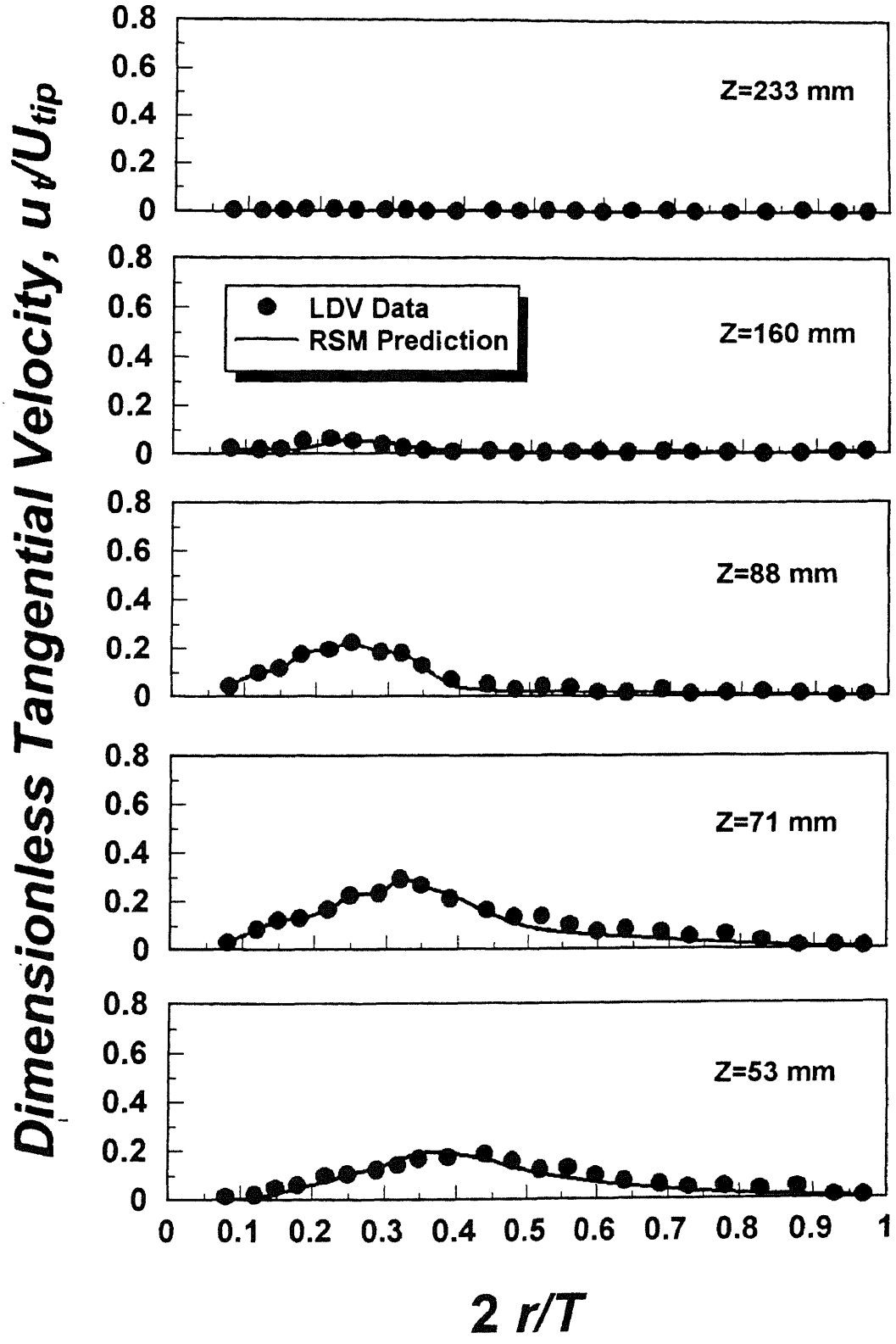

Figure 6-38 Comparison between LDV measurements and CFD predictions: tangential velocity (System C1, N = 159 rpm)

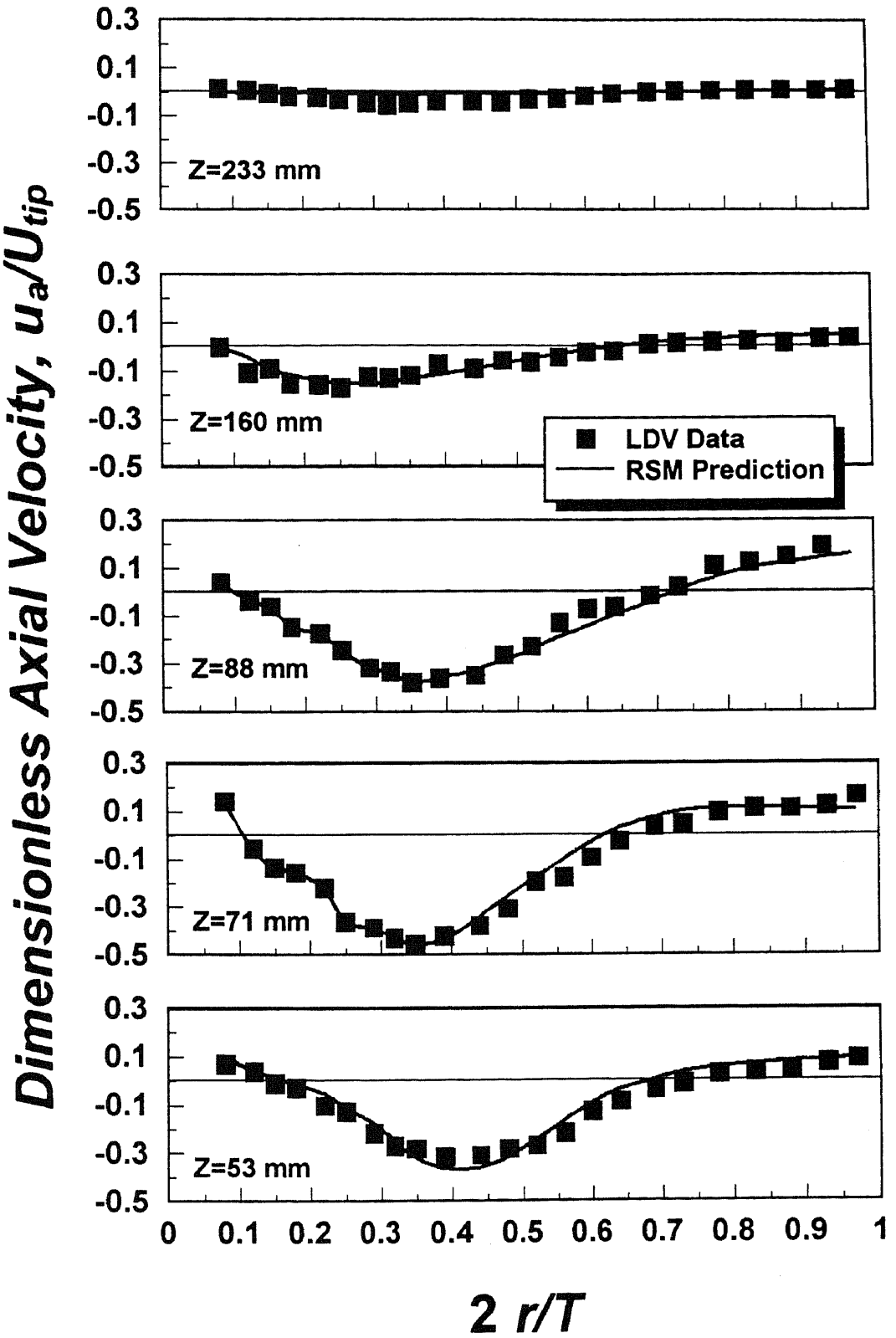

Figure 6-39 Comparison between LDV measurements and CFD predictions: axial velocity (System C1, N = 159 rpm)

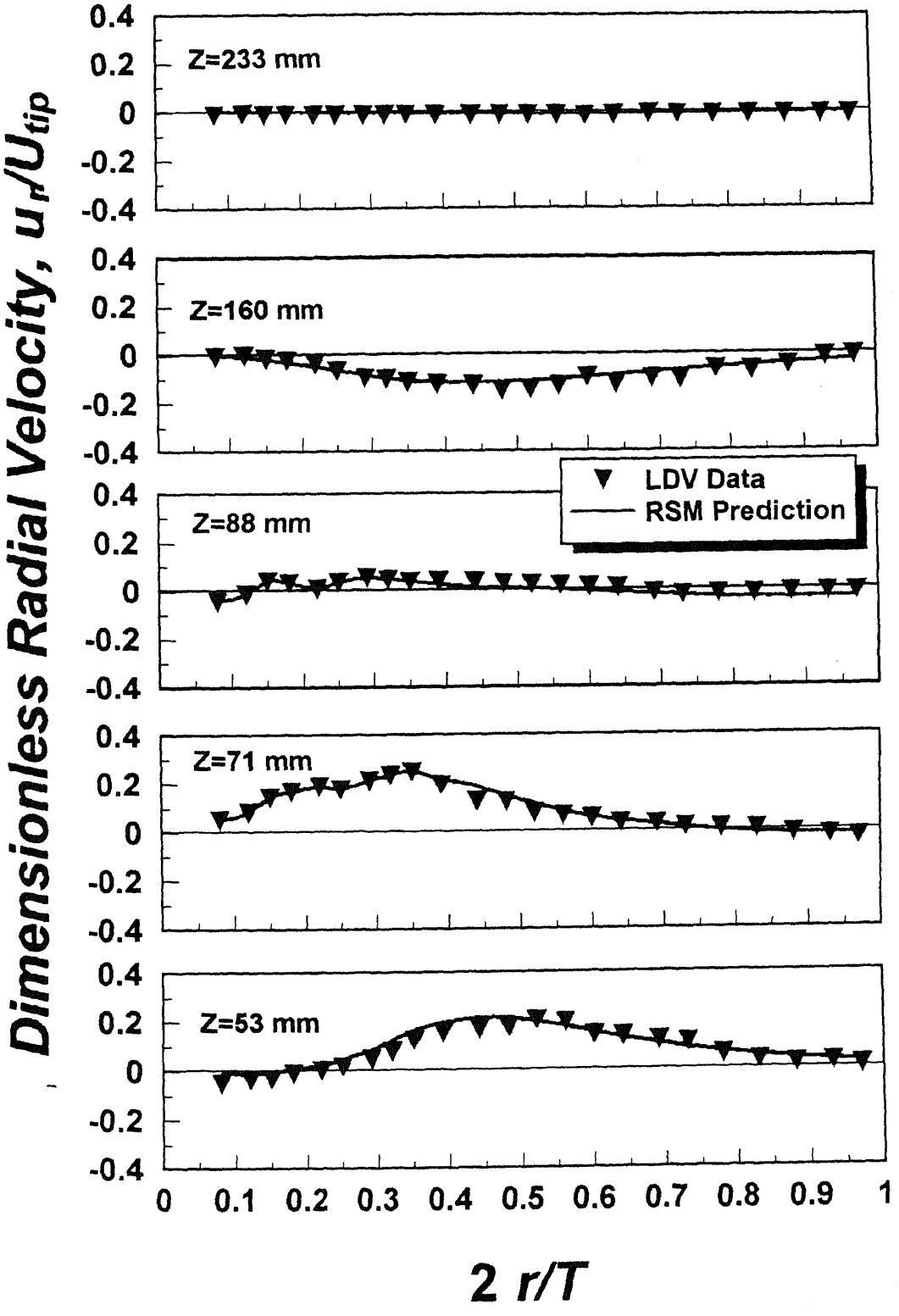

Figure 6-40 Comparison between LDV measurements and CFD predictions: radial velocity (System C1, N = 159 rpm)

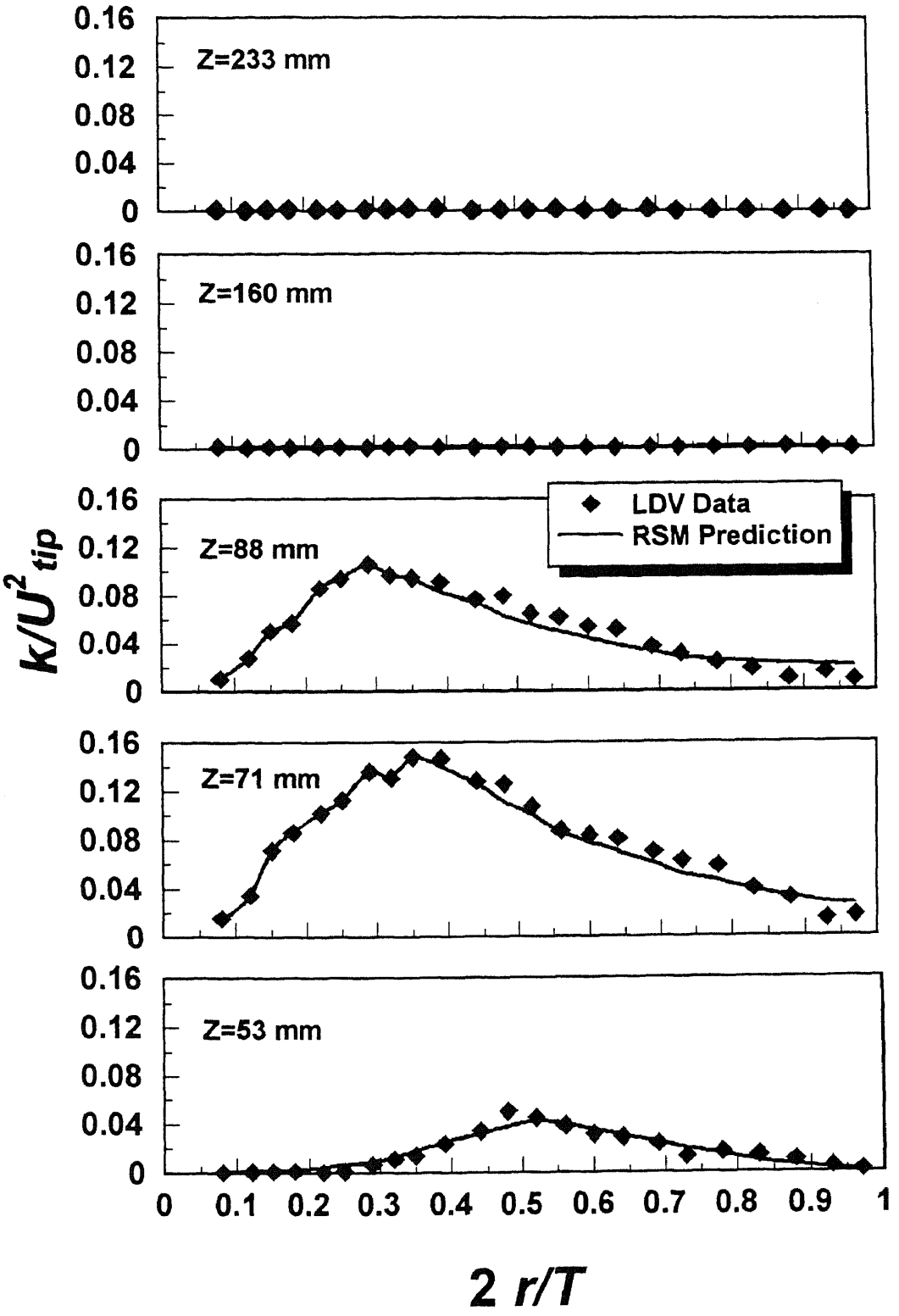

Figure 6-41 Comparison between LDV measurements and CFD predictions: turbulent kinetic energy (System C1, N = 159 rpm)

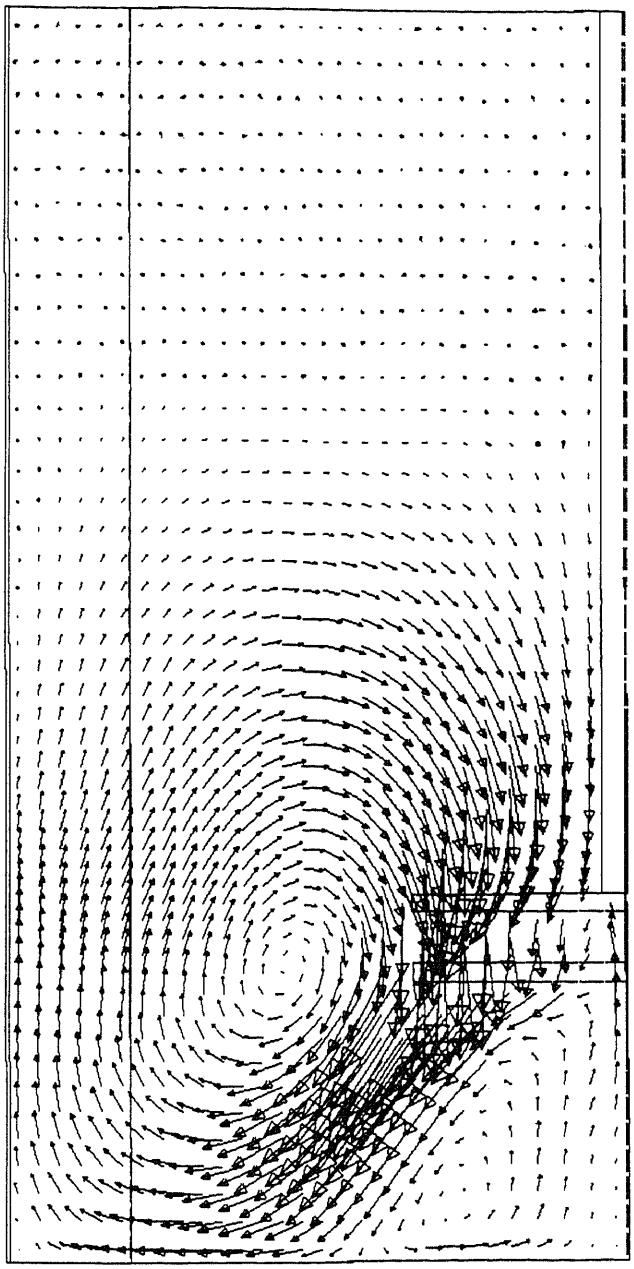

Figure 6-42 CFD prediction of velocity distribution in System C1 (2*D* view)

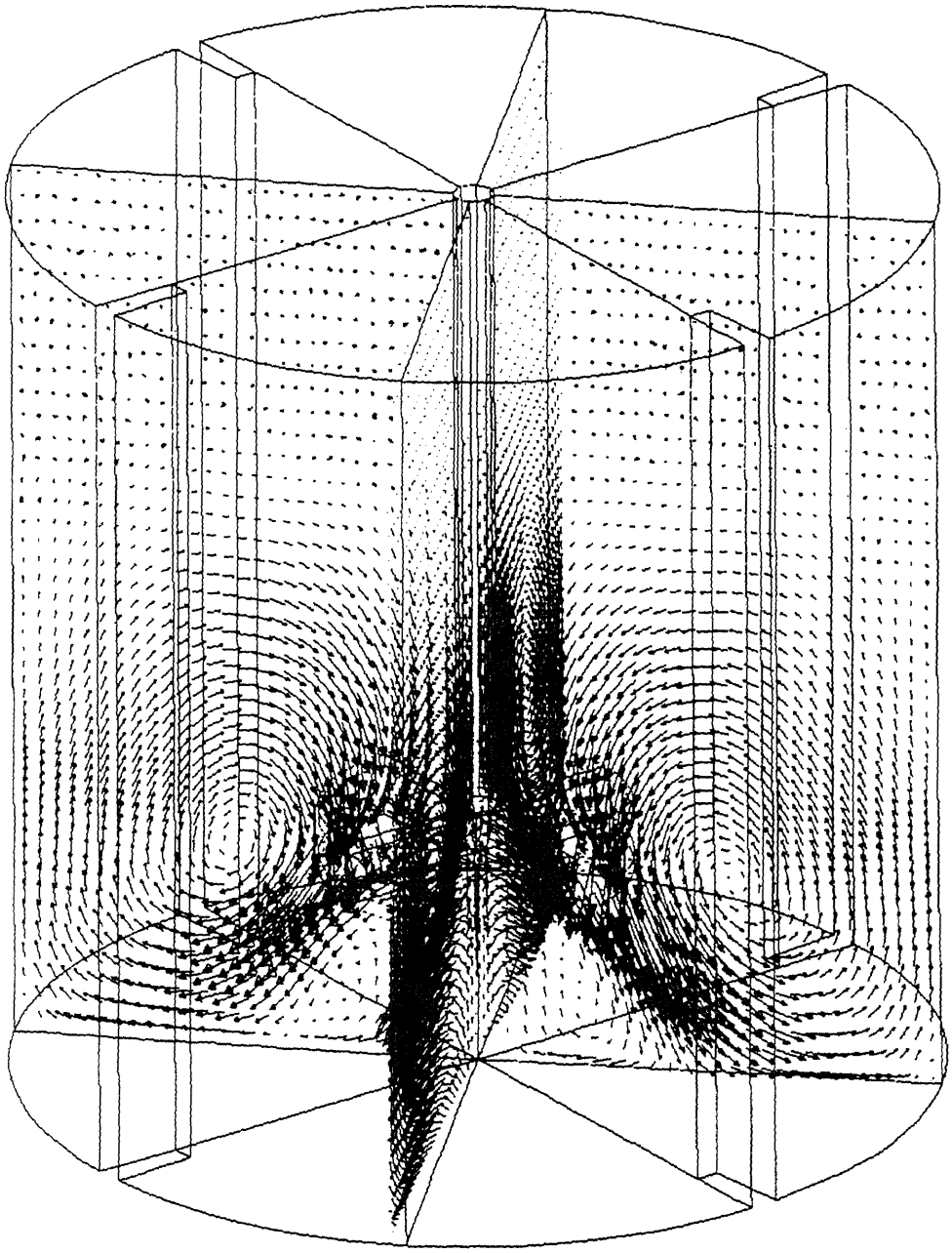

Figure 6-43 CFD prediction of velocity distribution in System C1 (3*D* view)

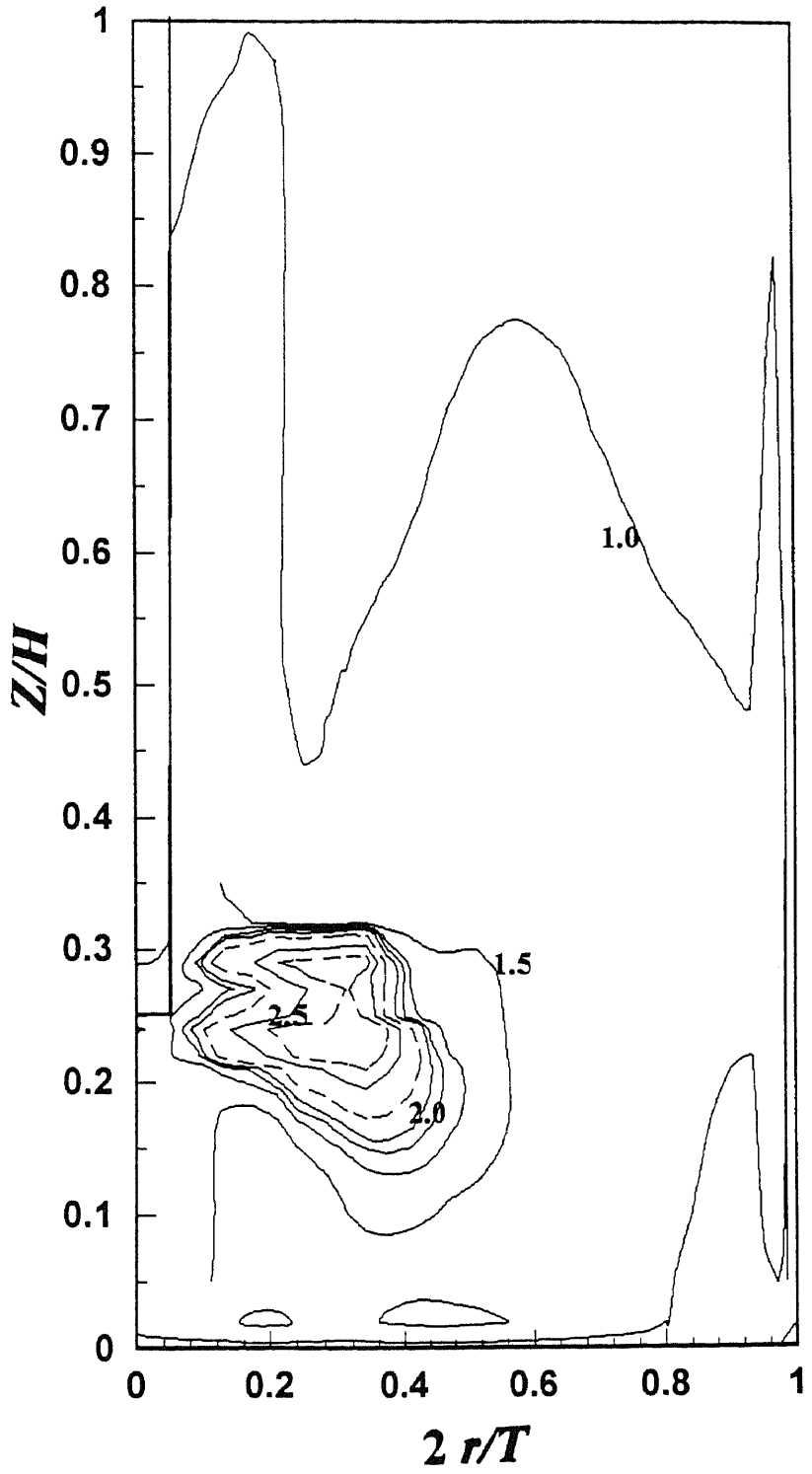

Figure 6-44 CFD prediction of velocity gradient distribution in System C1 (curve labels give the value of $\log_{10}G$, where G is in s^{-1})

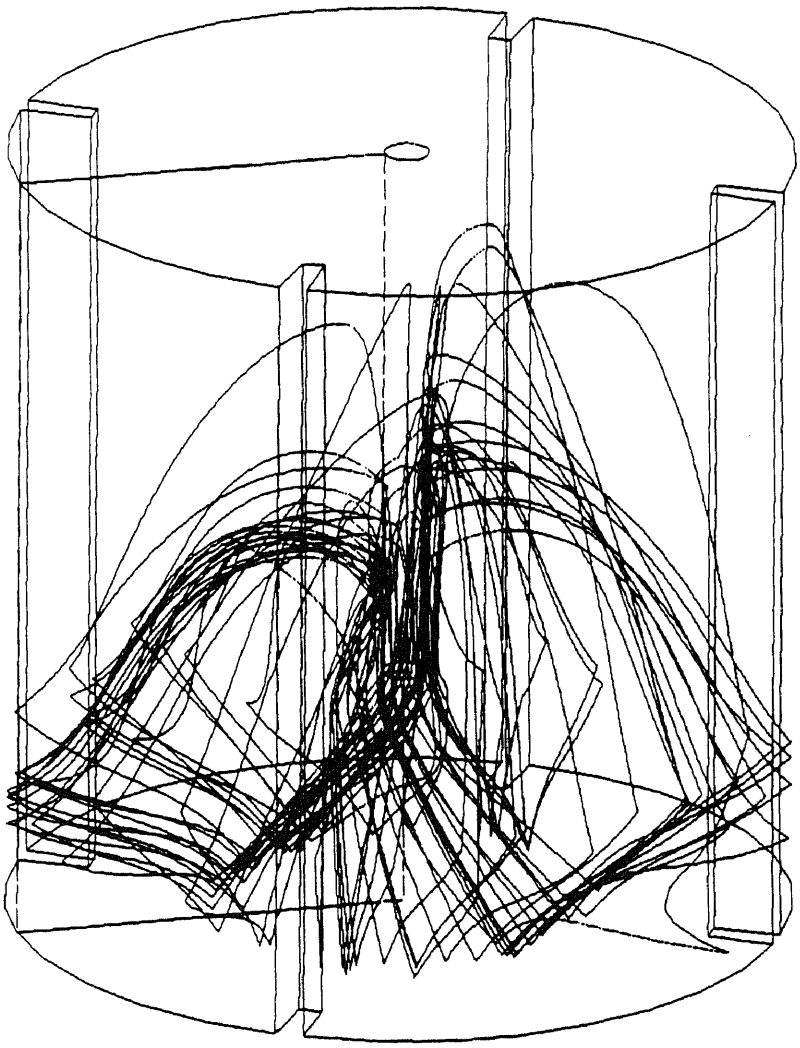

Figure 6-45 CFD prediction of particle trajectory in System C1 (t = 2,000 s)

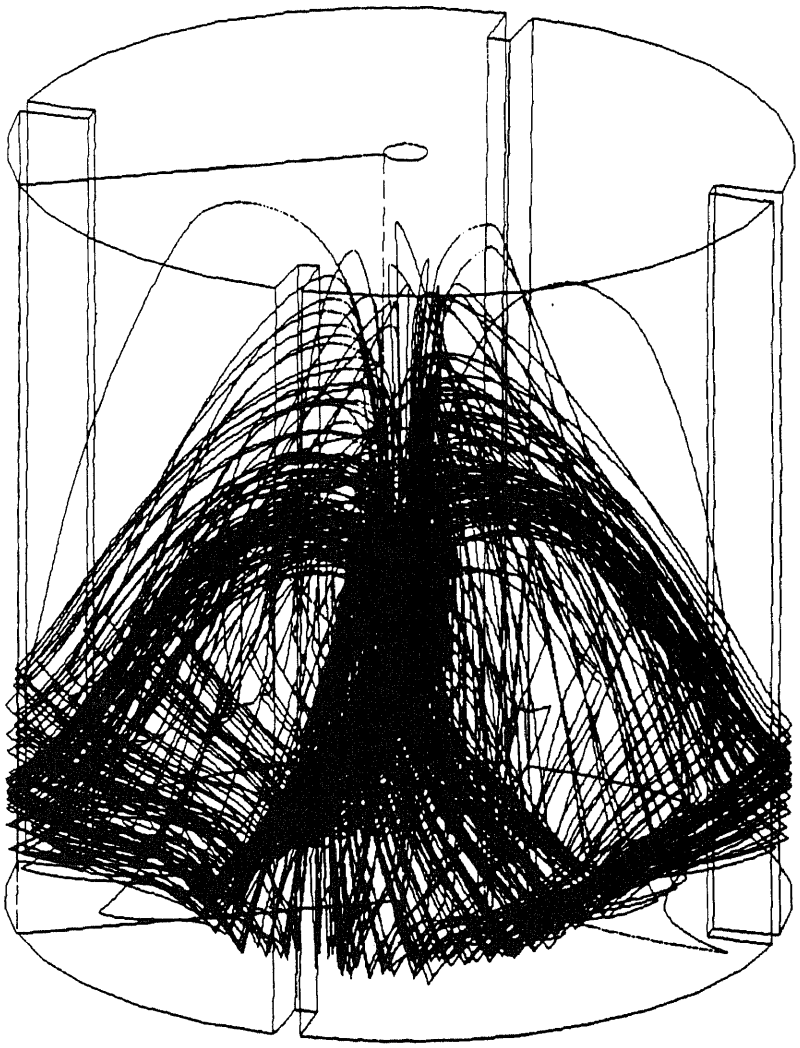

Figure 6-46 CFD prediction of particle trajectory in System C1 (t = 10,000 s)

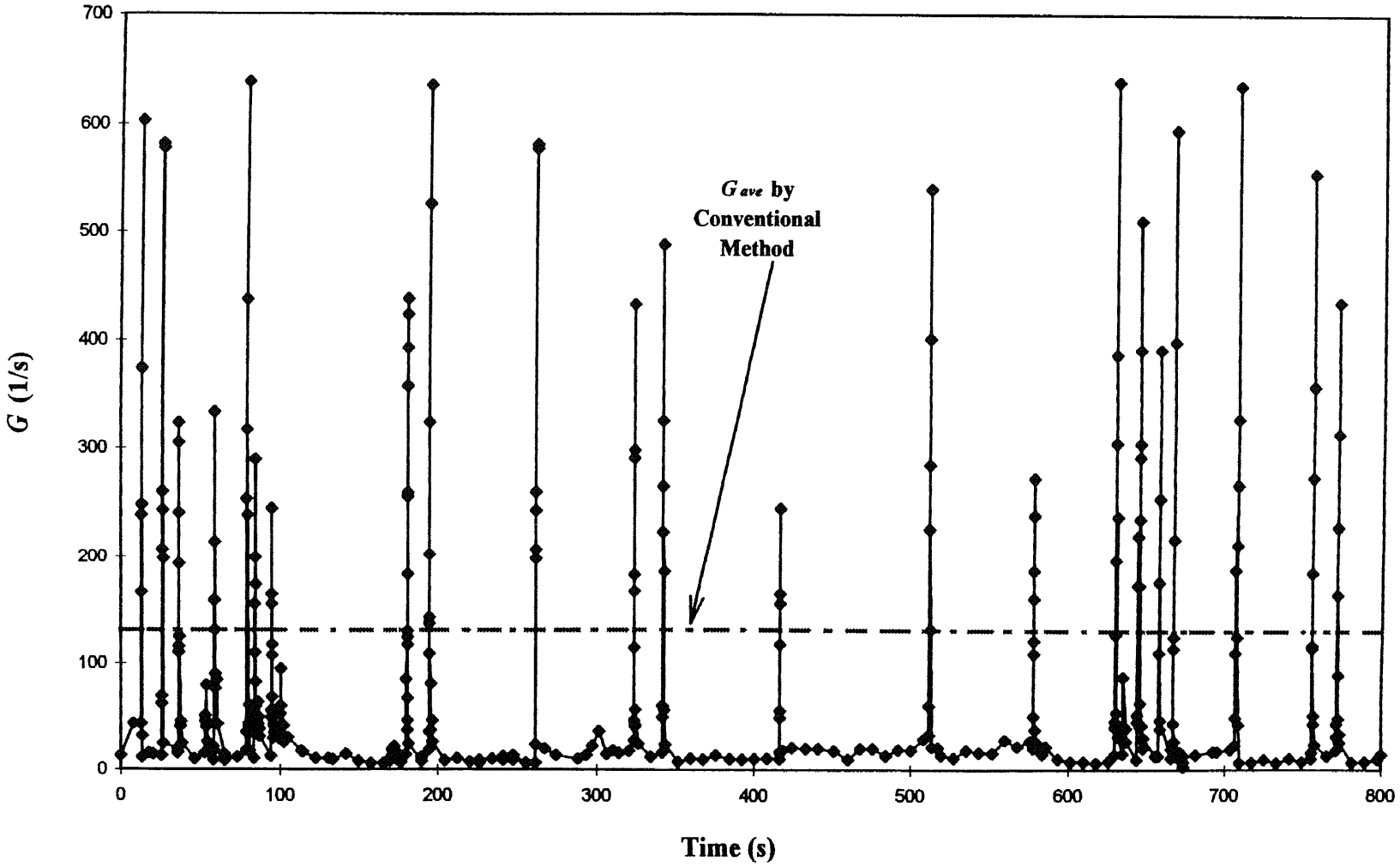

Figure 6-47 *G* value along the particle trajectory in system C1

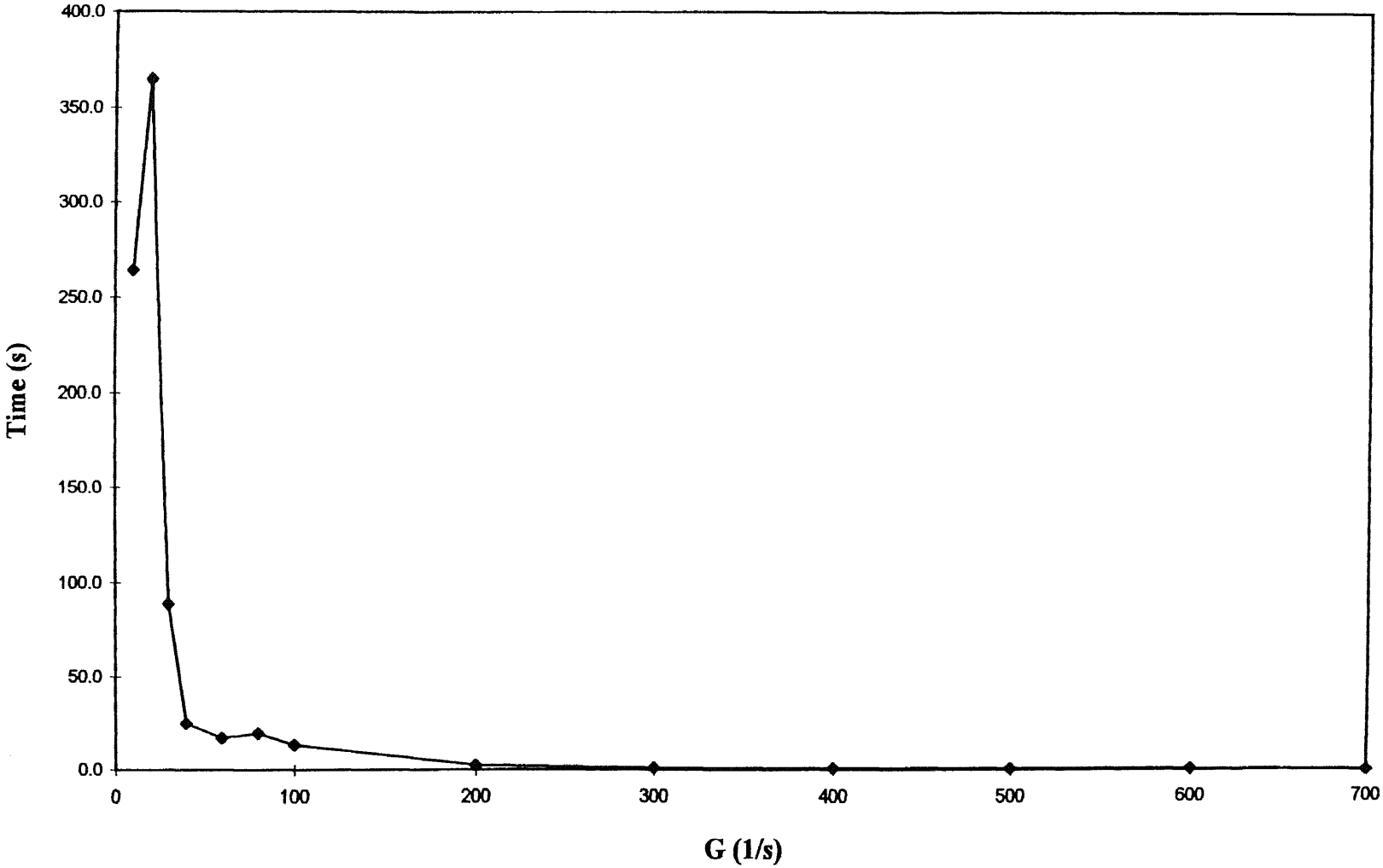

Figure 6-48 *G* value distribution curve along the particle trajectory in system C1

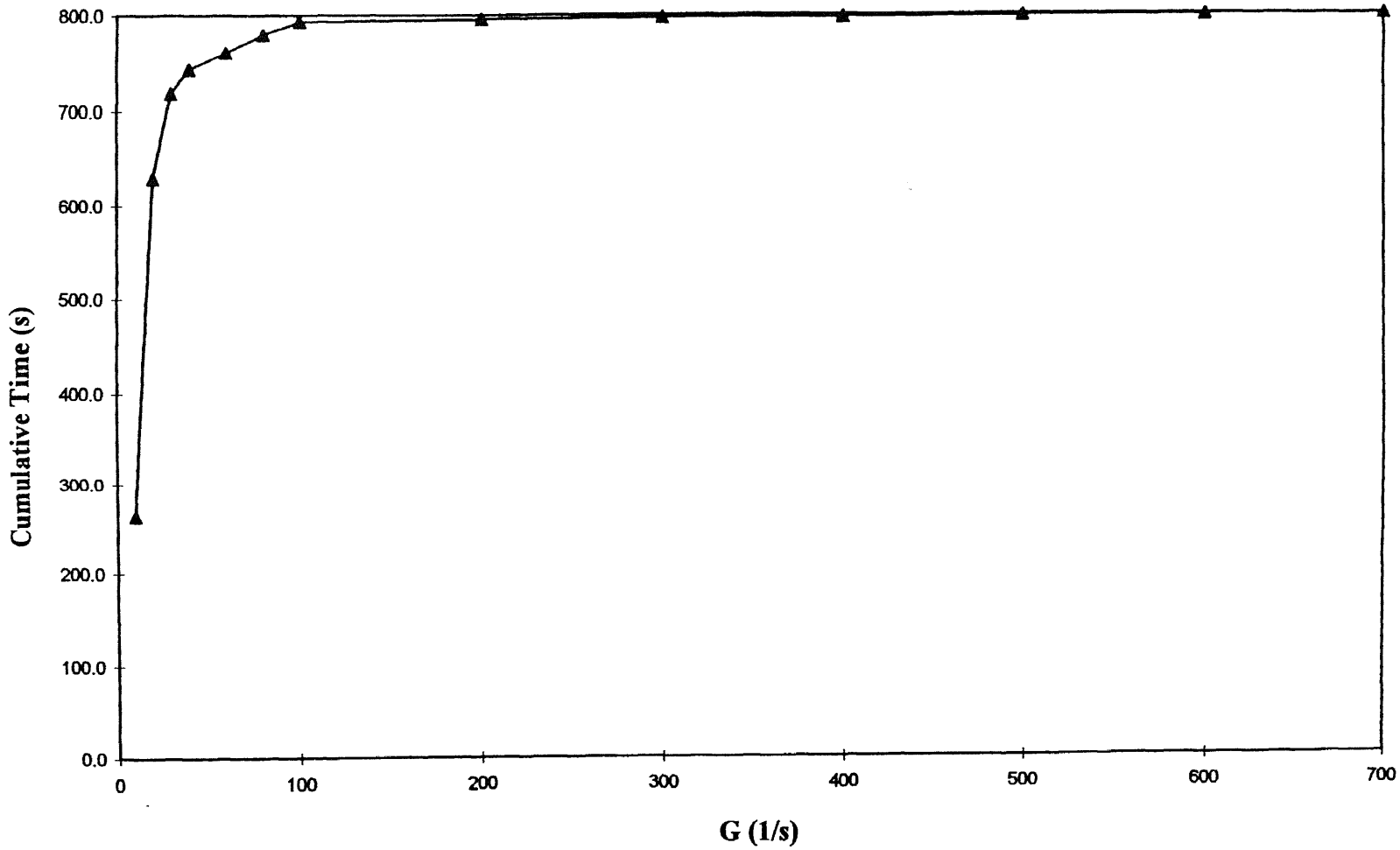

Figure 6-49 Cumulative G value distribution curve along the particle trajectory in System C1

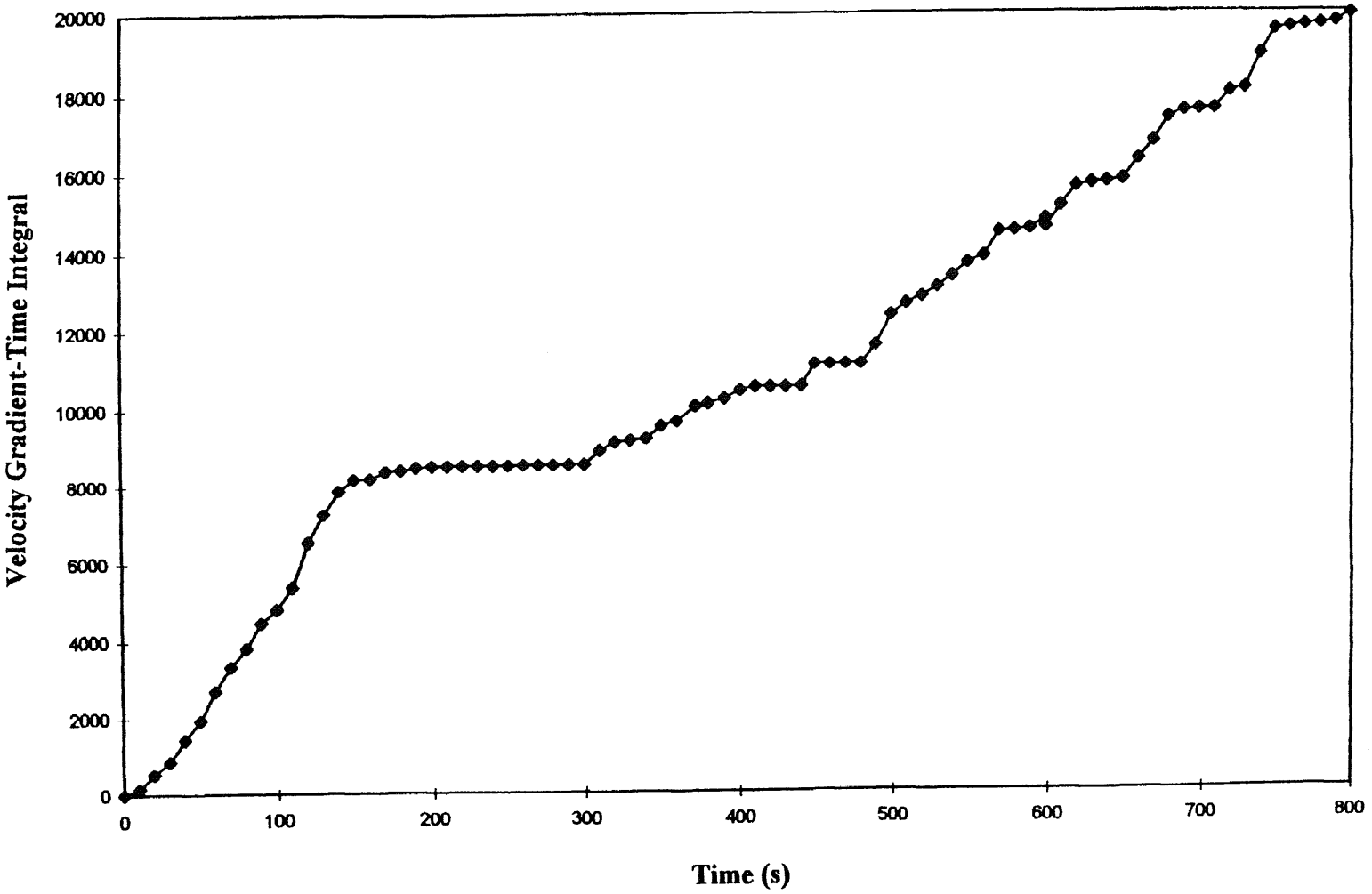

Figure 6-50 Numerical integration of (t * G) vs. time (along the particle trajectory) in System C1

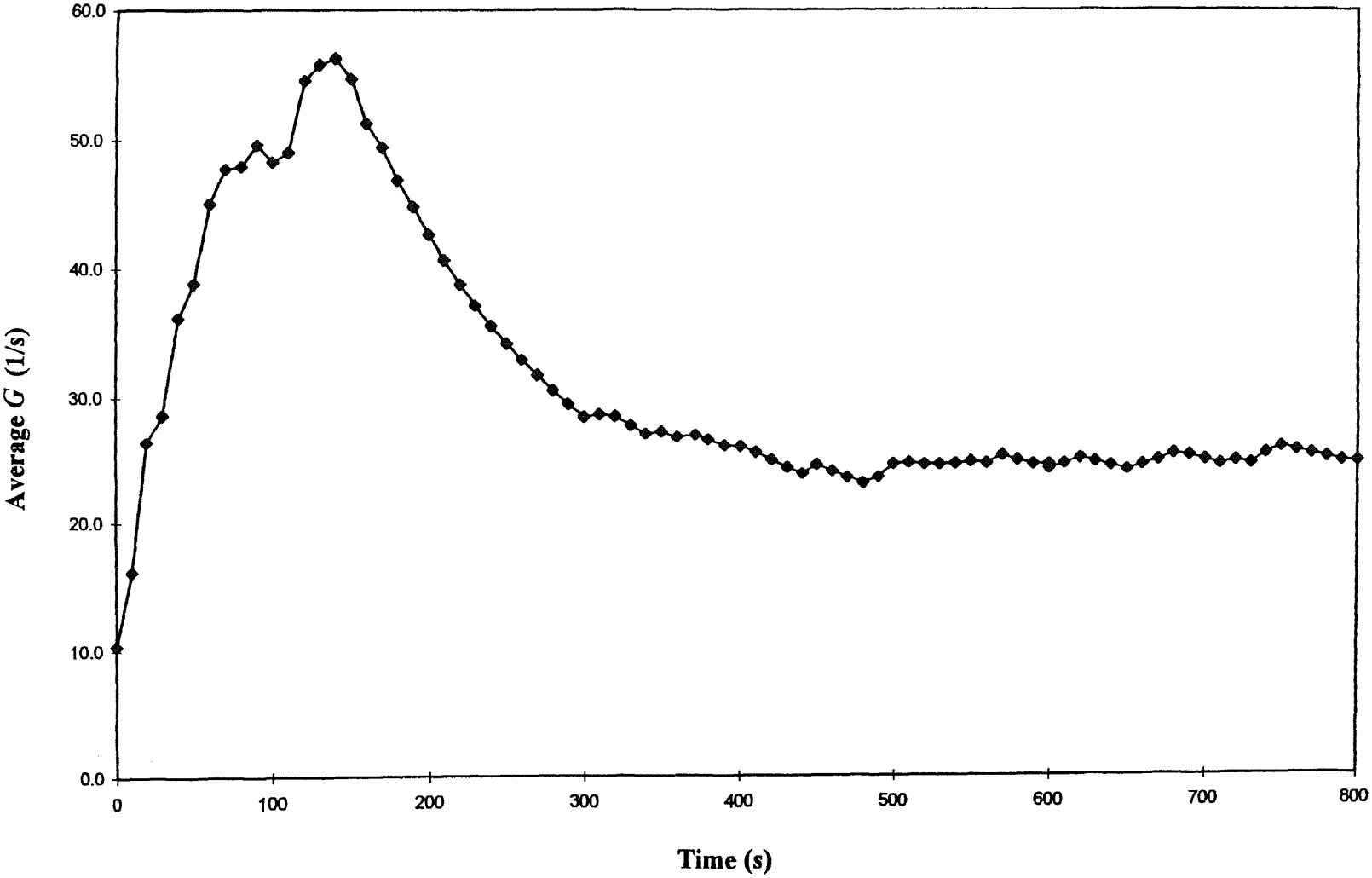

Figure 6-51 Average G value vs. time (along the particle trajectory) in System C1

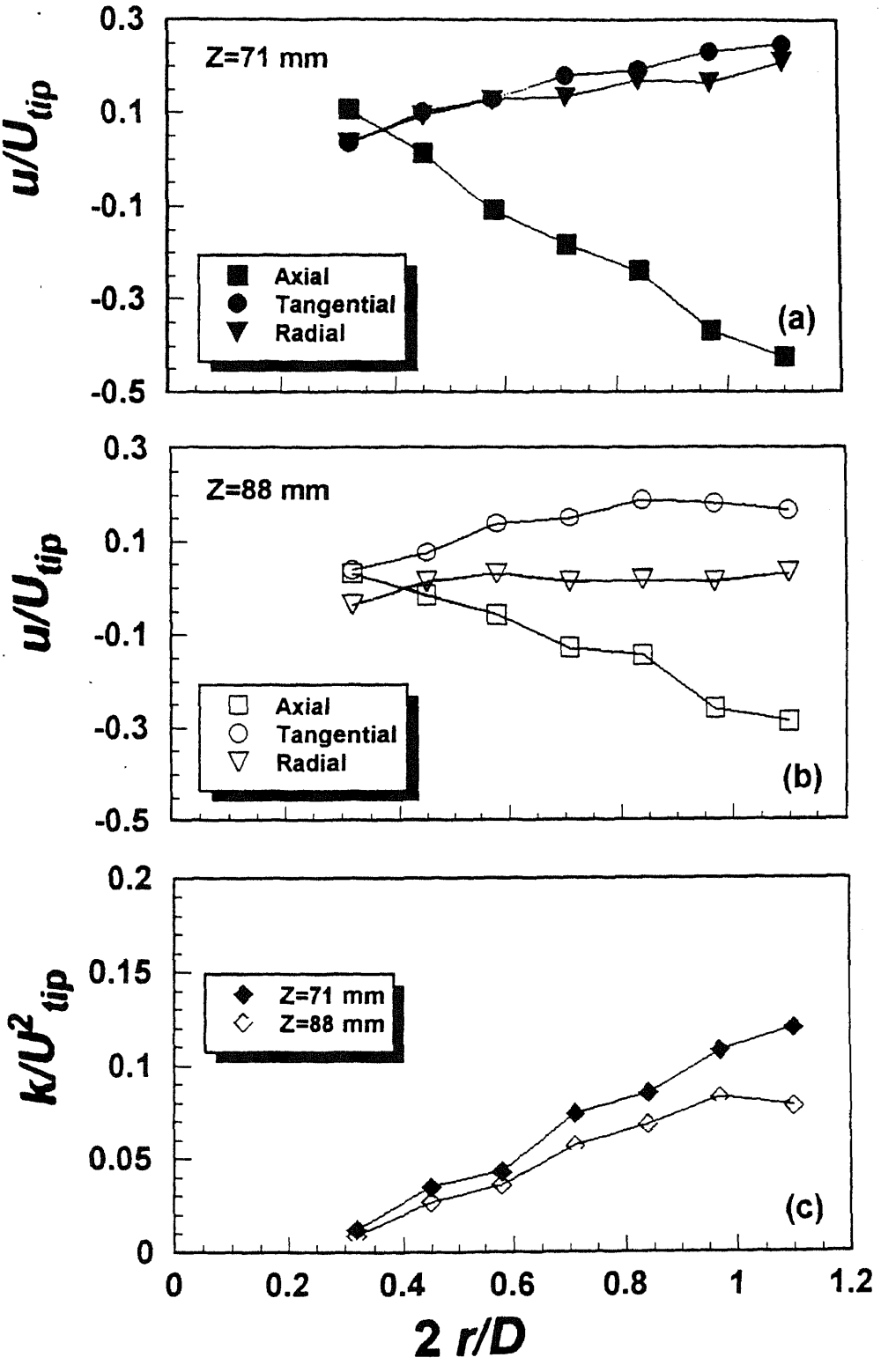

Figure 6-52 Experimentally determined (via LDV) dimensionless velocities and turbulent kinetic energies in the impeller region (System C2, $N = 256$ rpm)

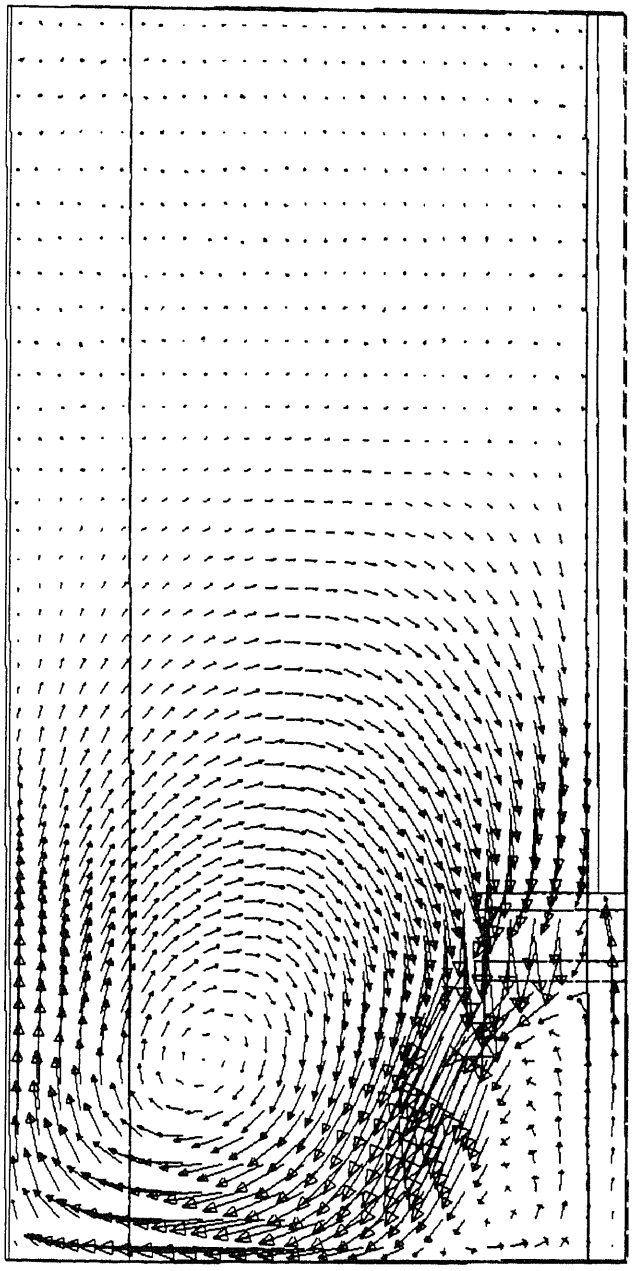

Figure 6-53 CFD prediction of velocity distribution in System C2 (2*D* view)

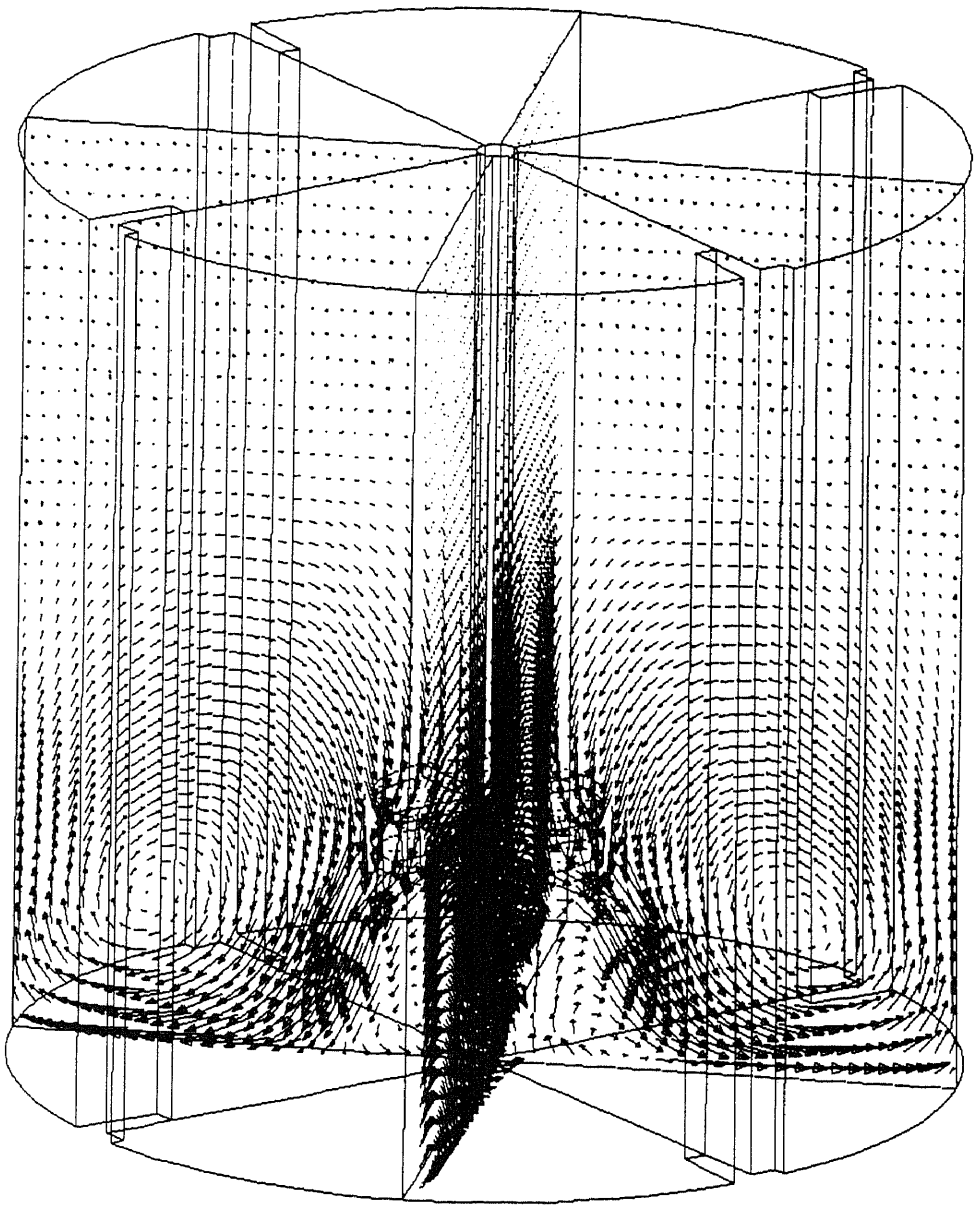

Figure 6-54 CFD prediction of velocity distribution in System C2 (3*D* view)

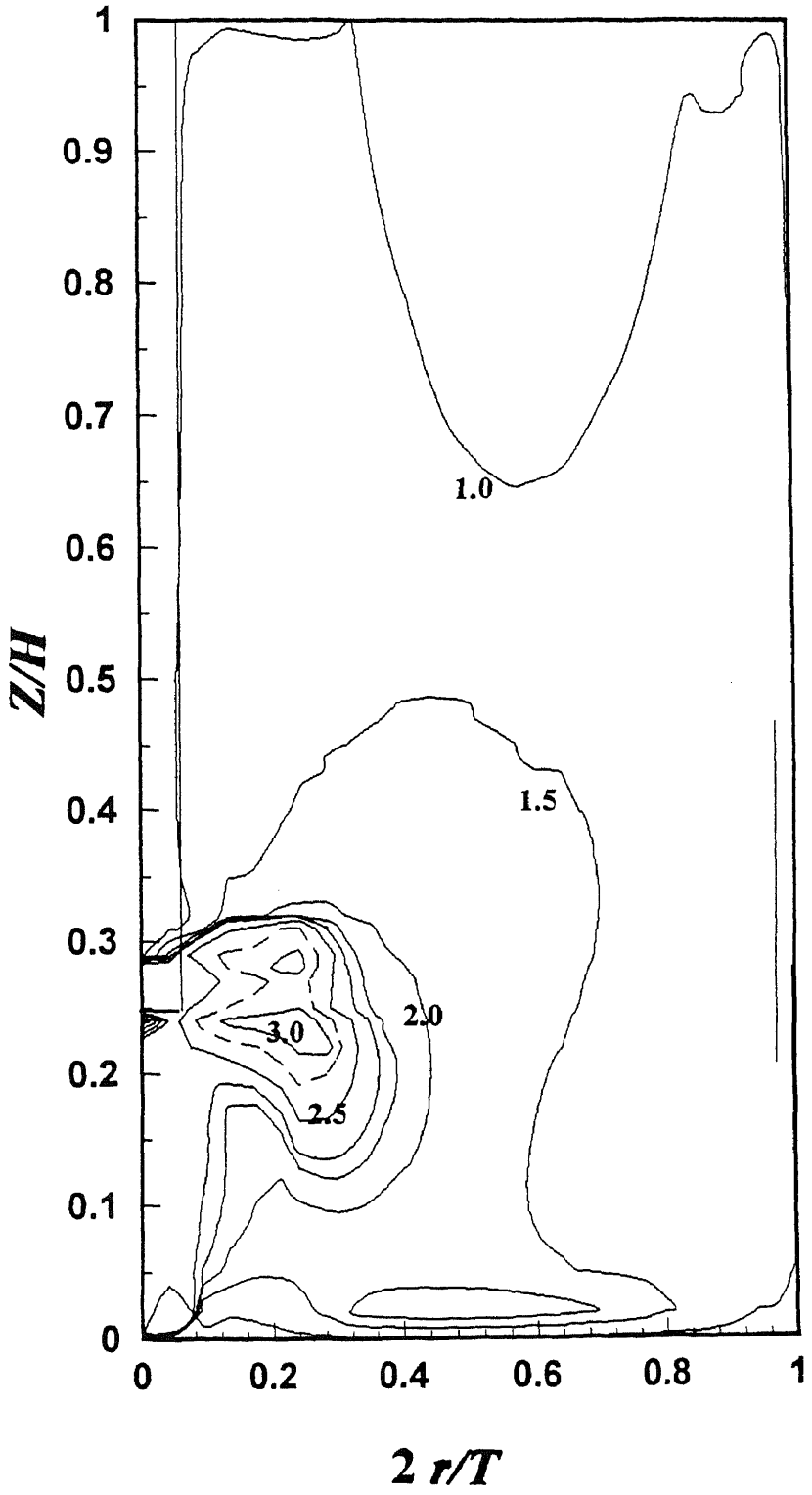

Figure 6-55 CFD prediction of velocity gradient distribution in System C2 (curve labels give the value of $\log_{10}G$, where G is in s^{-1})

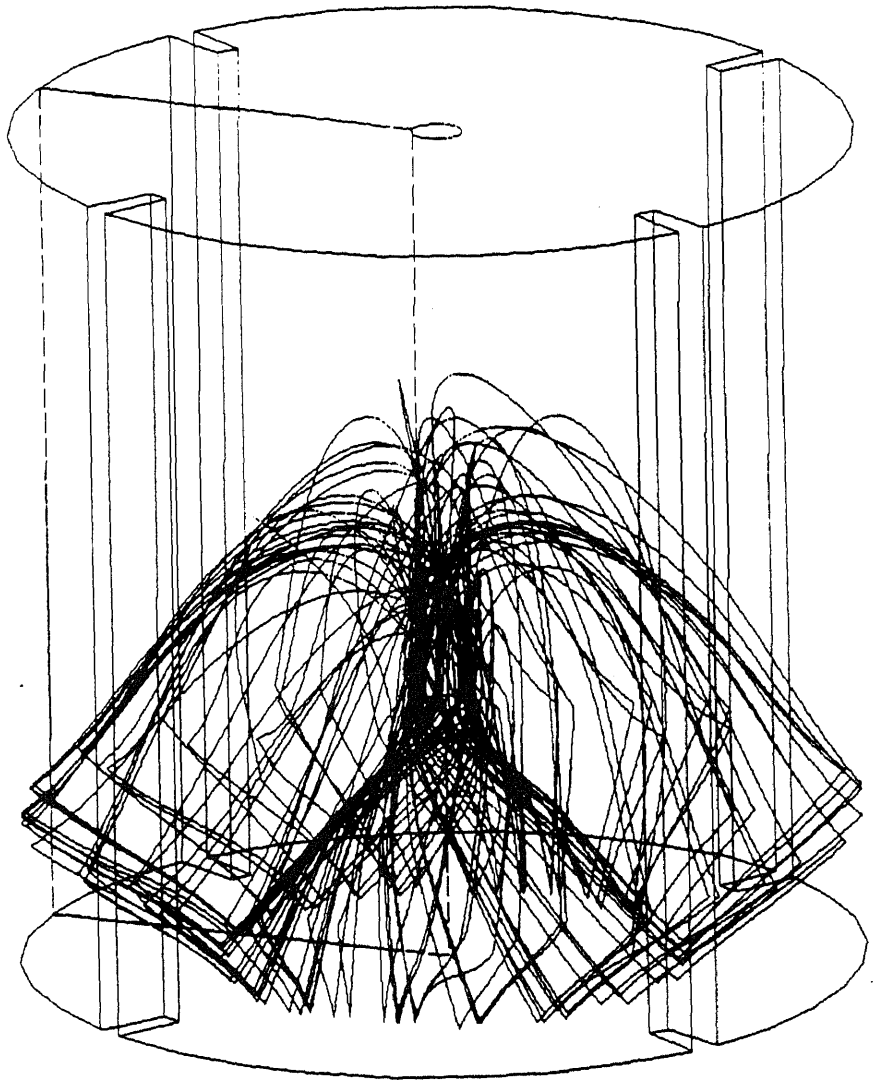

Figure 6-56 CFD prediction of particle trajectory in System C2 (t = 2,000 s)

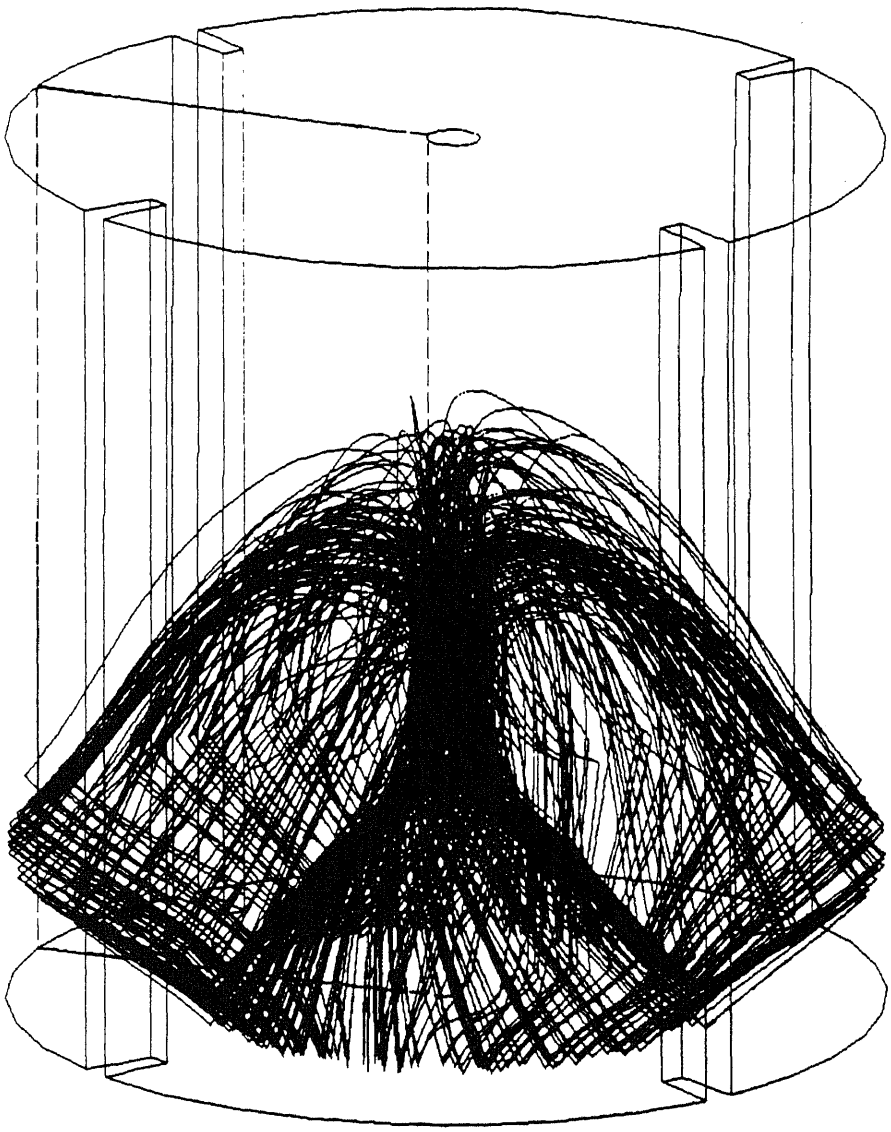

Figure 6-57 CFD prediction of particle trajectory in System C2 (t = 10,000 s)

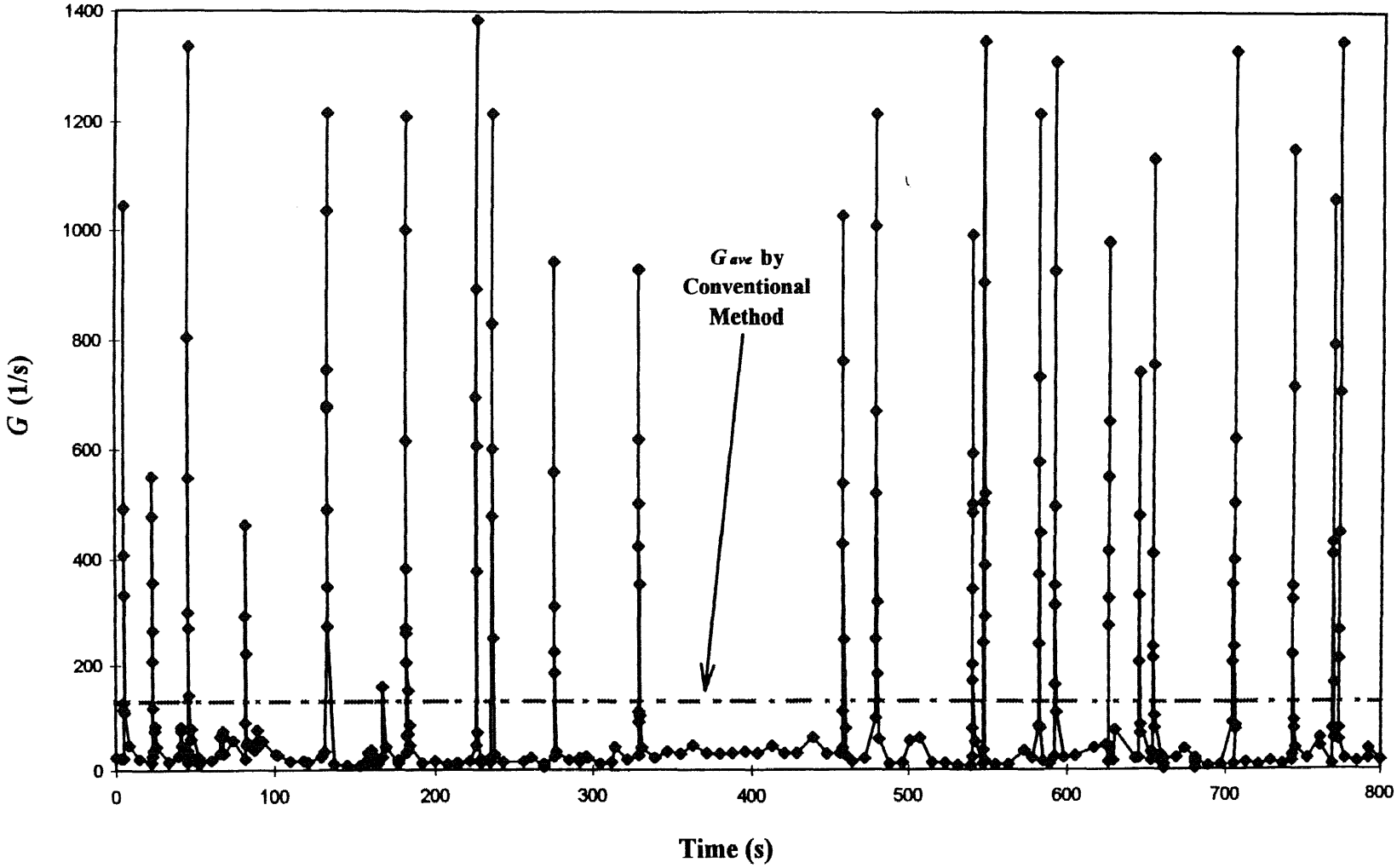

Figure 6-58 G value along the particle trajectory in System C2

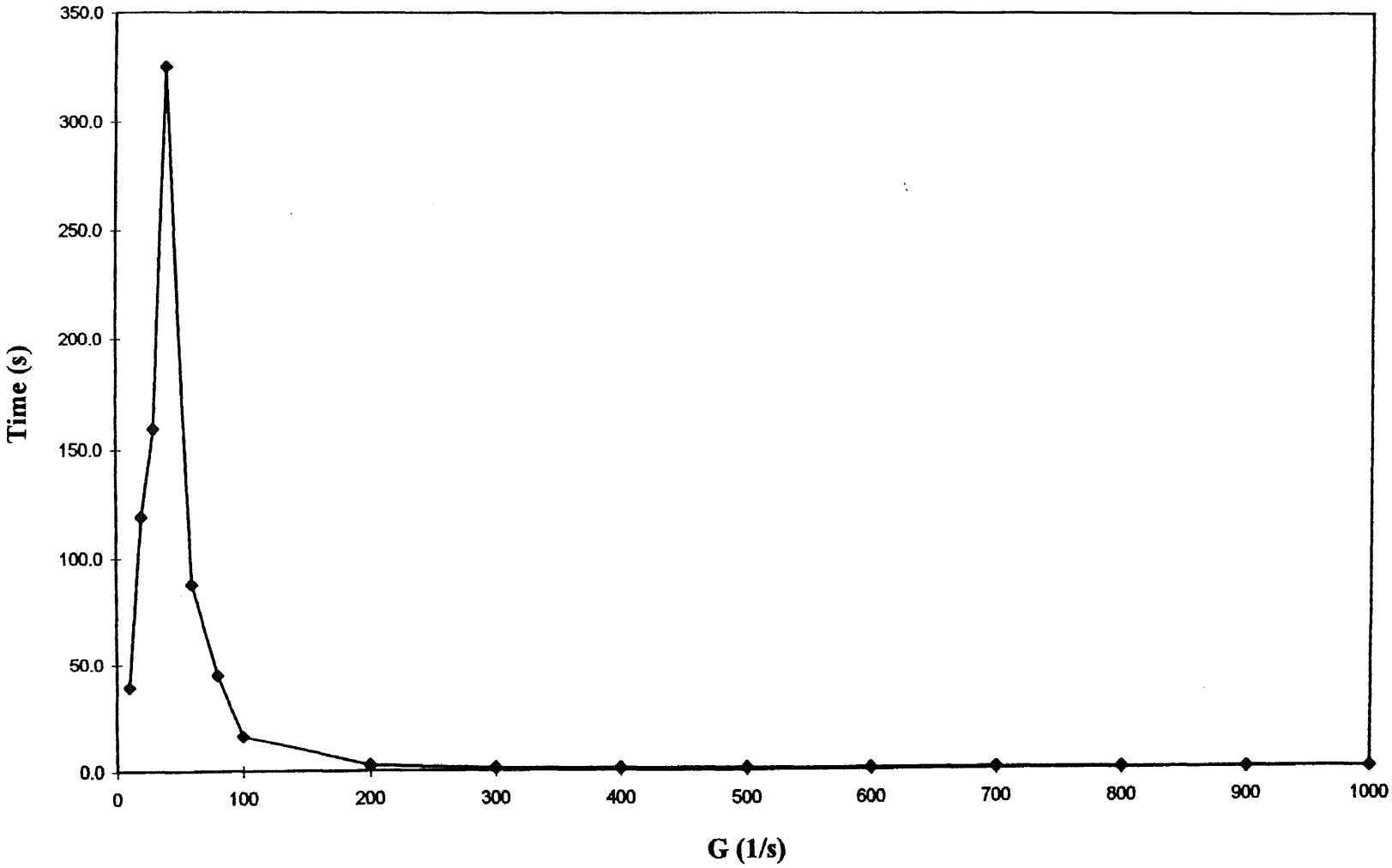

Figure 6-59 *G* value distribution curve along the particle trajectory in System C2

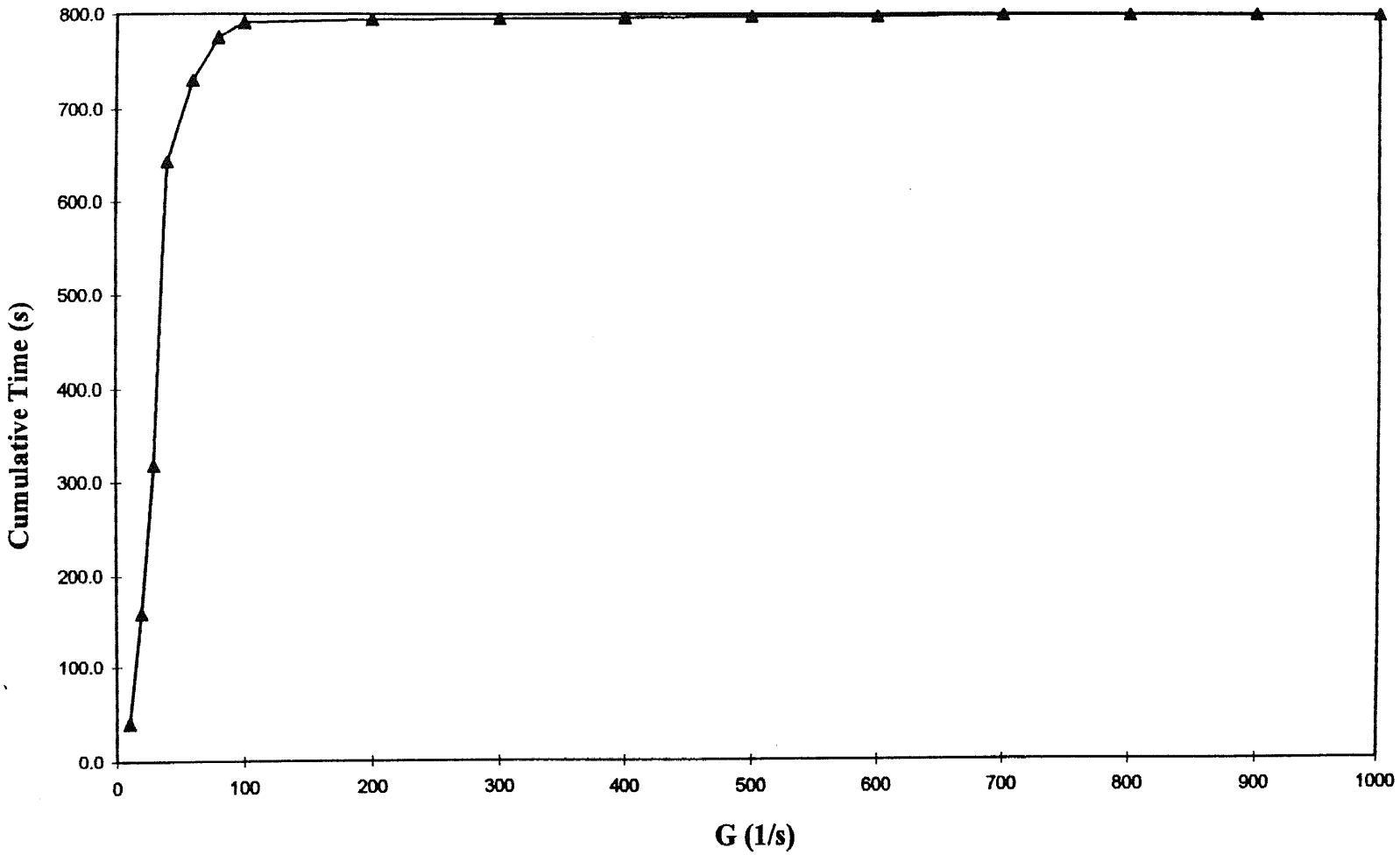

Figure 6-60 Cumulative G value distribution curve along the particle trajectory in System C2

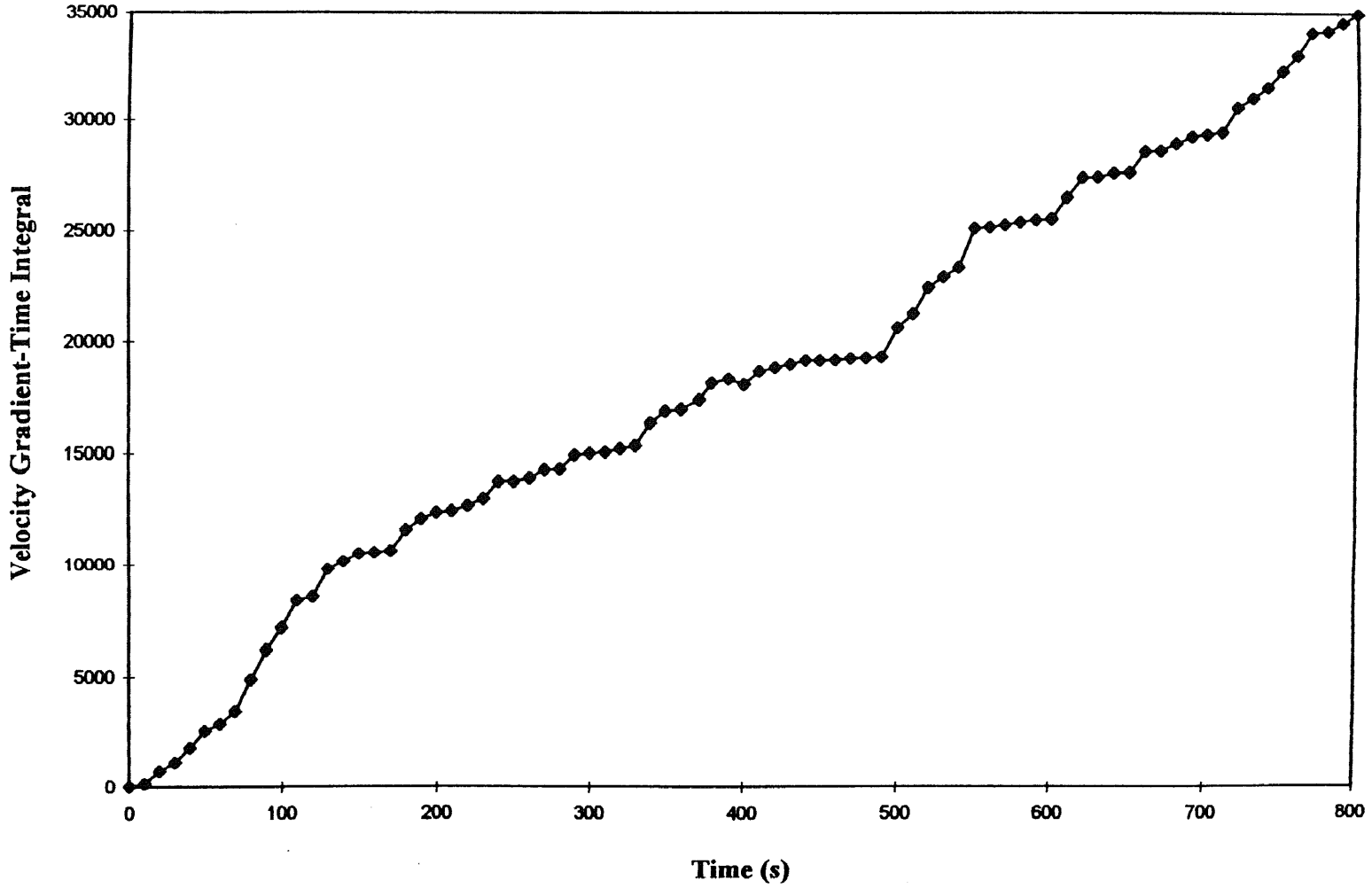

Figure 6-61 Numerical Integration of (t * G) vs. Time (along the Particle Trajectory) in System C2

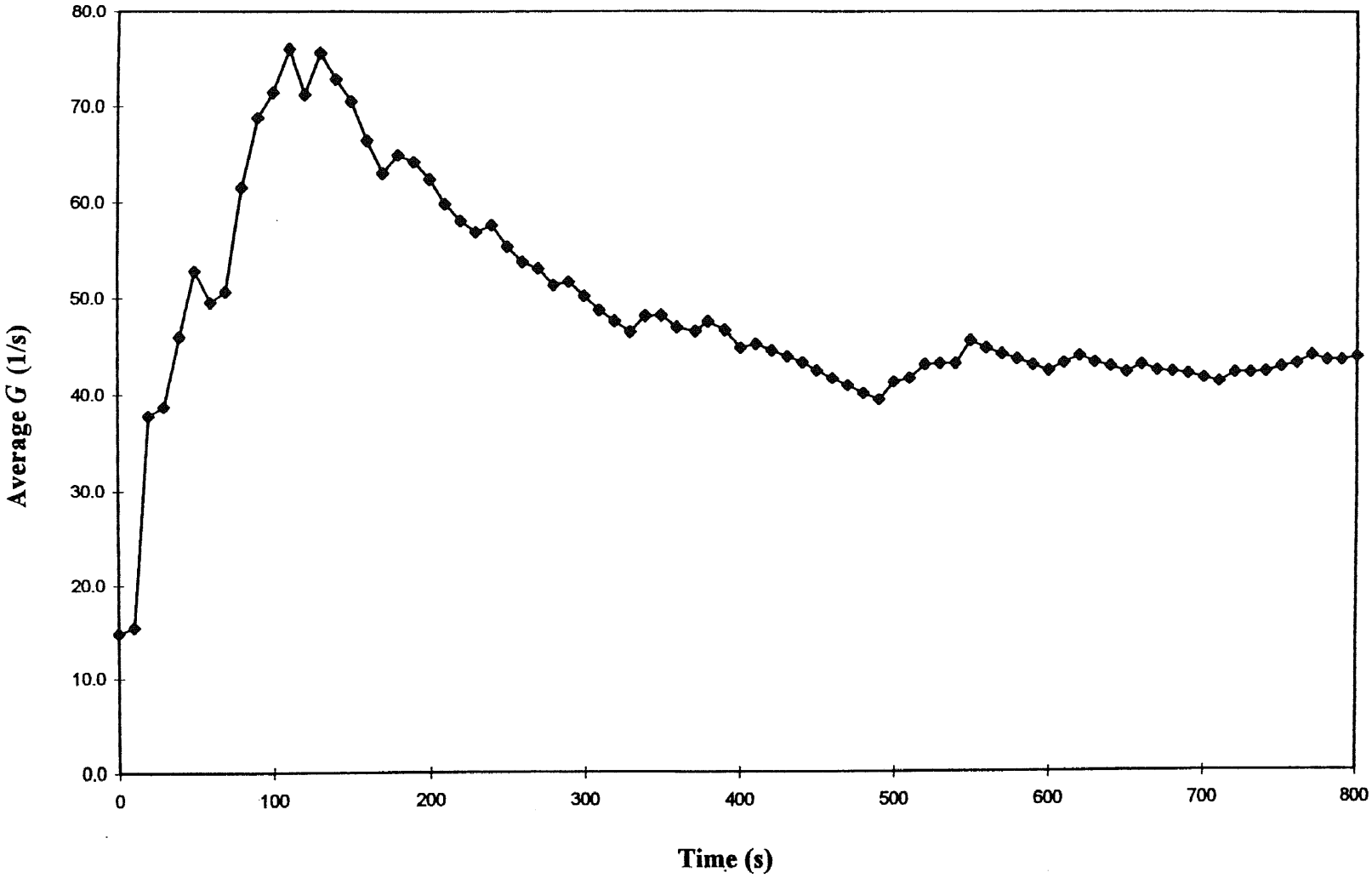

Figure 6-62 Average G Value vs. Time (along the Particle Trajectory) in System C2

APPENDIX B

PROGRAM CODE FOR THE LOCAL *G* VALUE CALCULATION

This appendix includes the program code used to perform the calculation of the local velocity gradient distribution via the complete definition of local velocity gradient method proposed in this work.

```
'          LOCAL VELOCITY GRADIENT CALCULATION PROGRAM
'
' Macro2 Macro
'
' Macro recorded in 04/27/1997 by Changgen Luo
'
' This Macro is created to calculated the local velocity gradient

' This is a mcaro programmed in MS Excel 5.0, working together with
'   data sheets imported from FLUENT V4.4,
' Following imported data sheets are included in this Excel Workbook:
'   xp: x position (cartesian coordinates)in each cell center,
'   yp: y position (cartesian coordinates)in each cell center,
'   zp: z position (cartesian coordinates)in each cell center,
'   uv: U velocity in each cell
'   vv: V velocity in each cell
'   wv: W velocity in each cell
'   zp: axial position (cylindrical coordinates)in each cell center,
'   tp: tangential position (cylindrical coordinates)in each cell center,
'   rp: radial position (cylindrical coordinates)in each cell center,
'   zv: velocity in axial dircetion in each cell
'   rv: velocity in radial direction in each cell
'   tv: velocity in tangential in each cell
'   eff:effective viscosity in each cell
'
' The results of local velocity gradient will be put in worksheet
'   "Gvalue" in the same workbook
'
Sub Macro()
Dim t, counter, Rownum, Colnum, GRownum, GColnum As Integer
Dim i, j, k, Maxi, Maxj, Maxk, Cood As Integer
Dim x1, x0, y1, y0, z1, z0, uv1, uv0, vv1, vv0, wv1, wv0 As Single
Dim dx, dy, dz, dux, duy, duz As Single
Dim Gxx, Gyy, Gzz, Gxy, Gyx, Gyz, Gzy, Gxz, Gzx As Single
Dim G1, G2, G As Single
Dim zv1, zv0, rv1, rv0, tv1, tv0 As Single
Dim duz, dur, dut, dutr As Single
Dim Gtt, Gzz, Grr, Grt, Gtr, Gtz, Gzt, Grz, Gzr As Single

VISCOSITY = 0.001

Cood = Val(InputBox("Please enter 1 if it is cartesian coordinate, or 0 if cylindrical",
"Which Coordinate System", 1))

Maxi = Val(InputBox("Please enter the number of i", "i Value Entry", 5))
```

```
Maxj = Val(InputBox("Please enter the number of j", "j Value Entry", 5))
Maxk = Val(InputBox("Please enter the number of k", "k Value Entry", 5))

If Cood = 1 Then

'This part is for the local velocity gradient calculation
'  in cartesian coordiate.
'=============================================================
For k = 1 To Maxk
   For j = 1 To Maxj
      For i = 1 To Maxi

   If ((i Mod 10) = 0) Then
   Rownum = (((k - 1) * 156 + 8) + (35 - j) + (((i \ 10) - 1) * 38))
   Colnum = 11
   Else
   Rownum = (((k - 1) * 156 + 8) + (35 - j) + ((i \ 10) * 38))
   Colnum = ((i Mod 10) + 1)
   'Where 156 is the number of rows for each k value block in "zx" sheet
   '     8  is the number of rows before the first x position value
   '     (35 - j) indicates that x position values were listed
   '           in reverse sequence
   '     (i mod 10) gives the reminder of this division
   '     (i \ 10) gives the integer of this division
   '     ((i \ 10) * 38) indicates for every 10 I values we have 38 rows
   '     the position values were listed in column 2 to 11
   End If
   GRownum = Rownum
   GColnum = Colnum
   x0 = Worksheet("xp").Cells(Rownum, Colnum).Value
   y0 = Worksheet("yp").Cells(Rownum, Colnum).Value
   z0 = Worksheet("zp").Cells(Rownum, Colnum).Value
   uv0 = Worksheet("uv").Cells(Rownum, Colnum).Value
   vv0 = Worksheet("vv").Cells(Rownum, Colnum).Value
   wv0 = Worksheet("wv").Cells(Rownum, Colnum).Value
   effv = Worksheet("eff").Cells(Rownum, Colnum).Value

   k = k + 1
   If ((i Mod 10) = 0) Then
   Rownum = (((k - 1) * 156 + 8) + (35 - j) + (((i \ 10) - 1) * 38))
   Colnum = 11
   Else
   Rownum = (((k - 1) * 156 + 8) + (35 - j) + ((i \ 10) * 38))
   Colnum = ((i Mod 10) + 1)
   End If
```

```
x1 = Worksheet("xp").Cells(Rownum, Colnum).Value
uv1 = Worksheet("uv").Cells(Rownum, Colnum).Value

k = k - 1
i = i + 1
If ((i Mod 10) = 0) Then
Rownum = (((k - 1) * 156 + 8) + (35 - j) + (((i \ 10) - 1) * 38))
Colnum = 11
Else
Rownum = (((k - 1) * 156 + 8) + (35 - j) + ((i \ 10) * 38))
Colnum = ((i Mod 10) + 1)
End If
y1 = Worksheet("yp").Cells(Rownum, Colnum).Value
vv1 = Worksheet("vv").Cells(Rownum, Colnum).Value

i = i - 1
j = j + 1
If ((i Mod 10) = 0) Then
Rownum = (((k - 1) * 156 + 8) + (35 - j) + (((i \ 10) - 1) * 38))
Colnum = 11
Else
Rownum = (((k - 1) * 156 + 8) + (35 - j) + ((i \ 10) * 38))
Colnum = ((i Mod 10) + 1)
End If
z1 = Worksheet("zp").Cells(Rownum, Colnum).Value
wv1 = Worksheet("wv").Cells(Rownum, Colnum).Value

dx = Abs(x1 - x0)
dy = Abs(y1 - y0)
dz = Abs(z1 - z0)
dux = Abs(uv1 - uv0)
duy = Abs(vv1 - vv0)
duz = Abs(wv1 - wv0)

Gxx = dux / dx
Gyy = duy / dy
Gzz = duz / dz
Gxy = duz / dy
Gyx = duy / dx
Gxz = dux / dz
Gzx = duz / dx
Gyz = duy / dz
Gzy = duz / dz

G1 = 2 * ((Gxx * Gxx) + (Gyy * Gyy) + (Gzz * Gzz))
```

```
    G2 = (Gxy + Gyx) ^ 2 + (Gyz + Gzy) ^ 2 + (Gxz + Gzx) ^ 2

    G = (effv / VISCOSITY) * (G1 + G2)

    'put this G value in worksheet Gvalue
    Worksheets("Gvalue").Cell(GRownum, GColnum).Value = G

        Next i
    Next j
Next k

Else
'This part is for the local velocity gradient calculation
'in cylindrical coordiate.
'=============================================================
For k = 1 To Maxk
    For j = 1 To Maxj
      For i = 1 To Maxi

    If ((i Mod 10) = 0) Then
    Rownum = (((k - 1) * 156 + 8) + (35 - j) + (((i \ 10) - 1) * 38))
    Colnum = 11
    Else
    Rownum = (((k - 1) * 156 + 8) + (35 - j) + ((i \ 10) * 38))
    Colnum = ((i Mod 10) + 1)
    'Where 156 is the number of rows for each k value block in "zx" sheet
    '     8  is the number of rows before the first x position value
    '     (35 - j) indicates that x position values were listed
    '           in reverse sequence
    '     (i mod 10) gives the reminder of this division
    '     (i \ 10) gives the integer of this division
    '     ((i \ 10) * 38) indicates for every 10 I values we have 38 rows
    '     the position values were listed in column 2 to 11
    End If
    GRownum = Rownum
    GColnum = Colnum
    z0 = Worksheet("zp").Cells(Rownum, Colnum).Value
    'this is the value in axial direction
    r0 = Worksheet("rp").Cells(Rownum, Colnum).Value
    'this is the value in radial direction
    t0 = Worksheet("tp").Cells(Rownum, Colnum).Value
    'this is the value in tangential direction
    zv0 = Worksheet("zv").Cells(Rownum, Colnum).Value
    'this is the veloctiy in axial dirction
    rv0 = Worksheet("rv").Cells(Rownum, Colnum).Value
```

```
'this is the velocitiy in radial  dirction
tv0 = Worksheet("tv").Cells(Rownum, Colnum).Value
'this is the velocitiy in tangential dirction
effv = Worksheet("eff").Cells(Rownum, Colnum).Value

k = k + 1
If ((i Mod 10) = 0) Then
Rownum = (((k - 1) * 156 + 8) + (35 - j) + (((i \ 10) - 1) * 38))
Colnum = 11
Else
Rownum = (((k - 1) * 156 + 8) + (35 - j) + ((i \ 10) * 38))
Colnum = ((i Mod 10) + 1)
End If
z1 = Worksheet("zp").Cells(Rownum, Colnum).Value
zv1 = Worksheet("zv").Cells(Rownum, Colnum).Value

k = k - 1
i = i + 1
If ((i Mod 10) = 0) Then
Rownum = (((k - 1) * 156 + 8) + (35 - j) + (((i \ 10) - 1) * 38))
Colnum = 11
Else
Rownum = (((k - 1) * 156 + 8) + (35 - j) + ((i \ 10) * 38))
Colnum = ((i Mod 10) + 1)
End If
r1 = Worksheet("rp").Cells(Rownum, Colnum).Value
rv1 = Worksheet("rv").Cells(Rownum, Colnum).Value

i = i - 1
j = j + 1
If ((i Mod 10) = 0) Then
Rownum = (((k - 1) * 156 + 8) + (35 - j) + (((i \ 10) - 1) * 38))
Colnum = 11
Else
Rownum = (((k - 1) * 156 + 8) + (35 - j) + ((i \ 10) * 38))
Colnum = ((i Mod 10) + 1)
End If
t1 = Worksheet("tp").Cells(Rownum, Colnum).Value
tv1 = Worksheet("tv").Cells(Rownum, Colnum).Value

dz = Abs(z1 - z0)
dr = Abs(r1 - r0)
dt = Abs(t1 - t0) 'refer to theta

duz = Abs(zv1 - zv0)
```

```
    dur = Abs(rv1 - rv0)
    dut = Abs(tv1 - tv0)    'refer to theta
    dutr = Abs((tv1 / r1) - (tv0 / r0))

    Grr = dur / dr
    Gtt = dut / dt
    Gzz = duz / dz
    Grt = dur / dt
    Gtr = dut / dr
    Gtz = dut / dz
    Gzt = duz / dt
    Gzr = duz / dr
    Grz = dur / dz

    G1 = 2 * ((Grr * Grr) + ((Gtt / r0) + Grr) ^ 2 + (Gzz * Gzz))
    G2 = (r0 * (dutr / dr) + (Grt / r0)) ^ 2 + (Gtz + (Gzt / r0)) ^ 2 + (Gzr + Grz) ^ 2

    G = (effv / VISCOSITY) * (G1 + G2)
    'put this G value in worksheet Gvalue
    Worksheets("Gvalue").Cell(GRownum, GColnum).Value = G

        Next i
    Next j
Next k

End If

MsgBox ("Good Job !")

End Sub
```

APPENDIX C

PROGRAM CODE FOR NEW PARAMETER CALCULATION

This appendix includes the program code used to perform the calculation of the local velocity gradient distribution, velocity gradient distribution along the particle trajectory, velocity gradient-time integral from *FLUENT* output data.

PROGRAM CODE FOR CALCULATION OF (DELT T * G) AND G VALUE DISTRIBUTION ALONG THE PARTICLE TRAJECTORY

```
'
' Macro1 Macro
' Macro recorded in 11/24/1996  and revised in 04/26/97 by Changgen Luo
' This is a mcaro programmed in MS Excel 5.0, working together with two data sheets,
'     i.e., tg and Epsilon_value.
' This Macro is created to calculated the integration of t*G for a particle moving
'     in a mixing tank, as well as the G value distribution data.
'
'In sheet "tg",
'  column 1 (A),  the time ending at each step of the particle movement;
'  column 2(B),3(C),4(D), corresponding x, y, z positions in the tank at each step;
'  column 5(E),6(F),7(G), corresponding cell locations expressed as I, J, K;
'  column 8(H), the time difference between each two steps;
'  column 9(I), the Epsilon value corresponding to the cell(I,J,K), getting from
'        sheet "Epsilon_value";
'  column 10(J), the CALCULATED G value;
'  column 11(K), the production of (G * delta t) was shown;
'  column 12(L), subtotal, summarize the above (G * delta t) values;
'  Values of time and I, J, K are imported from FLUENT output data file;
'  column 14(N), the G value
'  column 15(O), the time a particle spent in that G value
'
'
'In sheet "Epsilon_value",
'  we import the Epsilon value for the whole tank from FLUENT output data;
'  for each K = 1 ~ 40 we have I * J = 35 * 35 G values, listed in a 35 * 35 matrix,
'        i.e. 35 rows, and 35 columns;
'  we give some space so that each K = n level's first G value will be listed on
'        row(40*n + 1), col(1);
'  i.e. if K = 8, the G value of (1,1,8) is shown on cell(321,A), as ((40*8+1),1);
'For the case that we already have calculated the local G value, we put the
'  sheet  "G_value" instead of  "Epsilon_value".  The sheet "G_value" has the same
'  date configuration arrangement in sheet "Epsilon_value"
'


Sub Macro1()
Dim i, j, k, t, counter, temp, tempt, Steps, Gore As Integer
Dim Epsilon, g, deltt, subtotal As Single
Dim x, y, z, theta, ra As Integer
Dim t10, t20, t40, t60, t80, t100, t200, t300, t400, t500, t600 As Single
Dim t700, t800, t900, t1000, t1100, t1200, t1300, t1400, t1500, telse As Single
```

```
counter = 2
tempt = 0
t10 = 0
t20 = 0
t40 = 0
t60 = 0
t80 = 0
t100 = 0
t200 = 0
t300 = 0
t400 = 0
t500 = 0
t600 = 0
t700 = 0
t800 = 0
t900 = 0
t1000 = 0
t1100 = 0
t1200 = 0
t1300 = 0
t1400 = 0
t1500 = 0
subtotal = 0

Gore = Val(InputBox("Please enter 1 if imported G value, or 0 if imported Epsilon
Value", "Which Original Data You have?", 1))

If Gore = 1 Then
'=============================================================
'This part is for rectangular vessel
Steps = Val(InputBox("Please enter the number of steps", "Calculation Steps Entry", 5))
'Steps refers to the calculation steps in the particle trajectory simulation

While counter <= Steps

'convert the x position to cell I value
Cells(counter, 2).Select
x = Selection.Value
Select Case x
Case 0 To 0.013
   i = 2
Case 0.01301 To 0.026
   i = 3
Case 0.02601 To 0.038
   i = 4
```

```
Case 0.03801 To 0.05
   i = 5
Case 0.05001 To 0.062
   i = 6
Case 0.06201 To 0.073
   i = 7
Case 0.07301 To 0.083
   i = 8
Case 0.08301 To 0.092
   i = 9
Case 0.09201 To 0.1
   i = 10
Case 0.10001 To 0.108
   i = 11
Case 0.10801 To 0.115
   i = 12
Case 0.11501 To 0.121
   i = 13
Case 0.12101 To 0.127
   i = 14
Case 0.12701 To 0.134
   i = 15
Case 0.13401 To 0.141
   i = 16
Case 0.14101 To 0.147
   i = 17
Case 0.14701 To 0.153
   i = 18
Case 0.15301 To 0.16
   i = 19
Case 0.16001 To 0.166
   i = 20
Case 0.16601 To 0.172
   i = 21
Case 0.17201 To 0.179
   i = 22
Case 0.17901 To 0.185
   i = 23
Case 0.18501 To 0.192
   i = 24
Case 0.19201 To 0.2
   i = 25
Case 0.20001 To 0.208
   i = 26
Case 0.20801 To 0.217
```

```
    i = 27
Case 0.21701 To 0.227
    i = 28
Case 0.22701 To 0.238
    i = 29
Case 0.23801 To 0.25
    i = 30
Case 0.25001 To 0.262
    i = 31
Case 0.26201 To 0.274
    i = 32
Case 0.27401 To 0.287
    i = 33
Case 0.28701 To 0.3
    i = 34
Case Else
    MsgBox ("please check the x position") 'check if x value is in the correct range
    Debug.Print counter; x; y; z 'Display the position in the Debug Window
End Select


'convert the y position to cell J value
Cells(counter, 3).Select
y = Selection.Value
Select Case y
Case 0 To 0.013
    j = 2
Case 0.01301 To 0.026
    j = 3
Case 0.02601 To 0.038
    j = 4
Case 0.03801 To 0.05
    j = 5
Case 0.05001 To 0.062
    j = 6
Case 0.06201 To 0.073
    j = 7
Case 0.07301 To 0.083
    j = 8
Case 0.08301 To 0.092
    j = 9
Case 0.09201 To 0.1
    j = 10
Case 0.10001 To 0.108
    j = 11
```

```
Case 0.10801 To 0.115
   j = 12
Case 0.11501 To 0.121
   j = 13
Case 0.12101 To 0.127
   j = 14
Case 0.12701 To 0.134
   j = 15
Case 0.13401 To 0.141
   j = 16
Case 0.14101 To 0.147
   j = 17
Case 0.14701 To 0.153
   j = 18
Case 0.15301 To 0.16
   j = 19
Case 0.16001 To 0.166
   j = 20
Case 0.16601 To 0.172
   j = 21
Case 0.17201 To 0.179
   j = 22
Case 0.17901 To 0.185
   j = 23
Case 0.18501 To 0.192
   j = 24
Case 0.19201 To 0.2
   j = 25
Case 0.20001 To 0.208
   j = 26
Case 0.20801 To 0.217
   j = 27
Case 0.21701 To 0.227
   j = 28
Case 0.22701 To 0.238
   j = 29
Case 0.23801 To 0.25
   j = 30
Case 0.25001 To 0.262
   j = 31
Case 0.26201 To 0.274
   j = 32
Case 0.27401 To 0.287
   j = 33
Case 0.28701 To 0.3
```

```
    j = 34
Case Else
    MsgBox ("please check the y position") 'check if y value is in the correct range
    Debug.Print counter; x; y; z 'Display the position in the Debug Window
End Select

'convert the z position to cell K value
Cells(counter, 4).Select
z = Selection.Value
Select Case z
Case 0 To 0.016
    k = 2
Case 0.01601 To 0.035
    k = 3
Case 0.03501 To 0.046
    k = 4
Case 0.04601 To 0.06
    k = 5
Case 0.06001 To 0.073
    k = 6
Case 0.07301 To 0.084
    k = 7
Case 0.08401 To 0.094
    k = 8
Case 0.09401 To 0.103
    k = 9
Case 0.10301 To 0.11
    k = 10
Case 0.11001 To 0.116
    k = 11
Case 0.11601 To 0.123
    k = 12
Case 0.12301 To 0.129
    k = 13
Case 0.12901 To 0.135
    k = 14
Case 0.13501 To 0.142
    k = 15
Case 0.14201 To 0.148
    k = 16
Case 0.14801 To 0.155
    k = 17
Case 0.15501 To 0.161
    k = 18
Case 0.16101 To 0.167
```

```
    k = 19
Case 0.16701 To 0.174
    k = 20
Case 0.17401 To 0.18
    k = 21
Case 0.18001 To 0.189
    k = 22
Case 0.18901 To 0.198
    k = 23
Case 0.19801 To 0.208
    k = 24
Case 0.20801 To 0.219
    k = 25
Case 0.21901 To 0.231
    k = 26
Case 0.23101 To 0.244
    k = 27
Case 0.24401 To 0.257
    k = 28
Case 0.25701 To 0.271
    k = 29
Case 0.27101 To 0.287
    k = 30
Case 0.28701 To 0.302
    k = 31
Case 0.30201 To 0.319
    k = 32
Case 0.31901 To 0.336
    k = 33
Case 0.33601 To 0.354
    k = 34
Case 0.35401 To 0.373
    k = 35
Case 0.37301 To 0.392
    k = 36
Case 0.39201 To 0.411
    k = 37
Case 0.41101 To 0.43
    k = 38
Case 0.43001 To 0.45
    k = 39
Case Else
    MsgBox ("please check the z position") 'check if z value is in the correct range
    Debug.Print counter; x; y; z 'Display the position in the Debug Window
End Select
```

```
'put I value in column 5
Cells(counter, 5).Value = i

'put J value in column 6
Cells(counter, 6).Value = j

'put K value in column 7
Cells(counter, 7).Value = k

'copy the Epsilon value of cell(i,j,k) from sheet "Epsilon_value"
Worksheets("Epsilon_value").Select
If ((i Mod 10) = 0) Then
Cells((((k - 1) * 156 + 8) + (35 - j) + (((i \ 10) - 1) * 38)), 11).Select
Else
Cells((((k - 1) * 156 + 8) + (35 - j) + ((i \ 10) * 38)), ((i Mod 10) + 1)).Select
'Where 156 is the number of rows for each k value block in "Epsilon_value" sheet
'     8  is the number of rows before the first G value
'     (35 - j) refers to G values were listed on reverse sequence
'     (i mod 10) gives the reminder of this division
'     (i \ 10) gives the integer of this division
'     ((i \ 10) * 38) indicates for each 10 I values we have 38 rows
'
End If
temp = Selection.Value
Selection.Copy

'paste the Epsilon Value into Column 9 of sheet "tg"
Sheets("tg").Select
ActiveSheet.Paste destination:=Cells(counter, 9)
Application.CutCopyMode = False

Cells(counter, 9).Select
Epsilon = Selection.Value

'get the value of time , time difference
Cells(counter, 1).Select
t = Selection.Value
Cells(counter, 8).Value = t - tempt  'put the (time difference)in column 8
tempt = t
Cells(counter, 8).Select
deltt = Selection.Value


'calculate the G value, put in column 10
```

```
    Cells(counter, 10).Value = 1000 * ((Epsilon) ^ 0.5)
    'Cells(counter, 10).Value = Epsilon * 2   'This line just for testing
    Cells(counter, 10).Select
    g = Selection.Value

Else
'++++++++++++++++++++++++++++++++++++++++++++++
'This part is for cylindrical vessel

Steps = Val(InputBox("Please enter the number of steps", "Calculation Steps Entry", 5))
'Steps refers to the calculation steps in the particle trajectory simulation

While counter <= Steps

'convert the tangential position to cell I value
Cells(counter, 2).Select
theta = Selection.Value
Select Case theta
Case 0 To 0.121
    i = 2
Case 0.12101 To 0.181
    i = 3
Case 0.18101 To 0.242
    i = 4
Case 0.24201 To 0.302
    i = 5
Case 0.30201 To 0.362
    i = 6
Case 0.36201 To 0.423
    i = 7
Case 0.42301 To 0.483
    i = 8
Case 0.48301 To 0.543
    i = 9
Case 0.54301 To 0.604
    i = 10
Case 0.60401 To 0.664
    i = 11
Case 0.66401 To 0.725
    i = 12
Case 0.72501 To 0.785
    i = 13
Case 0.78501 To 0.845
    i = 14
Case 0.84501 To 0.906
```

```
    i = 15
Case 0.90601 To 0.966
    i = 16
Case 0.96601 To 0.103
    i = 17
Case 0.10301 To 0.109
    i = 18
Case 0.10901 To 0.115
    i = 19
Case 0.11501 To 0.121
    i = 20
Case 0.12101 To 0.127
    i = 21
Case 0.12701 To 0.133
    i = 22
Case 0.13301 To 0.139
    i = 23
Case 0.13901 To 0.145
    i = 24
Case 0.14501 To 0.151
    i = 25
Case 0.15101 To 0.157
    i = 26
Case Else
    MsgBox ("please check the x position") 'check if tangential value is in the correct
range
    Debug.Print counter; x; y; z 'Display the position in the Debug Window
End Select


'convert the radial position to cell J value
Cells(counter, 3).Select
ra = Selection.Value
Select Case ra
Case 0 To 0.0069
    j = 2
Case 0.0069 To 0.0125
    j = 3
Case 0.012501 To 0.0186
    j = 4
Case 0.018601 To 0.0245
    j = 5
Case 0.024501 To 0.0302
    j = 6
Case 0.030201 To 0.0357
```

```
    j = 7
Case 0.035701 To 0.0408
    j = 8
Case 0.040801 To 0.0455
    j = 9
Case 0.045501 To 0.05
    j = 10
Case 0.050001 To 0.0549
    j = 11
Case 0.054901 To 0.0597
    j = 12
Case 0.059701 To 0.0646
    j = 13
Case 0.064601 To 0.0694
    j = 14
Case 0.069401 To 0.0743
    j = 15
Case 0.074301 To 0.0791
    j = 16
Case 0.079101 To 0.0839
    j = 17
Case 0.083901 To 0.0888
    j = 18
Case 0.088801 To 0.0936
    j = 19
Case 0.093601 To 0.0985
    j = 20
Case 0.098501 To 0.1034
    j = 21
Case 0.103401 To 0.1082
    j = 22
Case 0.108201 To 0.113
    j = 23
Case 0.11301 To 0.118
    j = 24
Case 0.11801 To 0.123
    j = 25
Case 0.12301 To 0.128
    j = 26
Case 0.12801 To 0.133
    j = 27
Case 0.13301 To 0.137
    j = 28
Case 0.13701 To 0.142
    j = 29
```

```
Case 0.14201 To 0.147
   j = 30
Case Else
   MsgBox ("please check the y position") 'check if radial value is in the correct range
   Debug.Print counter; x; y; z 'Display the position in the Debug Window
End Select

'convert the z position to cell K value
Cells(counter, 4).Select
z = Selection.Value
Select Case z
Case 0 To 0.0066
   k = 2
Case 0.006601 To 0.0132
   k = 3
Case 0.013201 To 0.0196
   k = 4
Case 0.019601 To 0.0261
   k = 5
Case 0.026101 To 0.0323
   k = 6
Case 0.032301 To 0.0383
   k = 7
Case 0.038301 To 0.0443
   k = 8
Case 0.044301 To 0.0499
   k = 9
Case 0.049901 To 0.0553
   k = 10
Case 0.055301 To 0.0605
   k = 11
Case 0.060501 To 0.0653
   k = 12
Case 0.065301 To 0.07
   k = 13
Case 0.070001 To 0.074
   k = 14
Case 0.07401 To 0.078
   k = 15
Case 0.07801 To 0.082
   k = 16
Case 0.08201 To 0.086
   k = 17
Case 0.08601 To 0.09
   k = 18
```

```
Case 0.09001 To 0.094
   k = 19
Case 0.09401 To 0.0988
   k = 20
Case 0.098801 To 0.1035
   k = 21
Case 0.103501 To 0.1084
   k = 22
Case 0.108401 To 0.1134
   k = 23
Case 0.113401 To 0.1186
   k = 24
Case 0.118601 To 0.124
   k = 25
Case 0.12401 To 0.129
   k = 26
Case 0.12901 To 0.135
   k = 27
Case 0.13501 To 0.142
   k = 28
Case 0.14201 To 0.148
   k = 29
Case 0.14801 To 0.154
   k = 30
Case 0.15401 To 0.161
   k = 31
Case 0.16101 To 0.167
   k = 32
Case 0.16701 To 0.174
   k = 33
Case 0.17401 To 0.181
   k = 34
Case 0.18101 To 0.188
   k = 35
Case 0.18801 To 0.196
   k = 36
Case 0.19601 To 0.203
   k = 37
Case 0.20301 To 0.211
   k = 38
Case 0.21101 To 0.219
   k = 39
Case 0.21901 To 0.227
   k = 40
Case 0.22701 To 0.235
```

```
    k = 41
  Case 0.23501 To 0.243
    k = 42
  Case 0.24301 To 0.251
    k = 43
  Case 0.25101 To 0.259
    k = 44
  Case 0.25901 To 0.268
    k = 45
  Case 0.26801 To 0.276
    k = 46
  Case 0.27601 To 0.285
    k = 47
  Case 0.28501 To 0.293
    k = 48
  Case Else
    MsgBox ("please check the z position") 'check if z value is in the correct range
    Debug.Print counter; x; y; z 'Display the position in the Debug Window
  End Select


    'put I value in column 5
    Cells(counter, 5).Value = i

    'put J value in column 6
    Cells(counter, 6).Value = j

    'put K value in column 7
    Cells(counter, 7).Value = k

  'copy the G value of cell(i,j,k) from sheet "G_value"
    Worksheets("G_value").Select
    If ((i Mod 10) = 0) Then
    Cells((((k - 1) * 156 + 8) + (35 - j) + (((i \ 10) - 1) * 38)), 11).Select
    Else
    Cells((((k - 1) * 156 + 8) + (35 - j) + ((i \ 10) * 38)), ((i Mod 10) + 1)).Select
    'Where 156 is the number of rows for each k value block in "Epsilon_value" sheet
    '     8  is the number of rows before the first G value
    '     (35 - j) refers to G values were listed on reverse sequence
    '     (i mod 10) gives the reminder of this division
    '     (i \ 10) gives the integer of this division
    '     ((i \ 10) * 38) indicates for each 10 I values we have 38 rows
    '
    End If
    temp = Selection.Value
```

```
'  Put the G value in column 10 in Sheet "tg"
   Sheets("tg").Select
   Cells(counter, 10).Value = temp
   Cells(counter, 10).Select
   g = Selection.Value
'++++++++++++++++++++++++++++++++++++++++++++++++++++++++++++
End If

   'calculate the indivdual t*G value, put in column 11
   Cells(counter, 11).Value = g * deltt

   'calculate the subtotal of t*G value, put in column 12
   Cells(counter, 11).Select
   gg = Selection.Value
   subtotal = subtotal + gg
   Cells(counter, 12).Value = subtotal


   'The following part is for G value distribution calculation
   Select Case g
      Case 0 To 10
         t10 = t10 + deltt
      Case 10 To 20
         t20 = t20 + deltt
      Case 20 To 40
         t40 = t40 + deltt
      Case 40 To 60
         t60 = t60 + deltt
      Case 60 To 80
         t80 = t80 + deltt
      Case 80 To 100
         t100 = t100 + deltt
      Case 100 To 200
         t200 = t200 + deltt
      Case 200 To 300
         t300 = t300 + deltt
      Case 300 To 400
         t400 = t400 + deltt
      Case 400 To 500
         t500 = t500 + deltt
      Case 500 To 600
         t600 = t600 + deltt
      Case 600 To 700
         t700 = t700 + deltt
```

```
    Case 700 To 800
       t800 = t800 + deltt
    Case 800 To 900
       t900 = t900 + deltt
    Case 900 To 1000
       t1000 = t1000 + deltt
    Case 1000 To 1100
       t1100 = t1100 + deltt
    Case 1100 To 1200
       t1200 = t1200 + deltt
    Case 1200 To 1300
       t1300 = t1300 + deltt
    Case 1300 To 1400
       t1400 = t1400 + deltt
    Case 1400 To 1500
       t1500 = t1500 + deltt
    Case Else
       telse = telse + deltt
       'MsgBox ("G value out of range") 'check if G value is in the correct range
       'Debug.Print counter; x; y; z, g 'Display the position in the Debug Window
End Select

counter = counter + 1

'Output the distribution results
'put them in column 14 (G value), 15(time spent in the G value)
Cells(2, 14).Value = 10
Cells(2, 15).Value = t10

Cells(3, 14).Value = 20
Cells(3, 15).Value = t20

Cells(4, 14).Value = 40
Cells(4, 15).Value = t40

Cells(5, 14).Value = 60
Cells(5, 15).Value = t60

Cells(6, 14).Value = 80
Cells(6, 15).Value = t80

Cells(7, 14).Value = 100
Cells(7, 15).Value = t100

Cells(8, 14).Value = 200
```

```
Cells(8, 15).Value = t200

Cells(9, 14).Value = 300
Cells(9, 15).Value = t300

Cells(10, 14).Value = 400
Cells(10, 15).Value = t400

Cells(11, 14).Value = 500
Cells(11, 15).Value = t500

Cells(12, 14).Value = 600
Cells(12, 15).Value = t600

Cells(13, 14).Value = 700
Cells(13, 15).Value = t700

Cells(14, 14).Value = 800
Cells(14, 15).Value = t800

Cells(15, 14).Value = 900
Cells(15, 15).Value = t900

Cells(16, 14).Value = 1000
Cells(16, 15).Value = t1000

Cells(17, 14).Value = 1100
Cells(17, 15).Value = t1100

Cells(18, 14).Value = 1200
Cells(18, 15).Value = t1200

Cells(19, 14).Value = 1300
Cells(19, 15).Value = t1300

Cells(20, 14).Value = 1400
Cells(20, 15).Value = t1400

Cells(21, 14).Value = 1500
Cells(21, 15).Value = t1500

Cells(22, 14).Value = "Else"
Cells(22, 15).Value = telse

Cells(23, 14).Value = "total time"
```

```
    Cells(23, 15).Value = t

Wend
    MsgBox ("Good Job !")
    'End of program

End Sub
```

REFERENCES

Amirtharajah, A. and Mills, K. M., "Rapid Mix Design for Mechanisms of Alum Coagulation", *J. AWWA*, **74**: 210-216 (1982).

Amirtharajah, a. and Trusler, S. L., "Destabilization of Particles by Turbulent Rapid Mixing", *J. Environ. Eng.*, **112**: 1085-1108 (1987).

Argaman, Y., and Kaufman, W. J., "Turbulence and Flocculation", *Journal of the Sanitary Engineering Division,* ASCE, **96**(2): 223-241 (1970).

Armenante, P. M. and Chou, C. C., "Experimental LDV Measurement and Numerical CFD Determination of the Fluid Velocity Distribution in an Unbaffled Mixing Vessel", *AIChE Symp. Ser.*, **90** (299): 33-42 (1994a).

Armenante P. M., Chou, C. C. and Hemrajani, R. R., "Comparison of Experimental and Numerical Fluid Velocity Distribution Profiles in an Unbaffled Mixing Vessel Provided with a Pitched-Blade Turbine", *Proc. 8th Europ. Conf. Mixing (I. Chem. Eng. Symp. Ser. No. 136), Cambridge, U.K.*, **21**: 349-356, September (1994b).

Armenante, P. M. and Chou, C. C., "Velocity Profiles in a Baffled Vessel with Single or Double Pitched-Blade Turbines, " *AIChE J.*, January, **42**(1): 42-54 (1996).

Bakker, A., "Hydrodynamics of Stirred Gas-Liquid Dispersions", Ph.D. dissertation, Delft Univ. of Technology, Delft, The Netherlands (1992).

Bakker, A., Fasano ,J. B. and Myers, K. J., "Effects of Flow Pattern on the Solids Distribution in a Stirred Tank", *IChemE Symp. Ser.*, 136: 1-8 (1996).

Bakker, A. and Van Den Akker H. E. A., "A Computational Study on Dispersing Gas in a Stirred Reactor", 7th European Conference on Mixing, Proceedings Vol I: 199-207 (1991)

Bertrand, J., Abid, M. and Xuereb, C., "Modeling of the 3D Hydrodynamics of 2-Blade Impellers in Stirred Tanks Filled With a Highly Viscous Fluid", *The Canadian Journal of Chemical Engineering*, **72**: 184-193, April (1994).

Bhargava, D. S. and Ojha, C. S. P., "Models for Design of Flocculating Baffled Channels", *Wat. Res.*, **27**: 465-475 (1993).

Bird, R. B., Stewart, W. E. and Lightfoot, E. N., *Transport Phenomena*, John Wiley & Sons, Inc., New York, NY (1960)

Camp, T. R. and Stein, P. C., "Velocity Gradient and Internal Work in Fluid Motion", *J. Boston Soc.Civ. Eng.*, **30**: 219-237 (1943).

Camp, M. M., "Flocculation and Flocculation Basins", *Trans. ASCE*, **120**: 1-16 (1955).

Clark, M. M., et al., "Selection and Design of Mixing Processes for Coagulation", American Water Works Assoc. Res. Found. and American Water Works Assoc., Denver, Colo (1994).

Cleasby, J. L., "Is Velocity Gradient a Valid Turbulent Flocculation Parameter?", *J. Environ. Eng.*, **110**(5): 875-897 (1984).

Costes, J., Alran, C. and Couderc, J. P., "Characteristics of the Discharge Flow from a Rushton Turbine. Measurements by Thermal and Laser-Doppler Anemometry", *Int. Chem. Eng.*, **31:** 55-67 (1991).

Creare. x Inc., *Fluent - Computational Fluid Dynamics Software User's Manual*, Hanover, New Hampshire (1991).

De Groot, P. J., "LDA Used to Check Nagata's Model for Vortex Geometry in Stirred Vessels", Laser Anemom. Int. Conf. (ASME), **1:** 247-265 (1991).

Delichatsios, M. A. and Probstein, R. F., "Coagulation in Turbulent Flow: Theory and Experiments", *J. Colloid. Sci.*, **51**: 394-405 (1975).

Dharmappa, H. B., Verink, J., Fujiwara, O., and Vigneswaran, S., "Optimal Design of a Flocculator", *Wat. Res.*, **27**: 513-519 (1993).

Dong, L., Johansen, S. T. and Engh, T. A., "Flow Induced by An Impeller in an Unbaffled Tank - I. Experimental", *Chem. Eng. Sci*, **49**(4): 549-560 (1994a).

Dong L., Johansen, S. T. and Engh, T. A., "Flow Induced by an Impeller in an Unbaffled Tank - II. Numerical Modeling", *Chem. Eng. Sci.* **49**(20): 3511-3518 (1994b)

Ducoste, J. J., Clark, M. M. and Weetman, R. J., "The Evaluation of Mechanics Generated in the Flocculation Process: Effects of Tank Size and Impeller Type", *AIChE J.*, **43**(2):328-339 (1997).

Fluent. Inc. "FLUENT User's Guide", Version 4.3 (1995).

Fort, I., "Flow and Turbulence in Vessels with Axial Impellers", *In* Uhl, V. W. and Gray, J. B. (eds.) *Mixing: Theory and Practice*, Vol. III, Academic Press, New York (1986).

Geisler, R., Krebs, R. and Forschner P., "Local Turbulent Shear Stress in Stirred Vessels and its Significance for Different Mixing Tasks", *IChemE Symp. Ser.*, 136: 243-250 (1996).

Glasgow, L. A. and Kim, Y. H., "Characterization of Agitation Intensity in Flocculation Processes", *J. Environ. Eng.*, **112**: 1158-1163 (1986).

Glasgow, L. A. and Liu, X., "Response of Aggregate Structures to Hydrodynamic Stress", *AIChE J.*, **37**: 1411-1414 (1991).

Gray, J. B., "Flow Patterns, Fluid Velocities, and Mixing in Agitated Vessels", *In* Uhl, V. W. and Gray, J. B. (eds.) *Mixing: Theory and Practice*, Vol. I, Academic Press, New York (1966).

Harvey, A. D. and Rogers, S. E., "Steady and Unsteady Computation of Impeller-Stirred Reactors", *AIChE J.*, **42**(10): 2701-2712 (1996).

Hinze, J. O., *Turbulence*, Second Edition, McGraw-Hill Publishing Co., New York, NY (1975).

Hirata, Y., Nienow, A. W., and Moore, I. P., "LDA Studies of Velocity distributions and Cavern Sizes in a Yield Stress Fluid Agitated by a Rushton Turbine", *Proc. Eur. Conf. on Mixing, Brugge (Belgium)*, **1**: 167 (1991).

Jaworski, Z., Nienow, A. W. and Dyster, K. N., "An LDA Study of the Turbulent Flow Field in a Baffled Vessel Agitated By an Axial, Down-pumping Hydrofoil Impeller", *Can. J. Chem. Eng.*, **74**: 3-15 (1996).

Jaworski, Z., Nienow, A. W., Koutsakos, E., Dyster, K., and Bujalski, W., "An LDA Study of Turbulent Flow in a Baffled Vessel Agitated by a Pitched Blade Turbine", *Trans. Inst. Chem. Eng., Part A, Chem. Eng. Res. Des.*, **69**: 313-320 (1991).

Kresta, S. M. and Wood, P. E., "Prediction of the Three-Dimensional Turbulent Flow in Stirred Tanks", *AIChE J.*, **37**(3): 448-460 (1991).

Kresta, S. M. and Wood, P. E., "The Flow Field Produced by a Pitched Blade Turbine: Characterization of the Turbulence and Estimation of the Dissipation Rate", *Chem. Eng. Sci.*, **48**: 1761-1774 (1993).

Launder, B. E., and Spalding, D. B., *Mathematical Models of Turbulence*, Academic Press, London (1972).

Launder, B. E., "Second-Moment Closure: Present... and Future ?", *International Journal Heat and Fluid Flow*, **10**(4): 282-300 (1989).

Launder, B. E., Reece, G. J., and Rodi, W., "Progress in the Development of a Reynolds-Stress Turbulence Closure", *J. Fluid Mech.*, **68**(3): 537-566, Apr. 15 (1975).

Luo, J. Y., Gosman, A. D., Issa, R. I., Middleton, J. C. and Fitzgerald, M. K., "Full Flow Field Computation of Mixing in Baffled Stirred Vessels", *Chem. Eng. Res. Des.*, **71**: 342-344 (1993).

Mahouast, M., Cognet, and David, R., "Two-component LDV Measurement in a Stirred Tank", *AIChE J.*, **35**: 1770-1778 (1989).

Markopoulos, J. and Kontogeorgaki, E., "Vortex Depth in Unbaffled Single and Multiple Impeller Agitated Vessels", *Chem. Eng. Technol.*, **18:** 68-74 (1995).

McConnachie, G., "Turbulence Intensity of Mixing in Relation to Flocculation", *J. Environ. Eng.*, **117**: 731-750 (1989).

Mhaisalkar, V. A., Paramasivan, P., and Bhole, A. G., "Optimizing Physical Parameters of Rapid Mix Design for Coagulation-Flocculation of Turbid Waters", *Wat. Res.*, **25**: 43-52 (1991).

Morsi, S. A., and Alexander, A.., "An Investigation of Particle Trajectories in Two-Phase Flow systems", *J. Fluid Mech.*, **55**(2): 193-208, September (1972).

Nagata S., *Mixing*, John Wiley & Sons, New York (1975).

Nienow, A. W. and Miles, D., "Impeller Power Numbers in Closed Vessels", *Ind. Eng. Chem. Process Des. Develop.*, **10**(1): 41-43 (1971).

O'Melia, C. R., "Coagulation and Flocculation", in "*Physicochemical Processes for Water Quality Control*", by W. W. Weber (ed.), Wiley Interscience, New York, NY (1972).

Ranade, V. V., Joshi, J. B, and Marathe, A. G., "Flow Generated by Pitched Blade Turbines: II. Simulation Using k-ε Model", *Chem. Eng. Comm.*, **81**: 225-248 (1989).

Ranade, V. V. and Joshi, J. B., "Flow Generated by a Disc Turbine: Part II. Mathematical Modelling and Comparison with Experimental Data", *Chem. Eng. Res. Des.*, **68**: 34-50 (1990).

Ranade, V. V., Mishra, V. V., Saraph, V. S., Deshpande, G. B, and Joshi, J. B., "Comparison of Axial Flow Impellers Using a Laser Doppler Anemometer", *Ind. Eng. Chem. Res.*, **31**: 2370-2379 (1992).

Rodi W., "Turbulent Models and Their Application in Hydraulics -- A State of Art Review", Second Edition, *International Association for Hydraulic Research*, Delft, The Netherlands (1984).

Rutherford K., Mahmoundi, S. M. S., Lee, K. C. and Yianneskis, M., "The Influence of Rushton Impeller Blade and Disk Thickness on the Mixing Characteristics of Stirred Vessels", *Trans IChemE*, **74**(A): 369-378 (1996).

Sabersky, R. H., Acosta, A. J. and Hauptmann, E. G., *Fluid Flow, A First Course in Fluid Mechanics*, Third Edition, Macmillan Publishing Company, New York, NY (1989).

Stanley, S. J. and Smith, D. W., "Measurement of Turbulent Flow in Standard Jar Test Apparatus", *J. of Envir. Eng.*, **121**(12): 902-909 (1995).

Tatterson G.B., *Fluid Mixing and Gas Dispersion in Agitated Tanks*, First Edition, McGraw-Hill Inc., New York, NY (1991).

Wiesner, M. R., "Kinetics of Aggregate Formation in Rapid Mix", *Wat. Res.*, **26**: 379-387 (1992).

Wu, H., and Patterson, G. K., "Laser-Doppler Measurements of Turbulent-Flow Parameters in a Stirred Mixer", *Chem. Eng. Sci.*, **44**: 2207-2221 (1989).

Zhou, G. and Kresta, S. M., "Distribution of Energy between Convective and Turbulent Flow for Three Frequently Used Impellers", *Trans IChemE*, **74**(A): 379-389 (1996).